OPTIMAL AEROELASTIC TRIM FOR ROTORCRAFT WITH CONSTRAINED, NON-UNIQUE TRIM SOLUTIONS

A Thesis
Presented to
The Academic Faculty

by

Troy C. Schank

In Partial Fulfillment
of the Requirements for the Degree
Doctor of Philosophy in the
School of Aerospace Engineering

Georgia Institute of Technology
April 2008

Optimal Aeroelastic Trim for Rotorcraft with
Constrained, Non-Unique Trim Solutions

Approved By

Professor Dimitri N. Mavris, Advisor
School of Aerospace Engineering
Georgia Institute of Technology

Professor Dewey H. Hodges
School of Aerospace Engineering
Georgia Institute of Technology

Professor Daniel P. Schrage, Co-advisor
School of Aerospace Engineering
Georgia Institute of Technology

Professor J.V.R. Prasad
School of Aerospace Engineering
Georgia Institute of Technology

Professor David A. Peters
Department of Mechanical, Aerospace
and Structural Engineering
Washington University, St. Louis

Date Approved: January 16, 2008

ACKNOWLEDGEMENTS

I would like to thank my advisor, Dr. Dimitri Mavris, for providing me the opportunity to pursue my educational goals at Georgia Tech. I would also like to thank my co-advisor Dr. Schrage for providing many unique research opportunities in the area of rotorcraft performance and systems design. In addition, Dr. Dewey Hodges and Dr. David Peters provided invaluable guidance in the area of rotorcraft dynamics and aeroelasticity both in person and through their published work. Their examples of sincere kindness and technical excellence have been inspirational. Finally, I appreciate the gracious feedback on this work from Dr. J.V.R. Prasad.

I would also like to extend gratitude to my parents. My mother has a love for books and learning that set an example to me to ask questions and seek answers. I recall our home always having a fresh supply of books, replenished every couple weeks from the library. Likewise, my father's work ethic has been an example of getting up every day, rolling up your sleeves and accomplishing something worthwhile.

I must also acknowledge the love and support of my three boys, Randall, Quintan and Rhett. No matter what kind of day I have, their cheerful smiles greet me home each evening. Their unconditional love and support help to keep things in perspective. Lastly, I want to express gratitude to my life long friend and wife, Megan. Without her patience and support, I simply would not have completed this work. The journey we have experienced in this endeavor has stretched us both to a new understanding of life and of ourselves. Thank you.

Troy C. Schank

Georgia Institute of Technology

January 2008

TABLE OF CONTENTS

ACKNOWLEDGEMENTS iii
LIST OF TABLES vii
LIST OF FIGURES viii
LIST OF SYMBOLS xi
SUMMARY xiii
CHAPTER 1 INTRODUCTION 1
1.1 Rotorcraft Trim 4
1.1.1 Multidisciplinary Nature of Trim 4
1.1.2 Governing Equations 6
1.1.3 Periodicity Conditions 7
1.1.4 Trim Conditions and Constraints 8
1.2 Optimal Trim 9
1.2.1 Optimal Trim Formulation 10
1.2.2 Nonlinear Programming Methods 11
1.2.3 Optimal Trim Constraints 11
1.2.4 Optimal Rotorcraft Trim Considerations 12
1.3 Objectives and Scope of Work 13
1.4 Research Questions and Hypotheses 14
1.4.1 Primary Research Question and Hypothesis 15
1.4.2 Supporting Question and Hypothesis No. 1 15
1.4.3 Supporting Question and Hypothesis No. 2 15
CHAPTER 2 LITERATURE REVIEW 16
2.1 Rotorcraft Trim Methods 16
2.1.1 Direct Numerical Integration 17
2.1.2 Harmonic Balance 17
2.1.3 Periodic Shooting 19
2.1.4 Autopilot 20
2.1.5 Neural Net Function Approximation 21

2.2 Trim Optimization 22
2.2.1 Previous Applications 22
2.2.2 Nonlinear Programming Methods 24
2.3 Variable Rotor speed Autorotation 27
2.3.1 Background 27
2.3.2 Variable Rotor Speed Trim Methods 29
2.4 Rotor Blade Stress and Strain 30
2.5 Chapter Summary 32
CHAPTER 3 GENERALIZED REDUCED GRADIENT OPTIMAL TRIM 33
3.1 Mathematical Formulation 33
3.1.1 Reduced Gradient Determination 33
3.1.2 Inequality Constraints 36
3.1.3 Search Direction 38
3.1.4 Optimality Conditions 40
3.2 Optimal Trim Algorithm Implementation 40
3.2.1 Implementation Considerations 40
3.2.2 Algorithm Description 42
3.3 Method Validation 46
3.3.1 Validation Case: Hover 48
3.3.2 Validation Case: Forward Flight 51
3.3.3 Optimal Trim Results Discussion 56
3.4 Chapter Summary 58
CHAPTER 4 AUTOROTATIVE TRIM WITH VARIABLE ROTOR SPEED 59
4.1 Physics of Autorotation 59
4.2 Numerical Method for Variable Rotor speed 62
4.3 Rotor speed Correlation 65
4.3.1 Isolated Rotor Trim 66
4.3.2 6 DOF Vehicle Trim 74
4.4 Optimal Trim Application to Autorotation 78
4.5 Chapter Summary 80
CHAPTER 5 SURROGATE BLADE STRESS AND STRAIN 81

5.1 Rotor Aeroelastic and Structural Analysis Framework 82
5.2 Surrogate Stress/Strain Method 83
5.3 Neural Networks 86
5.4 Blade Surrogate Strain Model Validation 89
5.4.1 Identify Input Variables and Ranges 91
5.4.2 Sample Solution Space 92
5.4.3 Model Goodness of Fit 94
5.4.4 Surrogate Strain Validation Results 95
5.5 Chapter Summary 107
CHAPTER 6 CONSTRAINED OPTIMAL TRIM APPLICATION 109
6.1 Example Compound Gyroplane 109
6.2 Compound Gyroplane Optimal Aeroelastic Trim 113
6.2.1 Fixed Shaft Configuration 114
6.2.2 Tilting Shaft Configuration 117
6.2.3 Trim Configuration Results 118
6.2.4 Optimal Trim Purpose 120
6.3 Chapter Summary 121
CHAPTER 7 CONCLUSION 122
7.1 Summary and Conclusions 122
7.2 Future Work 124
REFERENCES 126

LIST OF TABLES

Table 1: Optimal Trim Validation Test Case Summary 47
Table 2: Sample Helicopter Properties 47
Table 3: Hover X^O=[40] 49
Table 4: Hover X^O=[28] 50
Table 5: Hover X^O=[34] 50
Table 6: Forward Flight X^O=[0, 40] 53
Table 7: Forward Flight X^O=[135, 35] 53
Table 8: Forward Flight X^O=[165, 48] 53
Table 9: Inequality Constrained Forward Flight X^O=[0, 40]; Dependent Ω 55
Table 10: Inequality Constrained Forward Flight X^O=[0, 40]; Independent Ω 55
Table 11: Total Function Calls for Inequality Constrained Optimization 56
Table 12: 10 Foot Diameter Wind Tunnel Rotor Properties 66
Table 13: VPM M16 Properties 75
Table 14: RSTA 69.75 Cross-Section Properties 91
Table 15: Design Variable Input Ranges 92
Table 16: Surrogate Model Goodness of Fit Summary 96
Table 17: Strain Recovery Time Summary 106

LIST OF FIGURES

Figure 1: Multi-dimensional, Constrained Trim Solution Spaces 2
Figure 2: Convex, Constrained Trim Solution Space to Optimize 3
Figure 3: Interdisciplinary Interaction in Rotorcraft Analysis and Design..... 5
Figure 4: NLP Method Classification 25
Figure 5: Rotor Airflow Direction and Net Forces [38] 28
Figure 6: Rotor Blade Dimensional Reduction Method 31
Figure 7: Elements and Input/Output of VABS..... 32
Figure 8: GRG Nonlinear Constraint Satisfaction 36
Figure 9: Trim Variable Radii of Convergence 39
Figure 10: RCAS Trim Algorithm 44
Figure 11: GRG Optimal Trim Algorithm..... 45
Figure 12: Hover Power vs. Rotor speed 48
Figure 13: Optimal Trim Convergence: 1 Independent Control Variable 51
Figure 14: Helicopter Power Map (HP)..... 52
Figure 15: Optimal Trim Convergence: 2 Independent Control Variables 54
Figure 16: Optimal Trim Convergence: Dependent vs. Independent Rotor Speed 55
Figure 17: Detailed Blade Element Flow in Autorotation [38] 60
Figure 18: Autorotational Diagram..... 61
Figure 19: Driving and Driven Regions [38]..... 63
Figure 20: Isolated Rotor Shaft Angle vs. Advance Ratio Test Resluts 68
Figure 21: Isolated Rotor Shaft Angle Model Prediction 68
Figure 22: Isolated Rotor θ_{1s} Correlation..... 69
Figure 23: Isolated Rotor Thrust Coefficient Correlation..... 69
Figure 24: Trimmed Rotor Speed Model Resluts 70
Figure 25: Rotor speed Convergence from 120% Nominal Rotor speed at $\mu = 0.29$ 71
Figure 26: Rotor Torque Convergence from 120% Nominal Rotor speed at $\mu = 0.29$..... 71
Figure 27: Rotor speed Convergence from 80% Nominal Rotor speed at $\mu = 0.29$ 72
Figure 28: Rotor Torque Convergence from 80% Nominal Rotor speed at $\mu = 0.29$..... 72

Figure 29: Inplane Force (lbs) Distribution at Advance Ratios 0.15 through 0.42 73
Figure 30: Periodic Shaft Torque with Two Shaft Boundary Conditions 74
Figure 31: University of Glasgow Instrumented Gyroplane..... 75
Figure 32: Pitch Attitude Correlation of Flight Test and Model 77
Figure 33: Rotor speed Correlation of Flight Test and Model..... 77
Figure 34: Rotor Torque and Lift vs. Shaft Angle..... 78
Figure 35: Rotor speed and Lift vs. Shaft Angle 79
Figure 36: Rotorcraft Aeroelastic Loads Framework 82
Figure 37: Surrogate Stress/Strain Feedback..... 84
Figure 38: Stress/Strain Field vs. Response Subset 84
Figure 39: Neural Network Conceptual Diagram..... 87
Figure 40: Nodal Output(s) as a Function of Weighted Inputs..... 87
Figure 41: Rotor Critical Strain Spanwise Location (in.)..... 90
Figure 42: Cross-sectional Strain Solution Space Sampling 93
Figure 43: Cross Sectional Surrogate ε_{vm} Model Fit 96
Figure 44: Cross-Sectional Strain Components Residual by Predicted (micro-strain)..... 97
Figure 45: Vertical Gust Velocity Profile..... 98
Figure 46: Case 1 Gust Response RSTA 69.75 Forces and Moments..... 100
Figure 47: Case 1 Time Dependent Max ε_{vm}..... 100
Figure 48: Case 1 Time Dependent Max ε_{11}..... 101
Figure 49: Case 1 Time Dependent Max ε_{12}..... 101
Figure 50: Case 1 Time Dependent Max ε_{13}..... 101
Figure 51: Case 1 Time Dependent Max ε_{22}..... 102
Figure 52: Case 1 Time Dependent Max ε_{23}..... 102
Figure 53: Case 1 Time Dependent Max ε_{33}..... 102
Figure 54: Case 2 Gust Response RSTA 69.75 Forces and Moments..... 103
Figure 55: Case 2 Time Dependent Max ε_{vm}..... 103
Figure 56: Case 2 Time Dependent Max ε_{11}..... 104
Figure 57: Case 2 Time Dependent Max ε_{12}..... 104
Figure 58: Case 2 Time Dependent Max ε_{13}..... 104
Figure 59: Case 2 Time Dependent Max ε_{22}..... 105

Figure 60: Case 2 Time Dependent Max ε_{23} 105
Figure 61: Case 2 Time Dependent Max ε_{33} 105
Figure 62: High Speed Compound Gyroplane 110
Figure 63: Rotor speed vs. Velocity Diagram (30,000 ft) 111
Figure 64: Compound Gyroplane Rotor Fundamental Frequencies vs. Rotor Speed 112
Figure 65: Compound Gyroplane Structural Model 113
Figure 66: Rigid Blade Flapping at Reduced Rotor speeds 117
Figure 67: Compound Gyroplane Optimal Rotor Speed Trends 119
Figure 68: Compound Gyroplane Optimal Velocity Trends 119
Figure 69: Compound Gyroplane Optimal Lift-to-Drag Trends 120

LIST OF SYMBOLS

a	artificial neural network input offset value
b	artificial neural network input weight parameter
B	total number of rotor blades
C_d	drag coefficient
C_l	lift coefficient
C_L	wing lift coefficient
C_T	thrust coefficient
D	drag
e	elevator
F_R	residual body force
$F(\vec{X})$	objective function
g	inequality constraint
h	equality constraint (average) value
$\hat{h}$	instantaneous constraint value
$\overline{h}$	specified azimuth constraint value
H	artificial neural network node
i	state variable first time derivative index
I	total state variables
I_R	rotor moment of inertia
j	slack variable index
J_{X_D}	dependent variable Jacobian matrix
J_{X_I}	independent variable Jacobian matrix
k	line search index
K	total state variables
l	implicit constraint index
L	lift
n	trim control variable index
N	total trim control variables
$\hat{N}$	total neural network nodes
m	trim equality constraint index
M	total trim equality constraints
M_{HR}	residual hub moment
M_R	residual body moment
o	force balance equation index
O	total force balance equations
p	inequality constraint index
P	total inequality constraints
$P(\vec{X})$	objective penalty function
q	artificial neural net node index
Q	rotor torque

r	radial distance along rotor radius
$\vec{r}$	dependent variable residual vector
r_p	penalty function scalar
$\hat{R}$	artificial neural net response
R	rotor radius
s	inequality slack variable
$\overline{S}$	line search direction vector
$\overline{S}*$	radius of convergence modified line search direction vector
S	reduced gradient subspace dimension
t	time
T	system period
T_E	engine thrust
u	state variable index
V_c	up-flow velocity through rotor disk
V_i	induced velocity
V	freestream velocity
x	state variable
$\dot{x}$	state variable time derivative
X	trim control variable
X_D	dependent control variable
X_I	independent control variable
$\vec{X}*$	control vector for optimum solution
z	quasi periodic states
$\hat{\alpha}$	line search step size
α	aerodynamic angle of attack
α_{shaft}	shaft incidence angle
α_{TPP}	tip path plane angle of attack
ε	material strain
λ	Lagrange multiplier
θ	geometric airfoil pitch angle
θ_{1s}	1/rev cyclic input at 90 degrees
μ	advance ratio
ρ	independent variable radius of convergence
σ	rotor solidity
τ_E	engine torque
ϕ	induced inflow angle
Φ	augmented objective function
ψ	rotor azimuth angle
ω_ξ	first rotor chordwise frequency
Ω	rotor angular velocity
$\dot{\Omega}$	time change in rotor angular velocity
$\nabla_r^T f(\vec{X}_I)$	reduced gradient

SUMMARY

New rotorcraft configurations are emerging, such as the optimal speed helicopter and slowed-rotor compound helicopter which, due to variable rotor speed and redundant lifting components, have non-unique trim solution spaces. The combination of controls and rotor speed that produce the best steady-flight condition is sought among all the possible solutions. This work develops the concept of optimal rotorcraft trim and explores its application to advanced rotorcraft configurations with non-unique, constrained trim solutions. The optimal trim work is based on the nonlinear programming method of the generalized reduced gradient (GRG) and is integrated into a multi-body, comprehensive aeroelastic rotorcraft code. In addition to the concept of optimal trim, two further developments are presented that allow the extension of optimal trim to rotorcraft with rotors that operate over a wide range of rotor speeds. The first is the concept of variable rotor speed trim with special application to rotors operating in steady autorotation. The technique developed herein treats rotor speed as a trim variable and uses a Newton-Raphson iterative method to drive the rotor speed to zero average torque simultaneously with other dependent trim variables. The second additional contribution of this thesis is a novel way to rapidly approximate elastic rotor blade stresses and strains in the aeroelastic trim analysis for structural constraints. For rotors that operate over large angular velocity ranges, rotor resonance and increased flapping conditions are encountered that can drive the maximum cross-sectional stress and strain to levels beyond endurance limits; such conditions must be avoided. The method developed herein captures the maximum cross-sectional stress/strain based on the trained response of an artificial neural network (ANN) surrogate as a function of 1-D beam forces and moments. The stresses/strains are computed simultaneously with the optimal trim and are used as constraints in the optimal trim solution. Finally, an optimal trim analysis is applied to a high-speed compound gyroplane configuration, which has two distinct rotor speed control methods, with the purpose of maximizing the vehicle cruise efficiency while maintaining rotor blade strain below endurance limit values.

CHAPTER 1
INTRODUCTION

The notion of trim is used in the aeronautical field to denote aircraft control settings, attitude and payload distribution required to obtain a steady flight condition. In the case of a fixed-wing aircraft, the steady flight condition can be characterized by constant lift and control surface (linear and angular velocity) state values relative to the aircraft body frame. The trim condition of a rotorcraft is more complex because its flight involves lifting/controlling surfaces that rotate with respect to each other, the aircraft body frame and with respect to the air mass through which the vehicle moves [1]. For a rotorcraft, no equilibrium condition exists such that the rates of all the aircraft states are constant. However, the controls and attitude can be adjusted to cause the rotor to achieve a particular periodic orbit where the average forces and moments achieve a desired steady flight condition. On this orbit each state value is unchanging at any given azimuth and the rotorcraft is characterized by periodic solutions of all the states, though the controls (or control parameters) are constant in time.

The mathematical basis for trim is well understood and the practical implementation of various trim methodologies has been successfully utilized in modern comprehensive rotorcraft codes for the trim solution of nonlinear rotorcraft models. The primary application of these trim methods has been the single main rotor (SMR) helicopter, often with a high level of model fidelity including elastic blades and unsteady aerodynamic effects. The SMR configuration, however, traditionally operates at a fixed rotor speed value and (assuming the yaw degree of freedom is fixed as is the normal convention) has a unique trim solution. A new generation of rotorcraft vehicle configurations and technologies is emerging which allows more flexible ways to fly the vehicle including variable main rotor speed and/or compound lift and thrust devices. Reference [2] describes a helicopter with a rigid rotor system that allows the rotor speed to operate over a large range to minimize power for maximum endurance, an important performance goal for unmanned aerial vehicles (UAVs). References [3,4] propose variants of the Slowed

Rotor Compound (SRC) configuration which share lift between the rotor and wing at various portions through the flight envelope. These concepts use the principle of autorotation to power the rotor and allow flexible rotor speed operation. Reference [5] speaks of a variable speed lifting rotor which allows high speed operation that, unlike the SRC, is loaded throughout the operating envelope. This concept, referred to as the Reverse Velocity Rotor (RVR) proposes higher harmonic control (HHC) to allow the main rotor to provide 100% of the lift up to speeds much higher than the conventional pure helicopter.

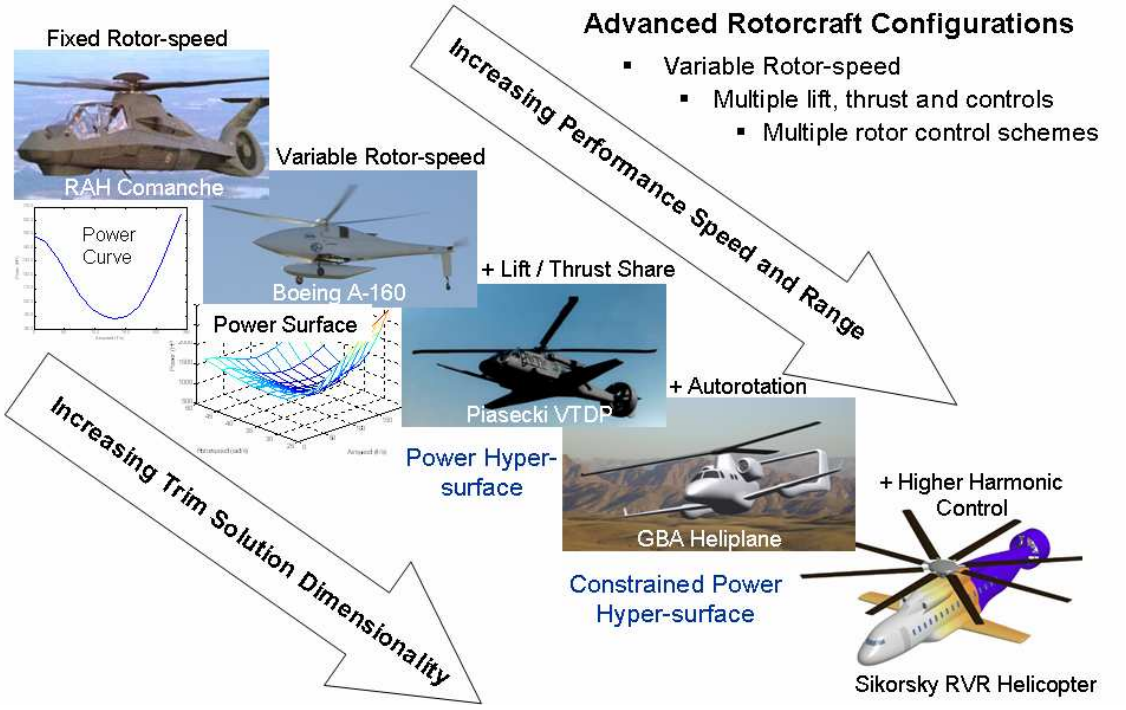

Figure 1: Multi-dimensional, Constrained Trim Solution Spaces

A defining characteristic of these advanced rotorcraft configurations is that they have a number of possible steady flight solutions for a given airspeed/altitude condition; the dimensionality of the trim solutions space increases. The question that faces the performance analyst is what combination of controls and rotor speed produce the best trim condition? The best condition may be driven by some performance measure such as minimum power or maximum lift-to-drag ratio and may have constraints such as rotor blade stress/strain, rotor induced vibration or maximum C_T/σ (a measure of the average

rotor lift coefficient). Performance codes may provide optimal lift and thrust sharing ratios based on simplified power formulations, but lack the ability to capture control moments, vibration, structural and aeroelastic constraints, which are dominant factors in rotorcraft flight operations, particularly if rotor speed varies over a wide range. To capture these details, a force-based approach is required that incorporates rotor equations of motion and a trimmed solution. The general procedure when using the force-based approach is to perform a number of trim analysis cases, sweeping additional trim variable(s) to produce carpet plots that give a graphical indication of the trim solution space. This approach becomes less tractable as the number of additional trim variables grows beyond one or two, especially when complex load or vibration constraints are involved. Therefore, a choice has to be made about which control variables to ignore and which ones to sweep, affecting the available trim solution space, and limiting the final solution to one potentially suboptimal. A trim method is desired that can remove the ambiguity of such trim sweep trades, and provide a rigorous way to systematically find the best possible trim solution achievable for the configuration. This thesis develops the concept of optimal (or optimum) rotorcraft trim through the application of nonlinear programming methods (NLP) and explores its application to advanced rotorcraft configurations with complex, constrained trim solution spaces. The term optimal trim is synonymous with optimum trim, that is to say the user defined objective function minimum or maximum has been obtained.

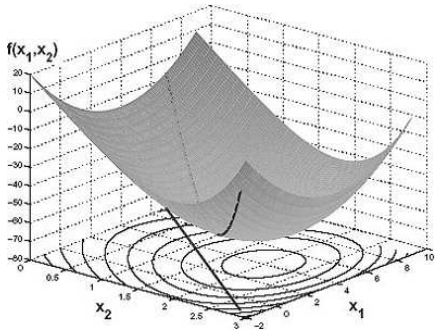

Figure 2: Convex, Constrained Trim Solution Space to Optimize

The thesis also develops methods for capturing two specific types of constraints that become important in the context of variable rotor speed capability, namely autorotation

constraints and rotor structural constraints. The development of the optimal trim method and these two constraints removes the ambiguity of limited, constrained trim solution space sweeps, and provides a rigorous method to systematically find the best possible trim solution achievable for a given configuration.

1.1 Rotorcraft Trim

A trim solution is a periodic solution for the set of governing differential equations with some unknown (control) parameters set such that a given set of constraints are satisfied. The constraints typically require the residual forces and moments to vanish for some steady flight condition. The trim solution is an important aspect of rotorcraft analysis for many reasons. The trim condition is required to calculate the net forces and moments on the rotor required for vehicle performance. The accurate calculation of trim is also crucial for the determination of loads. Furthermore the trim state affects the determination of flight mechanics and handling qualities since conventional stability derivatives are related in a strong, nonlinear way to the flight condition. Lastly, the aeroelastic stability of rotorcraft is strongly influenced by the trim settings. In fact, the dynamic and aeroelastic stability, and the handling qualities and control system design are commonly analyzed by perturbing the system about the periodic orbit corresponding to the trim condition. In other words, the analysis is based on the set of perturbation equations which strongly depend on the periodic solution that is perturbed. Therefore an inaccurate trim computation potentially undermines the validity of all these approaches.

1.1.1 Multidisciplinary Nature of Trim

The nature of rotorcraft flight yields a complex physical interaction between the elastic blades, the surrounding air mass and pilot control inputs. The analysis of such a system requires input from multiple disciplines, requiring comprehensive rotorcraft analysis tools to be highly multidisciplinary. For example, as the blade moves over one revolution, it encounters transonic flow, reverse flow, stall and unsteady effects including dynamic stall. Large azimuthal variations in lift result from changes in dynamic pressure and

angle of attack. The trailing and shed vortices leaving the blade result in a non-uniform wake. In addition to aerodynamic considerations, rotor blade structural dynamic behavior contributes to the system response. The rotor blade is slender and undergoes significant elastic deformation, requiring beam theories that accurately model large deflections. Strong structural nonlinearities such as Coriolis forces and radial shortening make the problem highly nonlinear. Finally, the aeroelastic system results in a set of average forces that must be modified by the pilot through available controls to yield a desired average flight condition. The complex interaction of these elements is illustrated in Figure 3. To reach a trimmed condition, some desired value of the aircraft attitude and (average) forces and moments are required to make the aircraft fly in a steady (periodic) way; thus, rotorcraft trim implies a periodic dynamic solution to a system of nonlinear differential equations with unknown control parameters. Therefore, the problem of finding a rotor trim solution involves both the calculation of the periodic solution to the system of nonlinear equations and a method to find the control settings that achieve a desired flight condition.

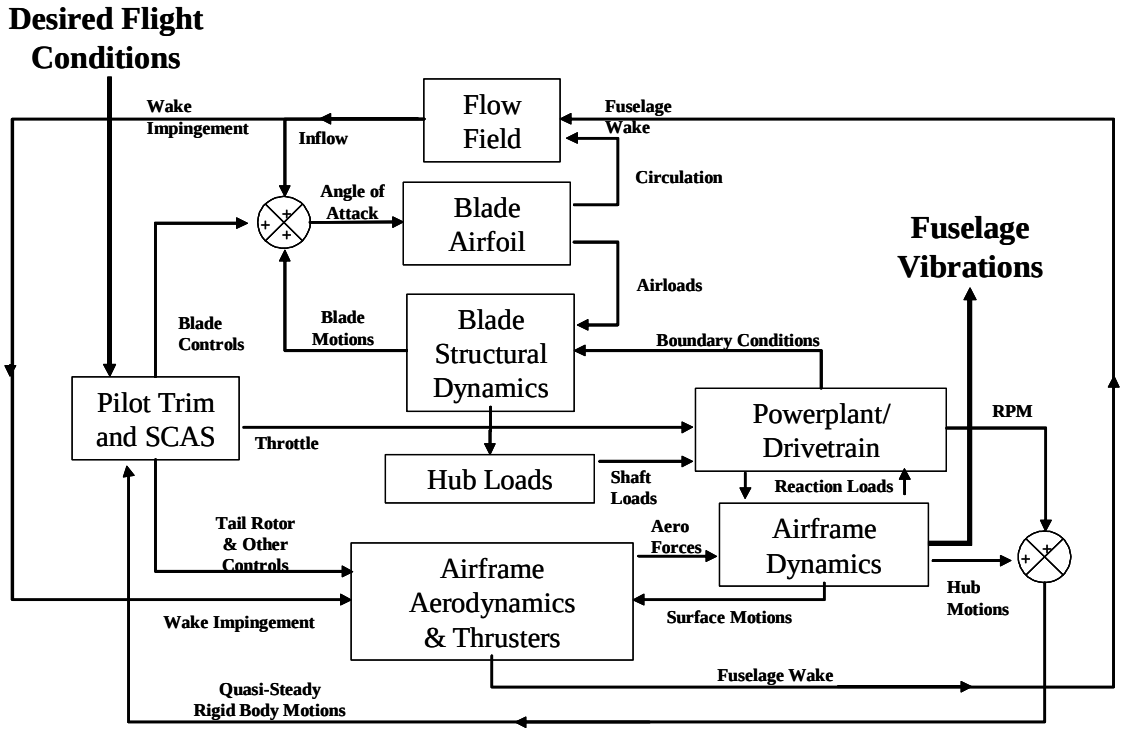

Figure 3: Interdisciplinary Interaction in Rotorcraft Analysis and Design

Due to the highly multidisciplinary nature of the rotorcraft analysis problem, formal multidisciplinary design optimization (MDO) techniques have been used for various aspects of rotorcraft design, including the optimization of: composite rotor blades, flight mechanics and handling qualities, aeromechanical stability etc. A comprehensive survey of recent developments in rotorcraft design optimization is presented in [6]. Regarding the use of MDO techniques to rotorcraft, reference [7] states that the predictions of optimization studies are suspect because of the (poor) predictive capability of aeroelastic analyses. On the other hand, the author also points out that in experiments conducted to verify optimization results, a reduction in the desired objective function (such as vibration) has always been found. Therefore, although aeroelastic analyses may not accurately predict the absolute values of quantities such as airloads and vibration, they do capture the essential physics of the problem; therefore, the relative changes in the design between the baseline and the optimum design may be more reliable than the absolute values themselves. The scope of this thesis concerns the methodology to achieve an optimal trim solution and does not concern absolute accuracy of the aerodynamic or structural math models, though accuracy ultimately will affect the trim solution.

1.1.2 Governing Equations

A convenient form of the trim formulation is a set of equations that represent the various model degrees of freedom as states. The general form therefore becomes

$$\dot{x}_i = f(x_u, X_n, \lambda_l) \qquad i, u = 1,2,\ldots K \qquad n = 1,2,\ldots N \qquad l = 1,2,\ldots L \qquad \textbf{1.1}$$

$$0 = F_o(x_j, X_n, \lambda_l) \qquad o = 1,2,\ldots O \qquad \textbf{1.2}$$

where x_i are the states, X_n are the controls, and λ_l are the internal forces associated with the multi-body formulations. The internal forces are Lagrange multipliers which arise from constraints in the multi-body formulation, and Equation 1.2 represents the internal force balance that must be satisfied at each time stem. The Lagrange multipliers can be

algebraically eliminated from the formulation and are not included in the remaining formulations. The number of states depends on the fidelity of the model and typically includes displacements, rotations, velocities, angular velocities and control states. Additional states can be added for more complex representations of engines, aerodynamics and structural dynamics in the context of modern comprehensive formulations when they are governed by differential equations. Engine states can include temperatures, pressures and other thermodynamic properties. For aerodynamic models, both local two-dimensional aerodynamic representations and global rotor inflow problems have been cast in efficient and concise state space forms. Finally, flexible components such as rotor blades can be spatially discretized to obtain governing ordinary differential-algebraic equations where degrees of freedom associated with the nodes of the spatial grids or modal amplitudes and their time derivatives are states.

Equations 1.1 and 1.2 are a completely general description of rotorcraft equations that can accommodate first-order forms, second-order forms, implicit forms, explicit forms, displacement versions, and multi body versions. These equations have a solution that depends on the initial conditions $x_i(0)$ and on the control parameters X_n. The X_n are any unknown parameters that appear in the equations that can be treated as invariant throughout the period. For example, primary cyclic or higher harmonic (HH) cyclic may be included as controls in the physical system. The actual control angular displacement values going into the swash plate or individual blade change with time. The time invariant control parameters would be the fundamental or n-per-rev (for HH control) coefficients of the control Fourier expansion. For the trim problem, these parameter values are chosen so as to satisfy the trim constraints. These trim control parameters can include, in addition to direct pilot controls, unknown linear and angular velocities, body positions or other constant parameters that are not functions of time.

1.1.3 Periodicity Conditions

In a trimmed condition the response of all the states will be harmonic. That is to say after one completion of the system period, the states values will equal their initial conditions

$$x_i(T) = x_i(0) \tag{1.3}$$

where T is the period. For various conditions of interest, some states have average velocities that are not zero, and therefore are not strictly periodic. For example, in climb the hub will have a velocity such that the position state will grow with time with respect to the inertial frame. Therefore, the periodic conditions can be formulated in the more generalized following way:

$$x_i(T) = x_i(0) + z_i(X_n) \tag{1.4}$$

where z_i are the differences between the 'quasi-periodic' states at the beginning and end of one period. The z_i are written as possible functions of the controls X_n because the quasi-periodic velocities and angular velocities can be sometimes be unknown parameters. If the state does not change with time, then z_i is zero.

1.1.4 Trim Conditions and Constraints

One of the basic concepts of trim is that the trim control parameters must be constant, i.e.

$$\dot{X}_n = 0 \tag{1.5}$$

The quantities to be trimmed, that is to say the quantities driven to a particular value (the trim target value), may include forces, moments and displacements and can always be written in terms of the states. Thus, a quantity that is to be trimmed can be expressed as $\bar{h}_m(x_j, X_n)$, where $\bar{h}$ represents the instantaneous value, h is the average over the period. However, in some cases the trimmed quantity may include a value at one point during the period, expressed as $\hat{h}_m(x_j, X_n)$. An example may include the blade flap angle at an azimuthal location. Therefore a general formulation for the trim conditions is

$$h_m = \frac{1}{T}\int_0^T \bar{h}_m(x_j, X_n)dt + \hat{h}_m(x_j, X_n) \tag{1.6}$$

where h_m is the desired value. In this way the trimmed steady flight condition can be defined by specifying desired values for the outputs of the system.

A time variant system that is periodic can be transformed from the time domain to the frequency domain using the Fourier Transform, where numerical iterative or nonlinear programming methods can be utilized on the system. The primary frequency of the system is the period, which is generally known. Therefore, the frequency domain information of interest in the trim problem is not the frequency content, rather the average value of the trim targets (0^{th} harmonic), which is precisely the quantity that is generated from 1.6. One of the oldest rotorcraft trim techniques, discussed in Chapter 2, is the Harmonic Balance method, and is essentially a truncated version of the Fourier series expansion of the system. Similar to other transformations such as the Laplace and Z transforms, the representation of the critical trim information through the Fourier Transform is simplified.

1.2 Optimal Trim

There exist certain conditions for a system to be trimmable, a primary condition being that the number of controls, *N*, be at least as great as the number of constraints, *M* [1]. Given that a trim solution exists (it is physically realizable), the trim constraints will always be able to be satisfied when the number of controls is equal to or greater than the number of constraints. If the number of controls is equal to the number of constraints, $M_h = N_X$, and a trim solution exists, the trim constraints implicitly define the trim controls, and the solution is generally (though not necessarily) unique. When the number of controls is greater than the number of constraints, $N_X > M_h$, then the system has an infinite number of solutions and the possibility of trimming an additional quantity to a maximum or minimum value becomes possible, i.e. an optimal trim solution.

Reference [1] gives a formulation for the optimal trim problem and qualitatively discusses the implications of such. The formulation utilizes the calculus of variations, where a functional is minimized akin to time variant optimal control problems. The field

of nonlinear mathematical programming (NLP) or optimization has been a rich area of development for methods and techniques that seek to minimize or maximize real functions for nonlinear (and linear) constrained systems. Typically NLP techniques are applied to time invariant systems. However, because the trimmed system is by definition periodic, the transformation of the states from the time domain to the frequency domain allows the system to be treated as quasi time invariant. Also, by definition the trim control parameters are not functions of time as stated in equation 1.5. Therefore, the methods of mathematical programming can be utilized on the optimal trim problem. The application of these methods to the rotorcraft trim problem has heretofore not been developed to any appreciable extent and holds promise for complex non-unique trim solution problems typified by advanced rotorcraft configurations.

1.2.1 Optimal Trim Formulation

The general problem of nonlinear constrained optimization is presented mathematically as follows:

$$\textbf{Minimize:} \quad F(\vec{X}) \qquad \vec{X} = [1,2,\ldots N]^T \tag{1.7}$$

$$\textbf{Subject to:} \quad g_p(\vec{X}) \le 0 \qquad p = 1,2,\ldots P \tag{1.8}$$

$$h_m(\vec{X}) = 0 \qquad m = 1,2,\ldots M \tag{1.9}$$

$$X_{n_l} \le X_n \le X_{n_u} \qquad n = 1,2,\ldots N \tag{1.10}$$

The trim control parameters $\vec{X}$ are the quantities that are varied to reach the minimum objective function in 1.7. Next, equation 1.8lists the inequality constraints, followed by equality constraints in equation 1.9. Finally, the side constraints, or the limits of the control parameters are listed in equation 1.10. The trim problem is characterized by a number of equality constraints as stated in 1.6; the number of trim constraints equals the number of trim control parameters. This poses somewhat of a challenge because many optimization techniques experience difficulty handling equality constraints. Therefore a consideration in choosing an optimization technique for trim problem is to utilize a

method that is able to handle a number of equality constraints, as well as inequality constraints.

1.2.2 Nonlinear Programming Methods

The area of nonlinear programming (NLP), also commonly referred to as optimization, involves automated computer algorithms that systematically probe a mathematical model to find the best solution as defined by the user. All NLP methods generally fall under one of two categories, functional comparison or geometric. As the name suggests, functional comparison methods explore a broad swath of the solution space based on functional values and have the capability to find global optimums. Functional comparison methods typically require a large number of function calls and are therefore best suited to computationally inexpensive problems. Geometric methods seek to find a local minimum based on the first or second derivative of the objective with respect to the variables. Geometric methods are based on the following iterative scheme:

$$\bar{X}^{k+1} = \bar{X}^{k} + \hat{\alpha}\bar{s}^{k}, \qquad k = 0,1,2... \tag{1.11}$$

where k is the iteration number, $\bar{X}$, is the design variable vector at the kth iteration (k=0 is the initial design), $\bar{s}^{k}$ is a search direction vector, and $\hat{\alpha}$ is the step size which varies among the many different methods. Geometric methods are better suited to computationally more expensive problems such as the rotorcraft trim problem. While geometric methods are limited to local minimums, this limitation is not seen as significant for rotorcraft problems with performance driven solution spaces. Therefore, emphasis is placed on geometric NLP methods for the optimal trim problem.

1.2.3 Optimal Trim Constraints

The design and operation of rotorcraft are characterized by a number of constraints, including power, weight, aeroelastic stability, vibration and loads (not to be confused with trim equality constraints defined in section 1.1.4). Dynamic loads and subsequently stress/strain values are of supreme importance because they determine the safe life of

dynamic components, particularly the rotor blade structure. Rotor blade stress/strain constraints can become important in optimal trim analysis, particularly with respect to configurations where the rotor speed operates over a large range. Both the Optimal Speed Helicopter and Slowed Rotor Compound, shown in Figure 1 respectively, have stiff-inplane and stiff flapwise rotor systems, which experience higher loads than the soft-inplane articulated or bearingless type [8]. In some reactionless modes, the rotor blade stresses and strains can become critical without any indication in the fixed system. The blade stress/strain values must not exceed allowable values and the stress/strain values themselves become constraints. However, the determination of rotor blade stress/strain values during the trim process is non-trivial due to the fact that the rotor blade representation in dynamic/aeroelastic models is typically a 1-D beam that does not contain stress/strain granularity. This thesis presents a novel way to compute the actual blade stresses and strains in the trim analysis and utilizes the capability to constrain the trim solution such that it does not violate specified stress/strain limits.

A second constraint to be investigated in this thesis is the condition of autorotation. Autorotation is a condition where the power required to turn a rotor for lift is extracted from the freestream; not directly from the engine. This operational state provides some advantages to advanced rotorcraft configurations where large rotor speed variations are conducted in the flight operations; i.e. the complexities of multiple speed transmissions can be completely avoided. However, the numerical computation of the specific rotor speed at which the correct power extraction from the freestream occurs presents a challenge for conventional trim methods. This thesis presents and applies a novel method to capture the varying rotor speed in the trim and optimal trim analysis by treating the rotor speed as a trim control parameter and constraining the shaft torque to vanish in the final solution.

1.2.4 Optimal Rotorcraft Trim Considerations

The ultimate goal of an optimal trim solution is to guide the designer and controls engineer to the best way to fly a vehicle. The control of modern flight vehicles is

supplemented to various degrees by flight control computers. The insights gained from the trim solution can be applied to the development of control laws for automatic flight control systems and in some cases may drive a control solution. In practice, the implementation of a vehicle control system that achieves the optimal trim condition may not be practical. For example, information that is available for each state in a modeling environment may not be available in flight, therefore information that determines an exact optimal trim solution may not be available. However, valuable insight can nevertheless be gained by understanding what is possible, and what factors contribute the most to achieve that state. Also when trim solution spaces are mapped out through parametric sweeps, one or more variables can be optimized to show the trends for a reduced, optimal solution space.

1.3 Objectives and Scope of Work

An objective of this thesis is to apply a NLP method that is suited for the multidisciplinary rotorcraft trim problem to optimize performance when the number of trim control parameters exceeds the trim constraints yielding non-unique trim solutions. The goal is to have the optimizer handle all the constraints directly, including trim constraints. To this end, a brief review of NLP methods will be conducted with emphasis on the characteristics that best allow application to the trim class of problem. The object is not to develop or modify any NLP method further than its current capabilities, rather to utilize its capabilities in application to the optimal trim problem. As part of this objective, a selected NLP method is integrated into a validated rotorcraft comprehensive program, RCAS [9]. Typically, a stand alone optimization code is interfaced with an analysis code to probe the solution space of the analysis code. For the problem of trim, an external optimizer becomes inefficient because much of the information internal to the analysis that can be used to improve the optimization efficiency can not easily be passed to the optimizer [29]. Therefore a contribution of this work is the selection and implementation of an NLP optimization method into an integrated multidisciplinary rotorcraft analysis native environment for routine optimal trim analysis.

A second objective of this work is to contribute to the sparse literature in computational methods for variable rotor speed in autorotational flight. Analytical techniques that allow for determination of rotor speed in autorotation require further development. Existing rotor trim methods require a priori knowledge of rotor speed and do not allow the rotor speed to vary with flight conditions. Therefore, another contribution of this work is the development and validation of a novel method that allows for determination of rotor speed in steady-state autorotation.

A third objective of this thesis is to capture rotor blade stresses and strains for accurate, computationally inexpensive feedback in optimal trim analysis. Rotorcraft dynamics is a multidisciplinary field, consisting of the usual constituents associated with aeroelasticity, i.e. structures, dynamics, and aerodynamics. The dynamicist is usually after stability, blade and rotor loads, and vibration (forced response), but not stress/strain in the blades. The latter are usually the responsibility of the structures group and require a different set of tools to obtain, i.e. FEA. For certain dynamic conditions, specifically where rotor speed operates over a wide range, it becomes important to include rotor blade stress/strain values in the dynamic trim analysis. This thesis presents a novel method of capturing rotor cross-sectional stress and strain via an artificial neural network surrogate to provide accurate, computationally inexpensive structural load information that can be used for trim constraint determination.

A final objective of this thesis is to apply the optimal trim method with variable rotor speed autorotation and rotor blade stress/strain constraints to a real multidisciplinary rotorcraft trim problem that has non-unique trim solutions. This application of optimal trim will demonstrate its usefulness and demonstrate the novel analytical capabilities.

1.4 Research Questions and Hypotheses

In light of the scope of work presented, the following research questions and hypotheses are posed:

1.4.1 Primary Research Question and Hypothesis

Question: What is the best way to fly an advanced rotorcraft configuration to maximize performance when it has constrained, non-unique trim solutions (one that has more trim control parameters than flight constraints) in steady flight?

Hypothesis: *An optimal trim solution can be systematically found through the use of nonlinear mathematical programming methods.*

1.4.2 Supporting Question and Hypothesis No. 1

Question: How can variable rotor speed be modeled, specifically for variable speed autorotation, in the context of comprehensive trim methods that require rotor speed to be specified a priori?

Hypothesis: *The rotor speed treated as a trim control parameter will allow variable rotor speed trim solutions.*

1.4.3 Supporting Question and Hypothesis No. 2

Question: How can rotor blade stresses and strains be recovered in a timely and accurate manner such that they provide trim solution structural constraints?

Hypothesis: *a) A good approximation of the stress and strain over a cross-section can be realized by through a surrogate model as a function of the 1-D beam loads (three forces and three moments) for the cross-section.*

b) Surrogate stress and strain can be computed with significantly less time and in a convenient form to be used during the aeroelastic trim optimization.

CHAPTER 2
LITERATURE REVIEW

This chapter contains a review of literature relating to the major contribution areas of this thesis. First, a review of general trim methods is presented. Then a review of research relating to the optimization of trim solutions is included. In the trim optimization review, the general types of NLP methods are covered, with specific emphasis on the generalized reduced gradient (GRG) method. Next a review of literature relating to variable rotor speed autorotation is presented. Finally, a survey of methods for rotor blade stress/strain recovery is presented.

2.1 Rotorcraft Trim Methods

As stated in section 1.1.2 through 1.1.4, the problem of finding a trim solution involves computing solutions for 1) the differential equations (including implicit equations), 2) (quasi) periodicity conditions and 3) trim constraints. Therefore any trim technique must address each aspect of these categories. The solution method for the differential equations is typically some version of the method of weighted residuals that uses trial functions as approximations and forms a residual error functional. Two methods to solve the differential equations are marching through time and temporal finite elements.

Solution methods must satisfy the periodicity conditions and include three basic types. The first type is simply time marching or applying finite elements in time on the equations of motion until the transients decay. The second type is enforced periodicity by assembly, where the solution and periodicity are solved in parallel. Harmonic balance is an example of an enforced periodicity solution technique. The third type of solution technique is based on (Floquet) transition matrix methods, where there is iteration on initial conditions and the solution and equations are solved sequentially or in parallel. Periodic shooting is an example of a transition matrix method [10].

The methods used to adjust the control settings to reach a trim solution can also be classified into three basic types: 1) closed-form force-balance equations that can be used as constraint equations to be solved in parallel with other equations, 2) Newton-Raphson iteration, 3) closed loop control law driving the control variables to a state that reduces the trim error signal. The solution methods for the trim control require a Jacobian of the trim constraint error due to perturbations in the trim controls. The following sections summarize trim techniques and their development in the literature.

2.1.1 Direct Numerical Integration

A method commonly used to compute the periodic solution for computer simulation models is the direct numerical integration of the equations of motion [11,12]. From some initial control parameter value set, the equations are integrated through time until all transients have decayed. Once the periodic solution is achieved, a Newton-Raphson or secant method is used to iterate on the controls, each iteration requiring the decay of all transients. Through this iterative process the converged trim solution is reached. For stable systems with a large number of states, this approach can be quite efficient because there is not iteration of the states or assembly processes. However, if the system exhibits one or more degrees of freedom with marginal damping, the time required to assure all transients have decayed becomes somewhat unknown. Systems exhibiting any instability will grow, and the system will never converge, preventing a trim solution. In addition, the method requires artificial springs to connect the vehicle to ground for a free flight trim convergence to prevent steady drifting.

2.1.2 Harmonic Balance

The harmonic balance trim method is perhaps one of the oldest techniques available to obtain the forced response of nonlinear differential equations with periodic coefficients. The basic notion of the harmonic balance method is that periodic functions may be represented by a Fourier series. The periodic function is then defined explicitly by the Fourier coefficients. Johnson discusses two alternative methods by which harmonic balance is employed [13]. One method, referred to as the substitutional method,

represents each degree of freedom explicitly as an *M*-th order Fourier series representation. The Fourier expansions and subsequent required derivatives are then substituted into the equations of motion. The coefficients of each sine and cosine harmonic are collected and equated to their corresponding sine and cosine periodic aerodynamic forcing harmonic. The result is a set of $M + 1$ algebraic equations for the harmonics for each of the blades generalized coordinates. The second method is similar to the first with the exception that the operators are applied numerically to the differential equations of motion to obtain the harmonics. This technique is therefore referred to as the operational method. The substitutional and operational methods result in the same set of algebraic equations and both methods are necessarily approximations since the Fourier series representing each of the generalized coordinates is truncated. The series is truncated depending on the level of harmonic fidelity required. For example, an articulated rotor with rigid blades would only require the first harmonics. A hingeless rotor with elastic blades would require a larger expansion to capture motion above the primary period. A primary advantage of the harmonic balance trim method compared to time domain methods is its insensitivity to system instabilities; the method will reach a trim solution even if eigenvalues with positive real components exist in the system.

Wheatley is one of the first researchers to employ harmonic balance trim to rotorcraft analysis, specifically to find the trim solution to a gyroplane rotor in autorotation [47]. Gessow and Myers utilize the method to present a closed form solution for rigid articulated helicopter blade motion [14]. This type of solution is convenient for simple flap articulated blade models. However, for more complex models that have numerous, nonlinear coupled degrees of freedom, the representation of each degree of freedom by as few as two Fourier coefficients creates an algebraically cumbersome challenge in managing the harmonic terms. Therefore Peters extended the method by developing a matrix formulation to enable improved efficiency in the analysis of larger systems having many coupled degrees of freedom [15]. When harmonic balance is used to find the states, the controls can be found in parallel by addition of augmented equations. The unknown trim settings are treated as additional harmonics that can easily be added to the set of algebraic unknowns formed by the unknown harmonics. The complete set of unknowns

may then be solved in a variety of iterative techniques. Eipe extended the method to include the trim variables in the system of equations and developed an iterative technique to trim to a desired condition [16]. The iterative method was particularly useful for the calculation of coupled rotor/body vibrations. However, the basic limitation of the method still presents itself as extensive bookkeeping required as models grows to include more degrees of freedom and harmonics.

2.1.3 Periodic Shooting

Periodic shooting is a method used to determine the solution to differential equations with periodic coefficients. Periodic shooting is based on linear system theory for periodic systems. Initially a sensitivity matrix is computed for all the states by perturbing each state, one at a time, and time marching through one period. A vector of the sensitivity of each perturbed state with respect to the other states computed; all vectors adding to the complete sensitivity matrix. The sensitivity matrix is then used to directly compute the forced solution. When applied to nonlinear systems, the method requires iteration on state initial conditions until the correct initial conditions are found that result in a periodic solution. One of the primary benefits of the periodic shooting method is its insensitivity to unstable degrees of freedom. For this reason, trim analysis requiring aeroelastic stability computation near or past stability boundaries is often performed utilizing the periodic shooting method. Because the sensitivity matrix is inverted each trim iteration, the method cannot handle zero eigenvectors in the identity minus transition matrix.

Peters and Izandpanah introduce periodic shooting as a rotorcraft trim method by including the trim variables in the sensitivity matrix in addition to the states [17]. The implementation of trimming with periodic shooting may include the controls to be varied in parallel with the states or serially. Achar and Gaonkar investigated serial and parallel periodic shooting with optimally damped Newton iterations to determine sensitivity to initial conditions [18]. The sequential method has proven in both theory and practice to diverge in free flight and is therefore somewhat limited. The parallel method was actually found to be more computationally efficient, though more sensitive to the initial

conditions. On the down side, periodic shooting can become prohibitively time consuming for systems having over approximately 100 states in the model. In addition, some models contain hidden states that present themselves in nonlinear regimes, and become problematic for the method. For example, free-wake inflow models are not finite state and are incompatible with periodic shooting. Peters and Peters developed a discrete control method that extends the capability of periodic shooting to systems with large number of states, including hidden states [19]. This is accomplished by a discrete-time observer that gives an estimate of the states, including hidden states during each period. A controller is applied to the original nonlinear simulation in that errors in each blade passage are fed back to give discrete control changes and effectively drive the system to trim.

2.1.4 Autopilot

Autopilot trim augments the system of equations with a control law that closes the loop between the trim control parameter values and the flight condition. The controller flies the system towards the desired trim condition as the equations are integrated through time. In this formulation, trim is cast in the form of a feedback control system. The advantage to the autopilot trim scheme is that the complexity of the controller itself depends only on the number of controls to trim; autopilot is very efficient for systems with a large number of degrees of freedom. Therefore, high fidelity models that incorporate a large number finite-element elastic beams and sophisticated aerodynamics become too large for some other trim methods and are best suited for auto pilot trim. Since autopilot trim is based on directly integrating the equations of motion in time, the method is susceptible to system instabilities, similar to direct numerical integration. Therefore any system that has insufficient damping is ill-suited for autopilot trim. In addition, the control laws exhibit their own dynamic behavior, independent of the rotorcraft system and can lead to instability. Because the controller changes the dynamics of the system, it cannot be used for flight mechanics analysis.

The control law is typically a set of dynamic equations coupled with those of the system. The equations are formulated with gains set by the user to determine the rate at which the error is eliminated. The actual feedback signal has to be filtered through equation 1.6 to remove the periodic nature of the system. In addition, higher order filters typically have to be added to suppress high-frequency oscillations in the error signal; only the average error signal is to be driven to zero based on the entire period. The correct setting of the gain and filter values often require a trial and error tuning phase. This phase can be time consuming and is optimal for the specific advance ratio and rotorcraft configuration for which the tuning occurs. Moving away from the condition often provides sub-optimal trim performance in terms of the trim time.

The autopilot trim method was developed and introduced by Peters, Kim and Chen [20]. Peters, Bayly and Li extended that work to develop a hybrid autopilot method [21] which combined the advantages of the periodic shooting method, the auto-pilot method and the discrete auto-pilot method. The hybrid method proved to overcome the inefficiency of the periodic shooting method for vary large systems and the instability of the auto-pilot system when the system is neutrally stable (such as free flight) or unstable.

2.1.5 Neural Net Function Approximation

Recent research in trim methods has utilized advances in adaptive neural networks (ANN) to model the plant dynamics. Neural networks are Gaussian processes which, through the process of 'training' can be conditioned to closely approximate nonlinear dynamic behavior. The main application of neural networks is approximating equations of motion for the process to be controlled when the functional forms are poorly known or the functional form is prohibitively computationally demanding. This is particularly the case for flight mechanics/control applications, where unsteady aerodynamic and elastic rotor effects affect flight qualities. Enns and Si developed a ANN based method to achieve trimmed flight of an Apache helicopter model [22]. The method consisted of training a neural network to capture the four control inputs and two body angles (holding yaw constant) as a function of multiple input parameters such as airspeed, weight, etc.

The relatively simple method was effective in capturing beginning trim states for flight mechanic maneuvers. Riviello developed a trim method based on nonlinear model predictive control, augmented by adaptive neural elements [23]. The predictive controller predicts the behavior of the plant (rotor) based on a reduced model and determines the control actions necessary to regulate the plant by solving an optimal control problem. For the rotor trim application, the reduced plant was a simple rotor with blade element quasi-steady aerodynamics and uniform inflow. The simple model was however augmented by an adaptive neural network trained to capture the differences in key parameters between the simple and a more complex unsteady, aeroelastic model subject to the same conditions. The method showed promise on an isolated, wind-tunnel type of rotor with no requirement to tune constants or gains, as required in autopilot trim.

2.2 Trim Optimization

2.2.1 Previous Applications

Peters and Barwey's treatise on the theory of rotorcraft trim [1] touches on all aspects of trim including optimal trim. They recognize that when the number of trim control parameters exceeds the number of trim constraints, a system has an infinite number of solutions, opening the possibility of maximizing or minimizing some additional quantity. The authors develop a formulation for trim optimization based on the calculus of variations, where a functional is minimized, resulting in a method akin to optimal control. The method is applied to a simple helicopter model to minimize the hover power in two separate cases. The first uses yaw angle as an optimization variable, and the second uses rotor speed. In both cases a minimum was obtained with improvements over the baseline condition.

Other researchers have applied modern nonlinear programming techniques to optimize some aspect of the rotorcraft flight through the trim solution. Jacob and Lehmann coupled an NLP optimization code with a dynamic rotor model to investigate vibration reduction through higher harmonic control of a rigid blade rotor, an elastic blade rotor, and an active twist rotor configuration [24]. They computed the vibration response based

on a frequency domain formulation, which enabled the control problem to be treated as time invariant. Parameters controlled to reduce vibration included 3/rev, 4/rev and 5/rev cyclic and time dependent twist of the rotor blades. Other researchers have utilized various open and closed loop control techniques to minimize vibration based on frequency domain (periodic trim) solutions [25, 26]. Active control of vibration has received much attention in the literature, a detailed review of the extensive work in this area is beyond the scope of this work. However, a comprehensive review is given by Friedmann and Millot [27].

Ormiston [28] investigates the induced power of rotors in forward flight with several trim variables to minimize the non-uniform induced power relative to the ideal (uniform inflow) induced power. He points out that the trim condition including collective pitch, shaft angle and (active) blade twist define the basic optimization problem for conventional one per rev cyclic control. An extension to the basic optimization is Higher Harmonic Control (HHC) which has the potential to significantly reduce induced power beyond that obtained with basic controls, particularly at high advance ratios. An induced power minimization study was investigated of advance ratios from 0 through 1.4 using a simple optimization algorithm coupled with RCAS, varying amplitude, phase and higher harmonics of 1P, 2P, 3P and 4P. His results were interesting in two regards with respect to optimal trim. First the simple optimization algorithm quite robustly reduced the induced power from the baseline condition. Second, the trim solution bifurcated with two separate rotor loading modes, indicating multiple trim modes for a given flight condition. Cheng and Celi also investigate improved rotor performance through optimum higher harmonic inputs [29]. They also used formal NLP methods to minimize rotor power with 2 per rev variation. Their study is interesting because they tried to couple the rotor model directly to the optimizer, bypassing the internal trim routine. In their formulation, they had 29 equality constraints, 11 represented the aircraft trim conditions, 4 for the inflow equations, and 14 for the main rotor equations. The optimizer was a commercial code and the technique applied was the method of feasible directions. The numerical formulation proved to be extremely poor and convergence was slow, often terminating due to lack of progress without reaching a minimum. The large scale

optimization was abandoned and the problem reformulated as an unconstrained minimization of just the higher harmonic controls. Thus the trim procedure was decoupled from the optimization, and was executed for every set of design variable values generated by the optimizer.

2.2.2 Nonlinear Programming Methods

Most engineering problems, including the rotorcraft optimal trim problem, are nonlinear. Nonlinear programming has developed into a mature field of research with many types of solution methods. Nonlinear methods can generally be categorized as Newton, quasi-Newton, conjugate gradient and functional comparison methods [30]. With the exception of functional comparison methods which are logical, all methods are geometric, meaning they use first or second derivative information of the variable space. There are essentially six types of methods to solve nonlinear constrained optimization problems. Two of these methods are successive, linear and quadratic programming. The other four convert the constrained problem into an unconstrained problem and apply an unconstrained search procedure. These four types are: penalty or barrier functions methods, the augmented Lagrangian functions, feasible directions, and generalized reduced gradients (GRG). The classification of many NLP methods is given in Figure 4. The feasible direction method, penalty function method and functional comparison class of methods are not inherently suited for the numerous equality constraints found in trim problems. The successive linear programming method can be used for nonlinear problems but has certain restrictions that limit is usefulness depending on the problem.

For small to medium sized nonlinear constrained problems, studies have concluded that the generalized reduced gradient (GRG) and sequential quadratic programming (SQP) methods are the most robust and efficient [31, 32]. Of these two methods, SQP typically yields a lower number of total function calls to arrive at a minimum solution due to its quasi-Newton superlinear convergence characteristics. SQP methods are an active area of research and the method's success often depends on the type of SQP algorithm employed and problem specifics. The GRG method has the benefit of interim solution

feasibility, meaning that all constraints are met throughout the search process; SQP only produces a feasible solution at completion. Finally, the GRG method has a structure that is similar to the many trim algorithm structures that use Newton's method for constraint satisfaction. Therefore, this thesis will use the GRG optimization technique for application to optimal rotorcraft trim.

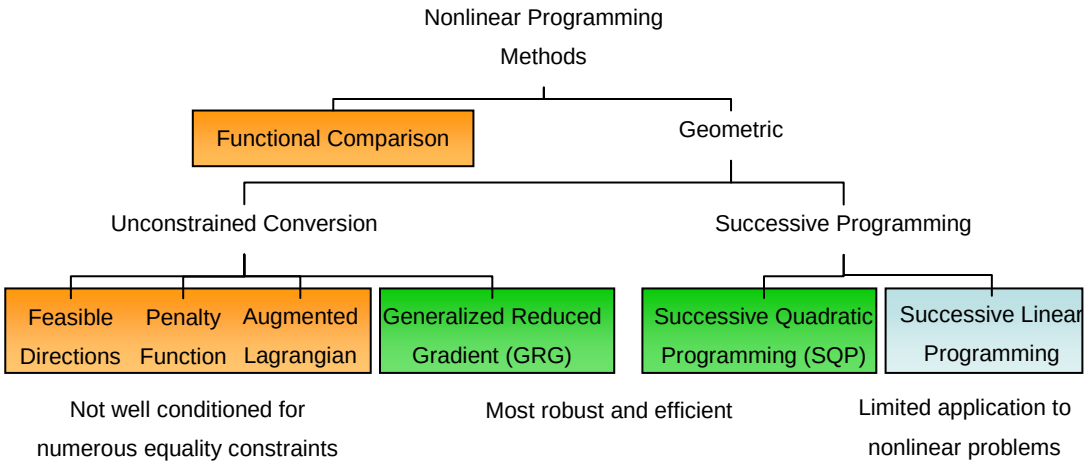

Figure 4: NLP Method Classification

2.2.2.1 Reduced Gradient Method

The concept of the reduced gradient is most often attributed to Wolfe [33,34] as a means for solving the nonlinear programming problem subject to linear constraints. In his work Wolfe first presented the concept of dividing the design variables into two classes: dependent variables, and independent variables. As the names imply, the independent variables become the decision variables and dependent variables are slaves to the decision variables, used only to satisfy the constraints. The number of dependent variables, therefore, must equal the number of constraints. The reduced gradient is the rate of change of the objective function with respect to the decision variables with the dependent variables adjusted to maintain feasibility. Geometrically, the reduced gradient can be described as a projection of the original N dimensional gradient onto the S dimensional feasible region described by the independent variables. Hence, the reduced gradient can be used in the same manner as the full gradient to search for a minimum

objective in the reduced space. Therefore, an advantage of the GRG method is the reduction of the problem dimension due to variable elimination.

2.2.2.2 Generalized Method

Adabie and Carpentier [35] extended the reduced gradient method to accommodate nonlinear constraints. The word "generalized" is included to underscore the presence of nonlinear constraints. When the constraints are linear, the state variable adjustment is given by the linear projection onto the dependent variable feasible space. However, when the constraints are nonlinear, the dependent variables must be adjusted by a nonlinear technique during each line search step to restore feasibility. Adabie and Carpentier employed the Newton-Raphson (N-R) method to readjust the dependent variables to satisfy the constraints. One of the defining characteristics of the GRG method is that at any point in the search algorithm, the solution is always feasible, that is to say all the constraints are satisfied.

Large-scale nonlinear programming problems often have many linear constraints with sparse structures. Gabriele [36] applied the GRG method to large scale structural optimization problems and used sparse solvers in the dependent variable solution to significantly increase the method efficiency. In this type of application, the GRG method is extremely efficient. Because one or more system of nonlinear equations have to be solved in the GRG method, its computation cost is high if the matrix is not sparse and without special structures for large-scale problems.

2.2.2.3 Hybrid Method

Parkinson and Wilson [37] developed a hybrid method that incorporates elements of both the GRG method and Sequential Quadratic Programming (SQP). The hybrid method uses a quadratic programming (QP) sub-problem, instead of the reduced gradient, to determine the search direction and initial step size. At each step along the search direction the constraints are satisfied through the N-R method. The advantages of using the QP search direction are 1) an initial step size was computed in addition to the search

direction and 2) variable metric, or quasi-Newton methods could be used to more efficiently determine the search direction based on previous searches. GRG optimization algorithms re-classify variables as dependent or independent before each line search to avoid singularities in the constraint Jacobian and degeneracy of the constraint variables. When the set of independent and dependent variables change from iteration to iteration, any update information associated with independent variables is lost. Because the SQP direction involves no partitioning, it is free from this problem. The hybrid method compared favorably to the SQP method in efficiency, yet had the significant advantage of solution feasibility at every point in the search process.

2.3 Variable Rotor speed Autorotation

2.3.1 Background

Autorotation can be defined as a self-sustained rotation of the rotor without the application of any shaft torque, i.e. the net shaft torque, Q = 0. Under these conditions the power to drive the rotor comes from the relative air stream, which is directed upward through the rotor [38]. Autorotation is commonly used in the context of helicopter emergency engine-out procedures where rotor power is exchanged for aircraft potential energy, i.e. altitude [14]. However, autorotation was originally used in the context of a sustained mode of flight for the first practical flying rotorcraft, the autogiro [39]. The autogiro or gyroplane tilts the rotor aft and power is indirectly supplied by the aircraft's propulsion system to overcome the rotor drag. Figure 5 shows the upward airflow through a rotor in autorotation compared to the downward airflow of powered helicopter rotor.

In the fully established autorotative state, the rotor speed will self adjust until a zero torque equilibrium is obtained; the rotor naturally seeks to find its own equilibrium angular velocity to any changing flight conditions. The change in rotor speed is documented for different flight conditions. Schad shows the rotor angular velocity trends for two light gyroplanes that have a fixed collective setting [40]. The variation of rotor angular velocity over the speed range for steady level flight is approximately 18%. In

steady level turns where load factor increases, Cierva states angular velocity can increase up to 120% that of level flight (fixed collective) [41]. Finally, when used in combination with a fixed wing (producing positive lift), an autorotating rotor tends to unload with the resulting angular velocity decreasing; if offloaded too much the rotor speed can decay to dangerously low values (for a rotor that relies on centrifugal force for equilibrium force balance) [42].

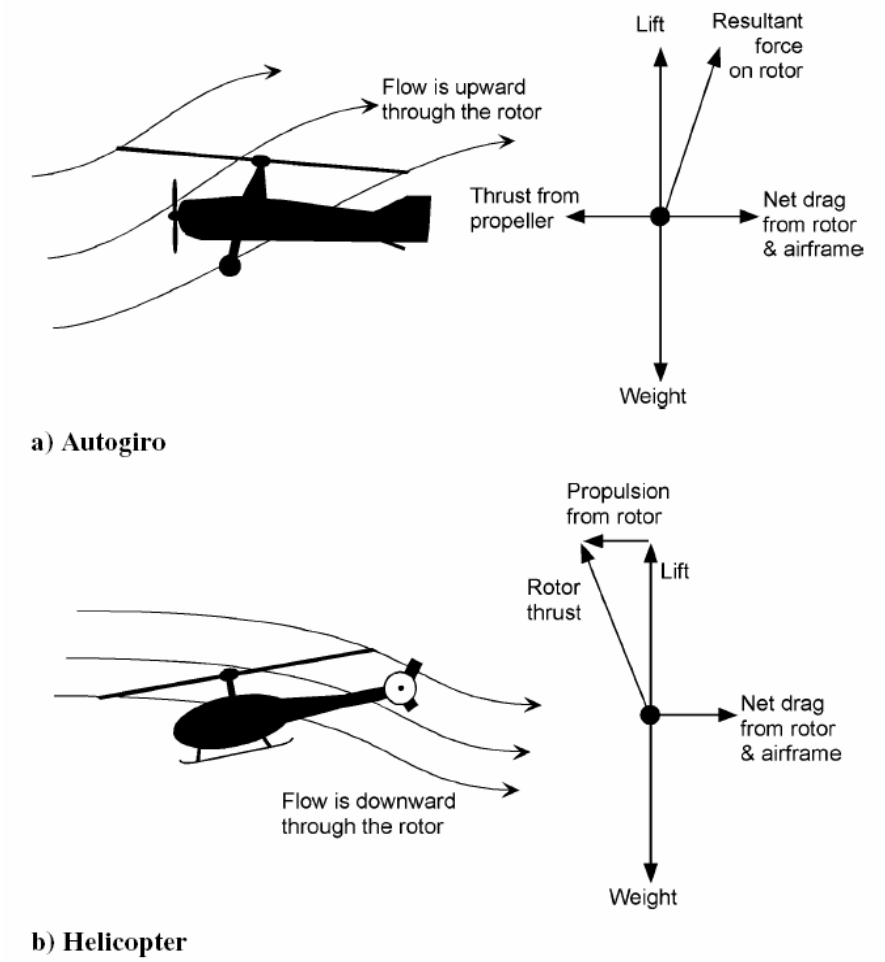

Figure 5: Rotor Airflow Direction and Net Forces [38]

Rotor angular velocity has a significant influence on the net forces and moments of the rotor and also the coupled body flight mechanics. McCormick found by numerical analysis of a gyroplane rotor that power required could be reduced by as much as 30% by carefully setting the collective to minimize rotor speed, compared to the same rotor with constant speed [43]. Ward conducted flight maneuvers to investigate loads of a rotor in

both helicopter flight and autorotation [44]. He observed a significant difference when rotor rpm was not constrained, stating there was "a complete lack of buildup in blade chordwise cyclic bending-moment amplitude during the maneuver, even though an aircraft angular velocity of 0.4 rad/sec was obtained." Finally, Houston found that accurate flight mechanics analysis for rotorcraft in autorotation requires the addition of the variable rotor speed to capture the complex flight mechanics of a coupled rotor speed and body dynamic system [45]. Houston states, "The ability of linearized models to capture the essential behavior of the aircraft in autorotation may be compromised [with constant rotor speed assumed] because large changes in rotor speed will give rise to significant changes in blade element in flow angle and therefore, angle of attack" [46].

A significant body of research, both analytical and experimental, was conducted in the area of autorotation before and during WW II [47, 48, 49, 50]. From that work an understanding of steady-state autorotation was developed for the basic aerodynamic phenomenon as well as operational considerations. Recent rotorcraft developments (within the last 30 years) in the basic fields of aerodynamics, structural dynamics, trim and dynamic analysis have been developed for and applied almost exclusively to powered rotor configurations. In certain circles, however, there has been growing interest in the further understanding of autorotational flight for unique applications. These applications include: improved simulation models for emergency pilot training [51], safer recreational aircraft [52], low flight speed capable unmanned aerial vehicles (UAVs) [53], low cost V/STOL aircraft [54], and high speed military vehicles [3].

2.3.2 Variable Rotor Speed Trim Methods

A few papers have addressed the issue of variable rotor speed in trim solution techniques. Barwey and Peters considered the case of varying rotor speed to minimize power of a hovering 6 DOF helicopter [1]. Their approach was novel in that it used rotor speed as one of the unknown trim control parameters in a periodic shooting approach. They showed a parametric sweep of the rotor speed versus power for hover trim with an

obvious minimum between two rpm extremes. Using an optimum trim method based on the calculus of variations, they trimmed to the optimum rotor speed.

McCormick also investigated the effects of rotor speed on the performance of an isolated gyroplane rotor [55]. He analyzed the effect that variable collective had on the autorotative rotor speed. The technique used to vary the rpm is described as an "interval halving technique" where rotor speed was adjusted to drive the shaft torque to aero. This appears to be a somewhat adhoc method, but was effective for the simple trim model to find the rotor speed producing zero torque. McCormick concluded in his study that a gyroplane rotor can operate over a wide range of air and rotor speeds. "An appreciable reduction in required power of an autogyro can be achieved by varying the collective pitch with airspeed" to yield a minimum rotor speed condition.

Finally, Morillo and Peters presented a method to trim an explicit set of coupled rotor equations for an unknown period with unsteady rotor speed [56]. This approach uses a harmonic balance method where space was treated as the independent variable instead of time. The purpose was to overcome problems in the traditional harmonic balance technique when the rotor speed is unsteady, unknown, or both. The research did not investigate the performance effects of rotor speed, but the technique could be applicable for autorotative trim, where the rotor speed required for zero shaft torque is unknown.

2.4 Rotor Blade Stress and Strain

Modern rotor blades are complex three-dimensional composite structures that often utilize anisotropic lay-up schemes to tailor the blade structural and aeroelastic characteristics. Three-dimensional finite element techniques are capable of accurate analysis of these designs, yet are impractical in terms of computational cost for routine rotorcraft structural analysis due to the complex rotating, aerodynamically loaded environment. However, rotor blades have one dimension that is much larger than the other two and can be approximated as a 1-D beam, simplifying the mathematical formulation compared to 3-D finite element techniques. Accurate beam approximations

must ensure that the reduced 1-D strain energy is equivalent to that of the original 3-D structure, including elastic couplings among the global deformations. Within the last 15 years, a large body of research has been developed to create elastic beam models that accurately capture the nonhomogenious, anisotropic, initially curved and twisted beams that rotor blades are [57,58]. Hodges and his coworkers have developed a framework that utilizes the variational-asymptotic method (VAM) to decouple 3-D nonlinear elasticity problems into 2-D linear cross-sectional analysis and 1-D nonlinear beams as illustrated in Figure 6 [59]. The method calculates the 3-D warping functions asymptotically and finds the constitutive model for the 1-D nonlinear beam analysis. The process is referred to as dimensional reduction and has been computer encoded into a tool called Variational-Asymptotic Beam Section Analysis (VABS).

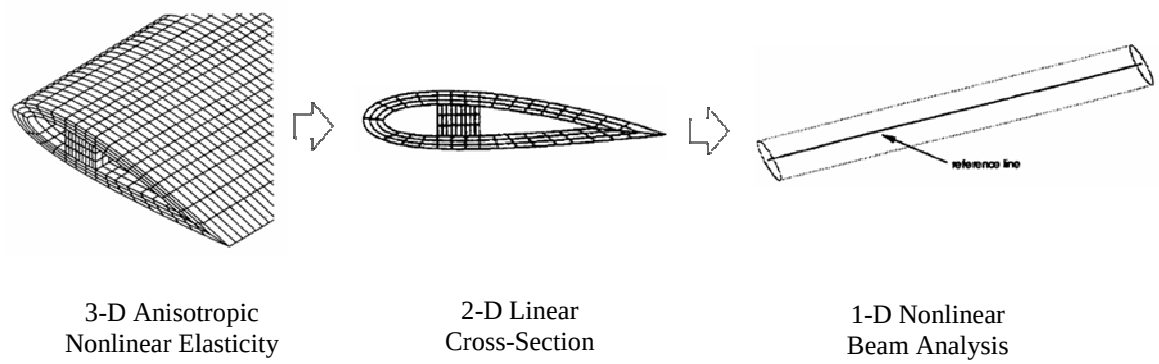

Figure 6: Rotor Blade Dimensional Reduction Method

An additional benefit of the VAM is information from the 1-D beam analysis can be fed back to the structural model from which 3-D fields (displacement, stress and strain) can be recovered using the 3-D warping functions, see Figure 7. VABS is capable of capturing the trapeze and Vlasov effects, which are useful for specific beam applications. VABS is also able to calculate the 1-D sectional stiffness matrix with transverse shear refinement for any initially twisted and curved, inhomogeneous, anisotropic beam with arbitrary geometry and material properties. The tool has been extensively correlated against higher order finite element and experimental results for coupled mode, composite beams. Correlation results show excellent predictive capabilities in terms of coupled

displacements, modal frequency calculation and recovered stress/strain distributions [60,61,62].

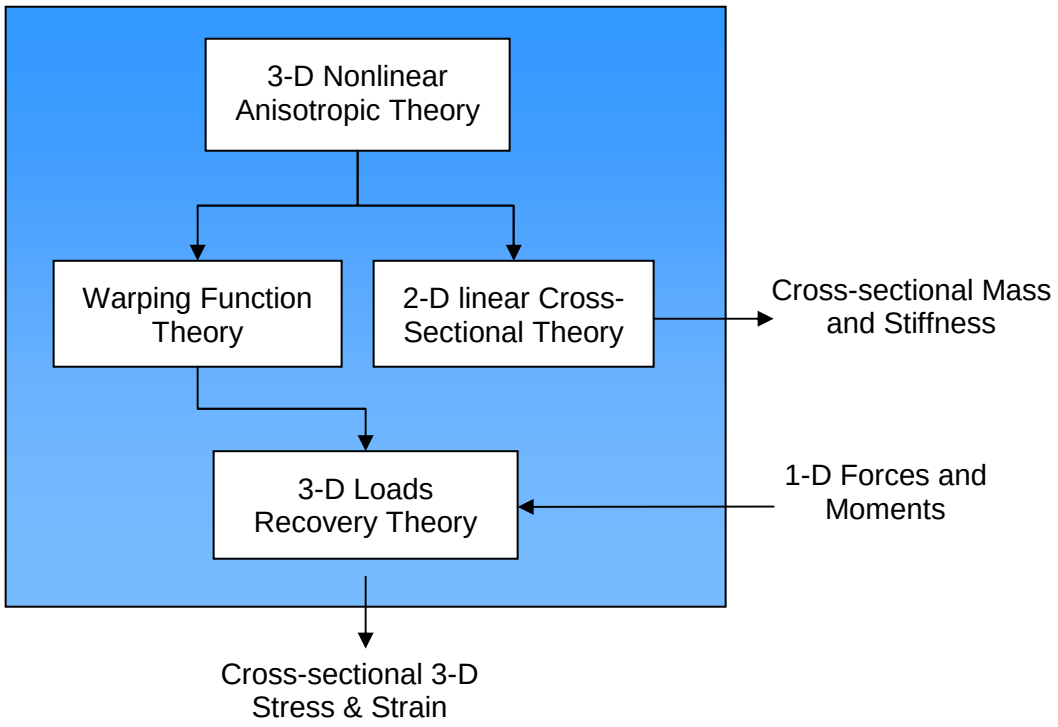

Figure 7: Elements and Input/Output of VABS

2.5 Chapter Summary

Literature concerning rotorcraft trim methods, optimal trim and nonlinear optimization techniques is summarized with concentration on the generalized reduced gradient method. In addition, literature relative to autorotation and variable rotor speed trim has been reviewed and summarized in this chapter. Finally, a review of rotor blade stress/strain recovery utilizing VAM and specifically the tool VABS has been presented. This review lays the foundation for the following chapters to build on relative to the objectives of this thesis.

CHAPTER 3
GENERALIZED REDUCED GRADIENT OPTIMAL TRIM

In this chapter a theoretical discussion of the generalized reduced gradient (GRG) method is given. The mathematical formulation of the GRG method, the search direction and optimality conditions are presented as part of the discussion. Next, the implementation of the GRG method into an optimal trim algorithm is presented and discussed. The flow of the algorithm and practical application considerations are provided. Finally, the implemented optimal trim method is validated with an optimization problem where the trim solution topography is known. The results of the method are discussed and evaluated in order to assess the accuracy of the method.

3.1 Mathematical Formulation

This section presents a concise description of the GRG method as it has been implemented in previous research. Only those basic steps required for the reader to gain an appreciation and understanding of the general theory are presented. The intent is to lay the foundation needed to discuss the method for application to the optimal trim problem. Additional considerations beyond the basic GRG method are discussed when applicable to the rotorcraft trim problem.

3.1.1 Reduced Gradient Determination

Recall the equality constrained nonlinear programming problem given by

Minimize:	$F(\vec{X})$	$\vec{X} = [1,2,\ldots N]^T$	**3.1**
Subject to:	$h_m(\vec{X}) = 0$	$m = 1,2,\ldots M$	**3.2**
	$X_{n_l} \le X_n \le X_{n_u}$	$n = 1,2,\ldots N$	**3.3**

The basic concept of the GRG method is to convert the equality constrained problem into an unconstrained problem and then utilize an unconstrained search procedure. The method requires the division of the variables into two classes: dependent variables $\vec{X}_D$, and independent variables $\vec{X}_I$.

$$\nabla^T f(\vec{X}_I) = \left[\frac{\partial f}{\partial X_{1I}}, \frac{\partial f}{\partial X_{2I}}, \cdots \frac{\partial f}{\partial X_{NI}} \right] \quad \textbf{3.4}$$

$$\nabla^T f(\vec{X}_D) = \left[\frac{\partial f}{\partial X_{1D}}, \frac{\partial f}{\partial X_{2D}}, \cdots \frac{\partial f}{\partial X_{ND}} \right] \quad \textbf{3.5}$$

As the names imply, the independent variables become the decision variables and dependent variables are slaves to the decision variables, used only to satisfy the constraints. In the computation of the reduced gradient, the Jacobian of the constraints is also partitioned with respect to the dependent and independent variables:

$$J_{X_I} = \begin{bmatrix} \frac{\partial h_1}{\partial X_{1I}} & \frac{\partial h_1}{\partial X_{2I}} & \cdots & \frac{\partial h_1}{\partial X_{NI}} \\ & & \ddots & \vdots \\ \frac{\partial h_{ND}}{\partial X_{1I}} & \frac{\partial h_{ND}}{\partial X_{2I}} & \cdots & \frac{\partial h_{ND}}{\partial z_{NI}} \end{bmatrix} \quad \textbf{3.6}$$

$$J_{X_D} = \begin{bmatrix} \frac{\partial h_1}{\partial X_{1D}} & \frac{\partial h_1}{\partial X_{2D}} & \cdots & \frac{\partial h_1}{\partial X_{ND}} \\ & & \ddots & \vdots \\ \frac{\partial h_{ND}}{\partial X_{1D}} & \frac{\partial h_{ND}}{\partial X_{2D}} & \cdots & \frac{\partial h_{ND}}{\partial X_{ND}} \end{bmatrix} \quad \textbf{3.7}$$

The differential of the objective function can be written as a function of the partitioned gradients

$$df = \nabla^T f(\vec{X}_I) d\vec{X}_I + \nabla^T f(\vec{X}_D) d\vec{X}_D \quad \textbf{3.8}$$

where $d\vec{X}_I$ and $d\vec{X}_D$ are vectors of differential displacements in independent and dependent variables respectively. Likewise the differential of the constraints can be written as function of the partitioned Jacobians and differential displacement vectors, which by definition of this method is zero.

$$d\vec{h} = \bar{J}_{X_I} d\vec{X}_I + \bar{J}_{X_D} d\vec{X}_D \equiv 0 \quad \textbf{3.9}$$

Solving for the dependent variable differential change in terms of the independent variables gives,

$$d\vec{X}_D = -\bar{J}_{X_D}^{-1} \bar{J}_{X_I} d\vec{X}_I \quad \textbf{3.10}$$

which when substituted into Equation 3.5 and rearranging gives the reduced gradient,

$$\nabla_r^T f(\vec{X}_I) = \nabla^T f(\vec{X}_I) - \nabla^T f(\vec{X}_D) \bar{J}_{X_D}^{-1} \bar{J}_{X_I} \quad \textbf{3.11}$$

The reduced gradient is the rate of change of the objective function with respect to the independent variables with the dependent variables adjusted to maintain feasibility. Hence, the reduced gradient can be used in the same manner as the full gradient to search for a minimum objective in the reduced space. Geometrically, the reduced gradient can be described as a projection of the original *N* dimensional gradient onto the *S* dimensional feasible region described by the independent variables. Changing the values of the independent variables will force a change in the dependent variables to maintain feasibility, at least over small changes where the constraints are linear. For nonlinear functions, changes in independent variable values beyond finite values will cause the linear approximation of the constraints to become invalid. Therefore, the dependent variables must be adjusted by a nonlinear technique during each line search step to restore feasibility. The method most commonly employed is the Newton-Raphson (N-R)

method to readjust the dependent variables to satisfy the constraints. The finite adjustment of the dependent variables is given by

$$\Delta \vec{X}_D = -\bar{J}_{X_D}^{-1} \vec{r} \qquad \textbf{3.12}$$

where $\vec{r}$ is the residual error vector of the constraints and $\bar{J}_{X_D}^{-1}$ is the inverse of the dependent Jacobian, already computed in Equation 3.7. Because the N-R method requires a square Jacobian for inversion, the number of dependent variables, ND, must equal the number of equality constraints, M.

The implementation of the GRG method generally consists of a number of line search steps in the (feasible) reduced gradient direction, each step followed by a N-R readjustment of the dependent variables to maintain feasibility. The GRG method is sometimes referred to as the 'saw-tooth' or 'hemstitching' method due to the readjustment of the dependent variables to satisfy the constraints, see Figure 8.

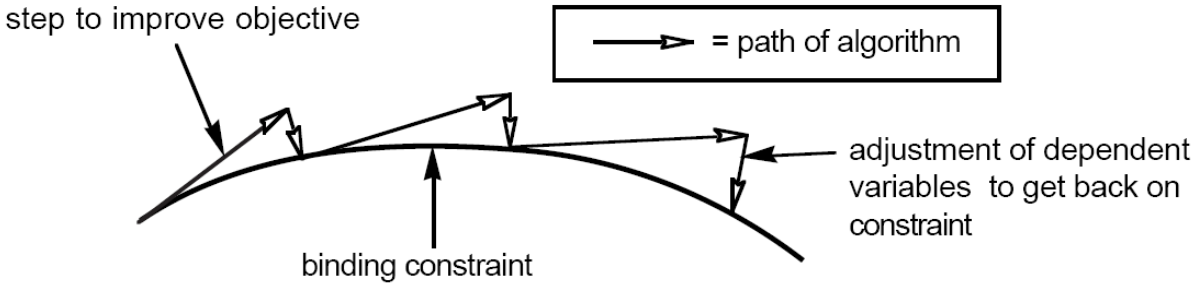

Figure 8: GRG Nonlinear Constraint Satisfaction

3.1.2 Inequality Constraints

The constrained nonlinear programming problem given by Equations 1.7 through 1.10 contains inequality constraints in addition to equality constraints. The GRG method is inherently set up to handle equality constraints, therefore inequality constraints are converted to equality constraints by the following transformation.

$$h_{M+j}(\vec{X}) = g_j(\vec{X}) - s_j \equiv 0 \quad \textbf{3.13}$$

$$0 \le s_j \le \infty \quad \textbf{3.14}$$

The variables s_j are nonnegative slack variables added to the original set of design variables. Hence, N now represents the total number of independent variables plus the slack variables used in 3.14. The parameter $M+J$ represents the total number of constraints, equality and inequality. The constraints considered in 3.2 and 3.13 include only functional constraints; variable bounds are contained in 3.3 and are handled separately.

GRG optimization methods in the literature use the slack variable method to handle inequality constraints almost exclusively [34,35,36]. The conversion of an inequality to an equality constraint results in an additional dependent variable. In some optimal trim applications, the addition of certain variables to the dependent type creates N-R convergence problems. This is the case for rotor speed in some situations (one of which is encountered in the example problem of Chapter 6). In this situation, inequality constraints must be handled in a manner that does not require rotor speed to be partitioned as a dependent variable. This can be accomplished by treating the inequality constraint as a penalty parameter to the objective as

$$\Phi(\vec{X}, r_p) = F(\vec{X}) + r_p P(\vec{X}) \quad \textbf{3.15}$$

where $F(\vec{X})$ is the original function, r_p is a multiple scalar and $P(\vec{X})$ is an imposed penalty. The form of $P(\vec{X})$ varies depending on its type, but for the exterior penalty function method is

$$P(\vec{X}) = \left\{\max[0, g_p(\vec{X})]\right\}^2 \quad \textbf{3.16}$$

The formulation for the inequality constraint allows the constraint to be satisfied and rotor speed to remain partitioned as an independent variable. Both slack variable and exterior penalty function methods are applied in this thesis.

3.1.3 Search Direction

Once the (reduced) gradient has been determined, it is used to define a search direction using any method that relies on gradients, such as steepest descent, conjugate gradient or quasi-Newton methods. The search direction in this work is based, in part, on the conjugate gradient method of Fletcher and Reeves [63]. The general optimization iterative algorithm steps along the search direction according to

$$\overline{X}^{k+1} = \overline{X}^{k} + \hat{\alpha}\vec{S}^{k}, \qquad k = 0,1,2... \tag{3.17}$$

where $\vec{S}$ is the search direction and $\hat{\alpha}$ the step length. In the GRG method, each step along the search direction is followed by a N-R convergence of the dependent variables. If the step size is too large, the system may not converge due to nonlinearity in the solution space; the convergence characteristics of the N-R method in any nonlinear space are dependent on the initial values of the variables and system nonlinearity. If the system does not converge, the step size must be progressively reduced [64]. Reference [37] uses the term 'radius of convergence' to define the step length beyond which the system will not converge. The radius of convergence has an important implication in the application of optimal trim, namely that the step size can not be arbitrarily large in the line search portion of the algorithm. If the minimum point is a relatively large distance away from the current point along the line search direction, the minimum point must be approached in steps of finite length, such that each step can converge from the previous point.

The radius of convergence depends on the nonlinearity of the local trim space topography and typically varies with the values of the independent variables and is not known a priori. In addition the radii of convergence of the independent variables are not equal in many optimal trim applications, depending on the set of independent variables. In practice,

some radii of convergence are different by an order of magnitude. Figure 9 illustrates this problem by showing the radii of convergence and component step-size magnitudes for two independent variables. The step-size in the X_{1I} direction is large, but its radius of convergence $\rho_{X_{1I}}$ is small. On the other hand, the step-size in the X_{2I} direction is small, but the radius of convergence $\rho_{X_{2I}}$ is large. If the composite search direction $\vec{S}$ is scaled to the smallest radius of convergence, $\rho_{X_{1I}}$, the progress in direction X_{2I} would be much smaller than could be, and may drive up the number of function calls during the line search.

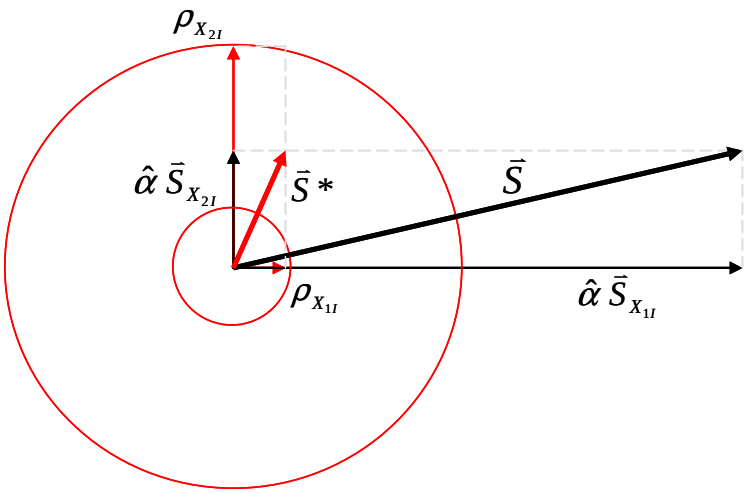

Figure 9: Trim Variable Radii of Convergence

A solution to this problem is to limit the step-size component of each variable to the radius of convergence. If the composite step in the search direction maintains each component within its respective radius of convergence, it is unmodified. However, if the composite step in the search direction exceeds a particular component radius of convergence, that component is reduced to the radius of convergence. This search direction is indicated as $\vec{S}*$ in Figure 9. This method requires a priori knowledge of radii of convergence for each independent variable, which must be determined through user experience with the trim problem. This radius-of-convergence modified, conjugate gradient step direction method is used in the optimal trim algorithm developed herein.

3.1.4 Optimality Conditions

The minimum of an unconstrained nonlinear problem occurs when the elements of the gradient vanish at the optimum point $\vec{X}^*$.

$$\nabla f(\vec{X}^*) = 0 \qquad \textbf{3.18}$$

The minimum of a constrained nonlinear problem is more complex to determine and requires the fulfillment of the Kuhn-Tucker conditions, namely that the Lagrangian vanishes,

$$\nabla^T f(\vec{X}^*) + \sum_{j=1}^{m} \lambda_p \nabla^T g_p(\vec{X}^*) + \sum_{k=1}^{l} \lambda_m \nabla^T h_m(\vec{X}^*) = 0 \qquad \textbf{3.19}$$

where *m* is for all equality constraints and *p* is only the active inequality constraints. The reduced gradient is a projection of the independent variable gradient on the feasible region defined by the dependent variables. If the reduced gradient is within some small region close to zero it can be shown that point is a constrained relative minimum that approximates the Kuhn-Tucker conditions [65].

$$\nabla_r^T f(\vec{X}_I^*) = \nabla^T f(\vec{X}_D^*) + \sum_{p=1}^{p} \lambda_p \nabla^T g_p(\vec{X}_D^*) + \sum_{m=1}^{M} \lambda_m \nabla^T h_m(\vec{X}_D^*) = 0 \qquad \textbf{3.20}$$

3.2 Optimal Trim Algorithm Implementation

3.2.1 Implementation Considerations

There are some practical considerations that must be dealt with when implementing the GRG method into a code. The issues include the relative scale of the variables, the radius of convergence, numerical noise and efficiency in computing the sensitivity matrix. A short discussion of each will provide insight into the limitations that are present when applied to the trim problem and the approaches used in this thesis.

A desirable optimization problem formulation is one in which the order of the magnitude of the variables are the same. Reference [30] discusses the importance of correctly posing an optimization problem in terms of the relative scale, suggesting that the magnitude of the components of the Hessian matrix diagonals be the same. In practice it is difficult to formulate all problems with variables of the same magnitude or scale components relative to their Hessian diagonal values. It is suggested that a simpler yet effective approach is to normalize each design variable by itself. Therefore the scaling array becomes

$$\overline{D} = \begin{bmatrix} \frac{1}{|X_1|} & 0 & \cdots & 0 \\ 0 & \frac{1}{|X_2|} & & \vdots \\ \vdots & & \ddots & \vdots \\ 0 & 0 & \cdots & \frac{1}{|X_N|} \end{bmatrix}. \qquad \textbf{3.21}$$

The type of problems encountered in trim optimization often have variables of different scale in terms of order of magnitude of the variables and also in terms of the span of the variable upper and lower limits. Therefore, the problem has to be scaled for efficient optimization. The implementation in this thesis is accomplished in the following way. First, the user specifies the step size for each variable, both dependent and independent, that is used in the finite difference gradient computation. The user therefore determines the relative scale in setting up the step size. Once the gradient is computed, it is scaled by the relative span of the independent variable upper and lower limit ranges that have the largest span.

Another consideration affecting the accuracy and efficiency of the optimum location is numerical noise. Numerical noise comes from several different sources including computer rounding error and convergence criterion. Noise from convergence criterion is the most significant in trim optimization problems. Numerical trim simulations have multiple levels of convergence including: numerical differential equation solutions from

one time step to the next, the periodic solution determination, the trim constraint determination and the optimum solution determination. The criterion used to determine the trim constraints is of particular concern. The convergence accuracy of the trim constraints by adjustment of the dependent trim variables must be less than the step size used in the finite difference determination of the reduced gradient. If the convergence criterion is too liberal, the magnitude or even the sign of the reduced gradient can have components that are spurious, causing problems in the line search procedure.

The N-R method requires the computation of the (inverse) Jacobian matrix at each iteration, Equation 3.12. For the typical forward or backward finite difference method to compute the Jacobian element derivatives, N function calls are required. This approach quickly becomes computationally expensive or even prohibitive, especially in the application of optimal trim were a N-R iteration is performed at each line search step to satisfy the trim constraints. Approaches have been devised to decrease the number of function calls. The first and most straightforward is to use the same Jacobian for a number of iterations. Eventually though, the Jacobian will go 'stale' as the nonlinear trim space topology changes, rendering the magnitude or even the sign of some of the components inaccurate. A more advanced type of approach is to update the Jacobian based on subsequent iterations, which is called the secant method. One of the more commonly used secant methods is Broyden's method [66]. In this thesis, the former method is used, where the user specifies the number of iterations performed before the Jacobian is recomputed. Additionally, the user can specify a maximum step size, under which the Jacobian is not recomputed. Near an optimum condition where the step sizes are small and frequent, a single computation of the Jacobian is quite effective in reducing the function calls, yet allowing the N-R iterations to converge.

3.2.2 Algorithm Description

The optimal trim algorithm uses several components of the RCAS comprehensive rotorcraft code trim algorithm, shown in Figure 10, with additional components to compute the reduced gradient, search direction and perform the line searches. The

algorithm components that implement the GRG optimal trim method are shown in Figure 11. The optimal trim algorithm begins with a normal trim solution convergence. To set up the trim problem, the user defines the dependent trim variables $\vec{X}_D$ to be controlled and their starting values along with the trim constraints. The native trim process uses a N-R type iteration which involves computing the Jacobian $\bar{J}_{X_D}$, then driving the residuals to zero. The process is actually a pseudo-Newton method because the Jacobian is not computed each iteration, rather the number of iterations between each finite difference Jacobian computation is specified. The end result of the trim procedure is the beginning point for the optimal trim algorithm; the optimization starts with all trim equality constraints satisfied.

The optimal trim algorithm also requires the independent trim variables $\vec{X}_I$ and their starting values be specified before the first trim iteration. Once the first trim solution is reached with the independent variable initial values $\vec{X}_I{}^O$, the optimization loop begins. In the first step the reduced gradient $\nabla_r^T f(\vec{X}_I)$ is computed. The gradient is used to determine the search direction $\vec{S}^k$ and can be used in any conventional gradient based unconstrained search technique. The actual search direction is determined by the conjugate gradient method and a scale factor. The scale factor is used to equalize any relative scale difference that may exist between independent trim variables and their ranges defined by the upper and lower limits. The search direction when scaled by the initial step size is checked to assure the independent variable values do not exceed the radius of convergence limits. If one or more of these limits are violated, the appropriate search direction component(s) are reduced to be equal to the radius of convergence limit.

Once the search direction is computed, the line search process begins. The line search consists of a number of steps that establish the minimum point on the line. After each step, the N-R adjustment of the dependent variables is executed to drive the solution to follow the constraints. The step size is limited by the radius of convergence, therefore if the minimum point is a significant distance from the beginning of the line search, it will

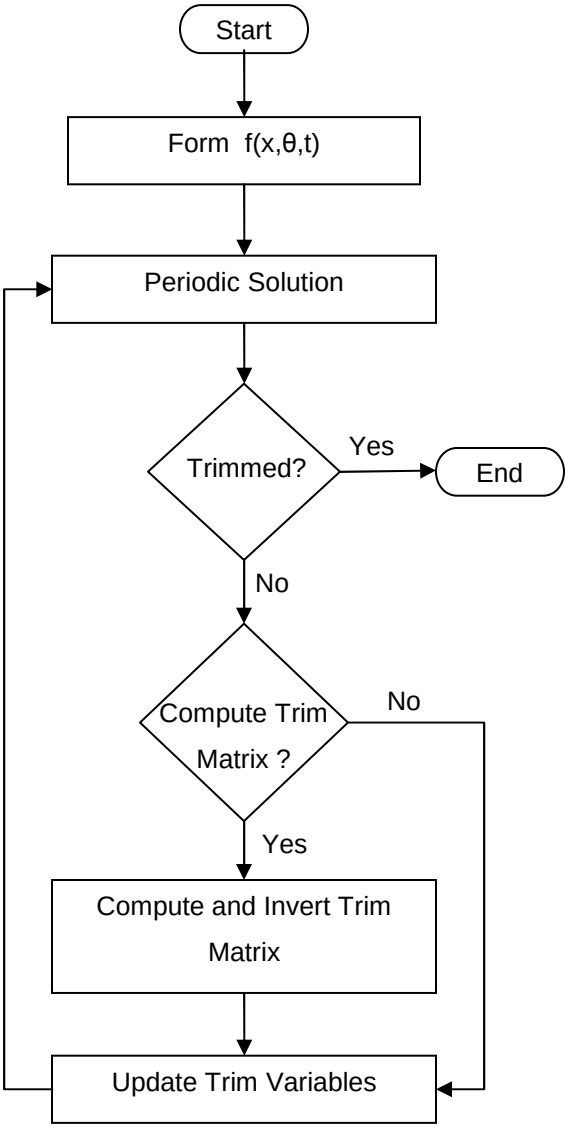

Figure 10: RCAS Trim Algorithm

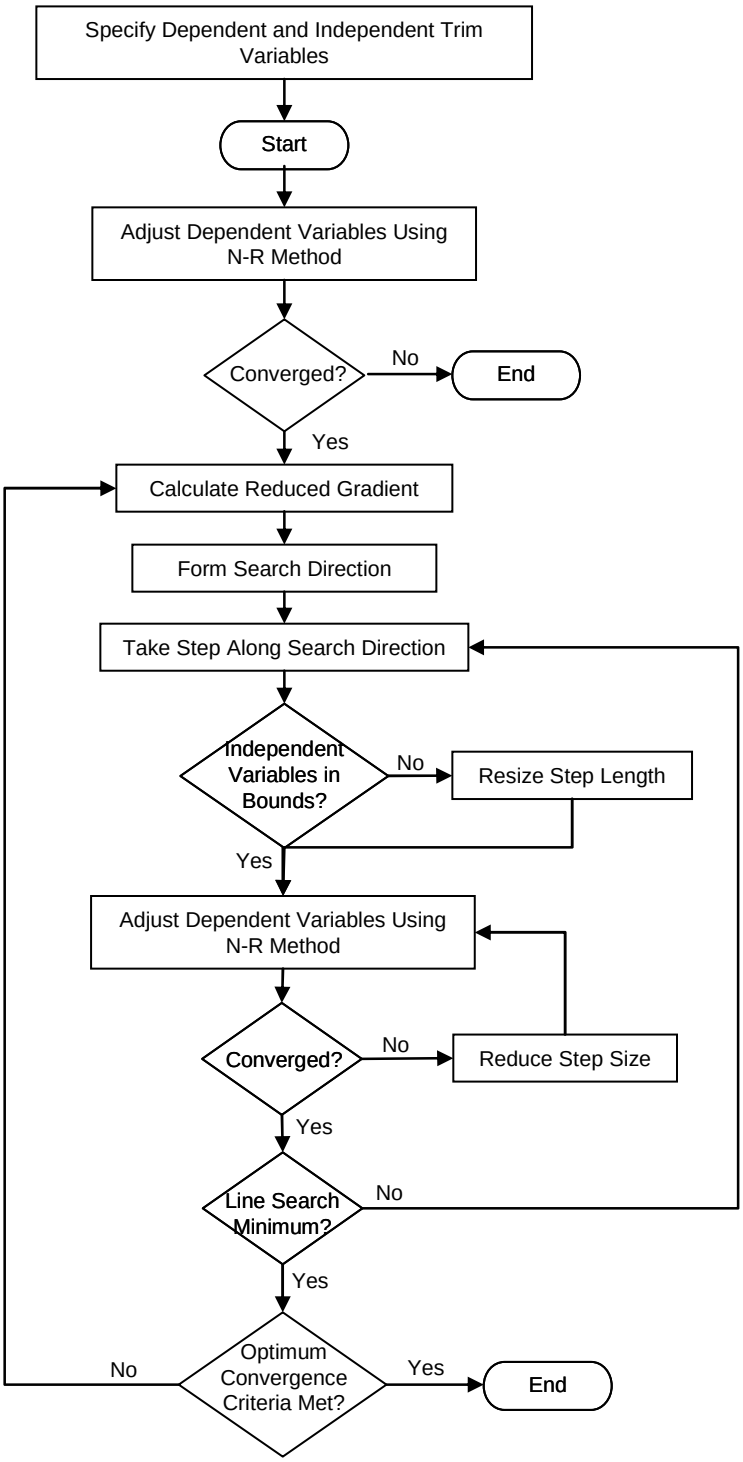

Figure 11: GRG Optimal Trim Algorithm

take a number of steps to reach. The line search progresses until the minimum is established or until the N-R fails to converge. If the N-R fails to converge, the step size is reduced and the N-R re-tries to converge. If the N-R iteration fails to converge more than a user specified number of times, the line search terminates. During each step of the line search, the values of the independent variables are tested to make sure they are within the prescribed limits.

The sequence of reduced gradient computation and line search is repeated until either the gradient approaches zero, or the line search step size becomes too small, indicating the optimum has been reached. The coding of the algorithm is relatively complicated compared to many non-constrained optimization techniques, but it is nonetheless fairly robust and relatively efficient due to its apparent ability to track the binding constraints to until an optimum is reached.

3.3 Method Validation

The GRG optimal trim algorithm is validated to show its capability to seek and find the constrained optimum objective. The method is validated by being exercised on a sample trim problem, where the solution topography as a function of the independent variables has been mapped out; all of the trim constraints are satisfied by adjustment of the dependent variables. The optimum solution is known a priori from the trim map. Once the algorithm shows its ability to effectively find the known minimum from several initial staring conditions, confidence is gained that it can find the optimum trim in solutions spaces where the topography is not known a priori. The purpose of this effort is to show the optimal trim capability, not to accurately map out the trim space based on high fidelity physics.

The algorithm is validated against two trim cases, each progressing in complexity. The first case consists of a hover condition with a single independent variable, the rotor speed. The problem of minimizing rotor power is solved with and without an inequality constraint on the average blade maximum lift coefficient. The second case consists of

forward flight with two independent variables, rotor speed and forward velocity, where again the optimum (minimum) power condition is sought. The second case also is run with and without an inequality constraint on the maximum average lift coefficient. A summary of the cases and the number and type of constraints are provided in Table 1.

Table 1: Optimal Trim Validation Test Case Summary

CASE DESCRIPTION	INDEPENDENT VARIABLES	EQUALITY CONSTRAINTS	INEQUALITY CONSTRAINTS
Hover	1	6	0
Hover	1	6	1
Forward Flight	2	6	0
Forward Flight	2	6	1

Table 2: Sample Helicopter Properties

HELICOPTER PARAMETER	VALUE
Blades	5
Lock no.	5.14
Solidity	.0925
Diameter_MR	38.0 ft
DL	12.65
Hinge Offset	0.22 r/R
Twist	8.29 deg
Diameter_TR	4.5 ft
L_TR	22 ft

Each case utilizes a helicopter model that is trimmed in 6 degrees of freedom. While the model is relatively simple, it has 5 individual articulated blades (in pitch and lead-lag) with non-uniform inflow over the rotor disk. The model also consists of a tail rotor for which the collective pitch is controlled to vary the yawing moment. The properties of the helicopter are given in Table 2. The model is constructed in a multi-body framework, allowing flexibility in the fidelity of the dynamic components. The mathematical representation is in the typical state space representation as presented in Equation 1.1.

Each blade has 2 degrees of freedom, the fuselage has 6 degrees of freedom, the tail rotor is a simple thrust fan representation with 1 DOF for thrust, finally the inflow model for the main rotor has 9 degrees of freedom for a total of 26 degrees of freedom.

3.3.1 Validation Case: Hover

The first validation case is simple hover with the independent variable being the rotor speed. Figure 12 shows the 1 dimensional topography of the rotor power with rotor speed, which qualitatively matches the behavior in Reference [1]. The nature of the hover power is clearly evident. On the high end of the rotor speed variable, the power is dominated by profile drag and increases proportional to the square of dynamic pressure. On the low end of the rotor speed, the dynamic pressure is low and in order to maintain the vertical force constraint, the collective pitch is increased. Therefore, the local angle of attack increases and subsequently the profile drag also increases sharply, more so than the profile drag with rotor speed. The minimum value of the rotor speed is 27.5 rad/s, as values below that point failed to converge to meet the constraints, due to stall.

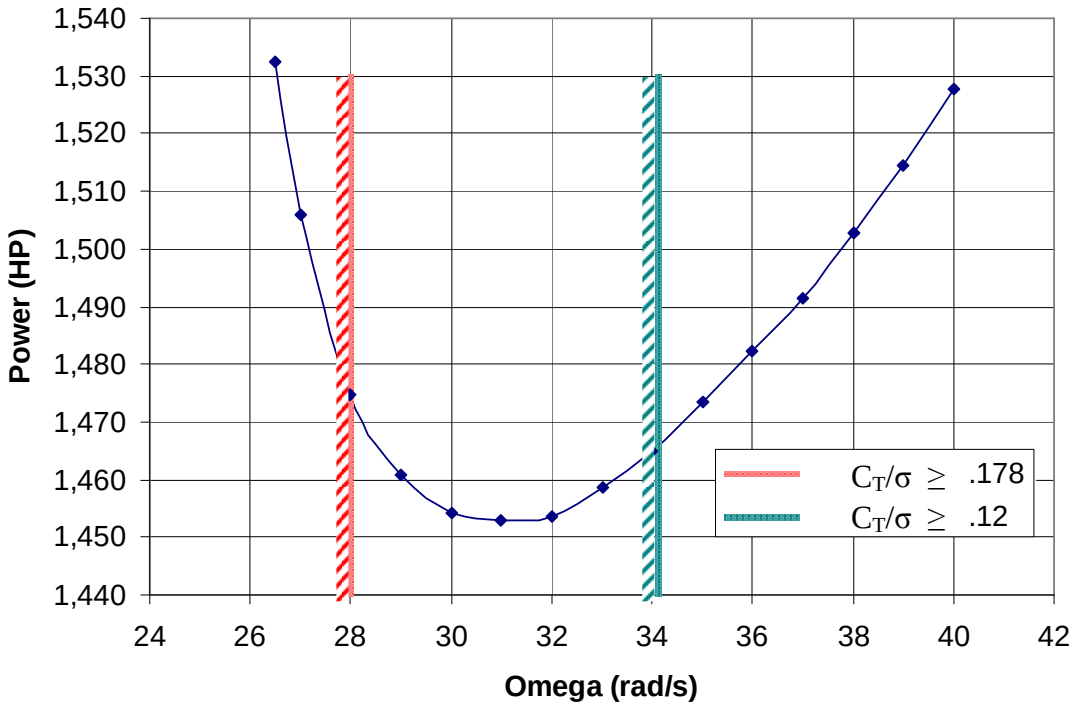

Figure 12: Hover Power vs. Rotor speed

Problem Statement:

Minimize: Power **3.22**

Subject to:

$$F_{Rx}(\vec{X}_D) = 0 \quad \textbf{3.23}$$

$$F_{Ry}(\vec{X}_D) = 0$$

$$F_{Rz}(\vec{X}_D) = 0$$

$$M_{Rx}(\vec{X}_D) = 0$$

$$M_{Ry}(\vec{X}_D) = 0$$

$$M_{Rz}(\vec{X}_D) = 0$$

$$28 \le X_{1I} \le 40 \quad \textbf{3.24}$$

$$\vec{X}_D = [\theta_0, \theta_{1s}, \theta_{1c}, \alpha, \phi, \theta_{TR}];\ \vec{X}_I = [\Omega] \quad \textbf{3.25}$$

Table 3: Hover X^O=[40]

Iteration	*Power*	X_{1I}	X_{1D}	X_{2D}	X_{3D}	X_{4D}	X_{5D}	X_{6D}	*delta*	*Function*
0	1,527.00	40.20	9.29	-0.52	0.63	23.61	-0.08	0.07	---	---
1	1,457.50	30.00	15.04	-1.17	0.80	27.49	-0.11	0.06	69.52	72
2	1,453.90	31.00	14.23	-1.04	0.82	26.89	-0.10	0.06	3.54	170
3	1,453.50	31.29	14.01	-1.01	0.82	26.73	-0.10	0.06	0.00	268

For practical purposes, a rotor is not operated at the minimum power condition due to potential blade stall; there is usually some constraint on the blade loading. The quantity of trust coefficient over solidity (C_T/σ) is a measure of the average lift coefficient and reference [67] gives an empirical relationship for C_T/σ versus forward speed non-dimensionalized by advancing tip speed (μ)

$$C_T/\sigma \le 0.15 + 0.12\mu - 0.15\mu^2 \quad \textbf{3.26}$$

This constraint is applied to the hover solution at two different zero velocity values to show the effectiveness of the optimal trim method with inequality constraints. The location of these constraints relative to the rotor speed and power curve for the sample rotor is shown in Figure 12. As outlined in equation 3.13and 3.14, the GRG method

treats inequality constraints by adding a slack variable to the independent variable set. The resulting constraint formulation is:

$$g_1 = \left(\frac{C_T}{\sigma_0} + 0.12\mu - 0.15\mu^2 \right) - \frac{C_T}{\sigma} - s_1 = 0 \qquad \textbf{3.27}$$

$$0 \le s_1 \le \infty \qquad \textbf{3.28}$$

where μ is zero at hover. The constraint therefore becomes an equality constraint which is included with the dependent variable matrix. The dependent trim variable correlating to the equality constraint is rotor speed, which becomes X_{7D}. The slack variable s_1 becomes an independent variable and is set to zero initially. At each line search step in the optimization, all dependent variables are adjusted such that each equality constraint is satisfied. Table 4 and Table 5 show the optimal trim convergence results for two C_T/σ constraint conditions. Note that when the constraint is at an effective rotor speed below the minimum, the solution finds the optimum and the slack variable X_{2I} becomes a nonzero positive value. The trim optimization terminates as the reduced gradient vanishes. For the condition that the constraint is at an effective rotor speed above the minimum value, the final solution terminates at the constraint, with the slack variable equal to zero. The trim terminates as the objective value change between two successive iterations is below the convergence tolerance. The optimization results are shown graphically in Figure 13.

Table 4: Hover X^O=[28]

Iteration	*Objective*	X_{1I}	X_{1D}	X_{2D}	X_{3D}	X_{4D}	X_{5D}	X_{6D}	X_{7D}	*delta*	*Function*
0	1,482.10	0.00	16.07	-1.37	0.75	28.28	-0.11	0.06	28.87	---	---
1	1,453.80	0.03	14.11	-1.02	0.82	26.80	-0.10	0.06	31.15	28.32	138

Table 5: Hover X^O=[34]

Iteration	*Objective*	X_{1I}	X_{1D}	X_{2D}	X_{3D}	X_{4D}	X_{5D}	X_{6D}	X_{7D}	*delta*	*Function*
0	1,467.60	0.00	11.70	-0.74	0.76	25.16	-0.09	0.07	34.90	---	59
1	1,467.60	0.00	11.70	-0.74	0.76	25.16	-0.09	0.07	34.90	0	72

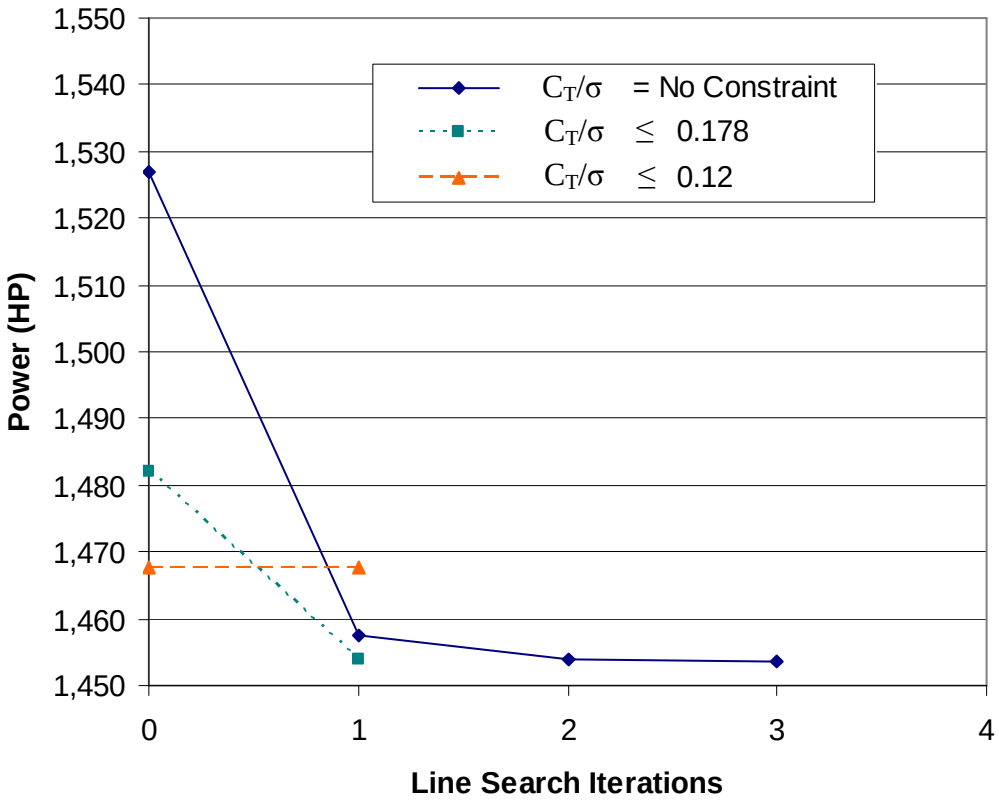

Figure 13: Optimal Trim Convergence: 1 Independent Control Variable

3.3.2 Validation Case: Forward Flight

The second validation case is an extension of the first with the addition of forward speed as an independent variable. Again, the objective of the optimization is to minimize power. The so called 'power bucket' has the known characteristics of the power reducing from hover to some minimum and then rising again as the parasite, divergence and retreating blade stall power increase. Figure 14 shows the topography of the power as functions of air speed and rotor speed. There is a clear minimum power location in the approximate location of 130 ft/s and 36 rad/s. Also note the lower right portion of the map has a region where the dependent variables do not converge. In forward flight the thrust capability diminishes as the dynamic pressure over the retreating side decreases. The phenomenon of (advancing tip) divergence and retreating blade stall drag combine to reduce the thrust capability as a function of the advance ratio. Therefore, in practice the C_T/σ limit of 3.26 must not be exceeded; this limit is depicted on the power map.

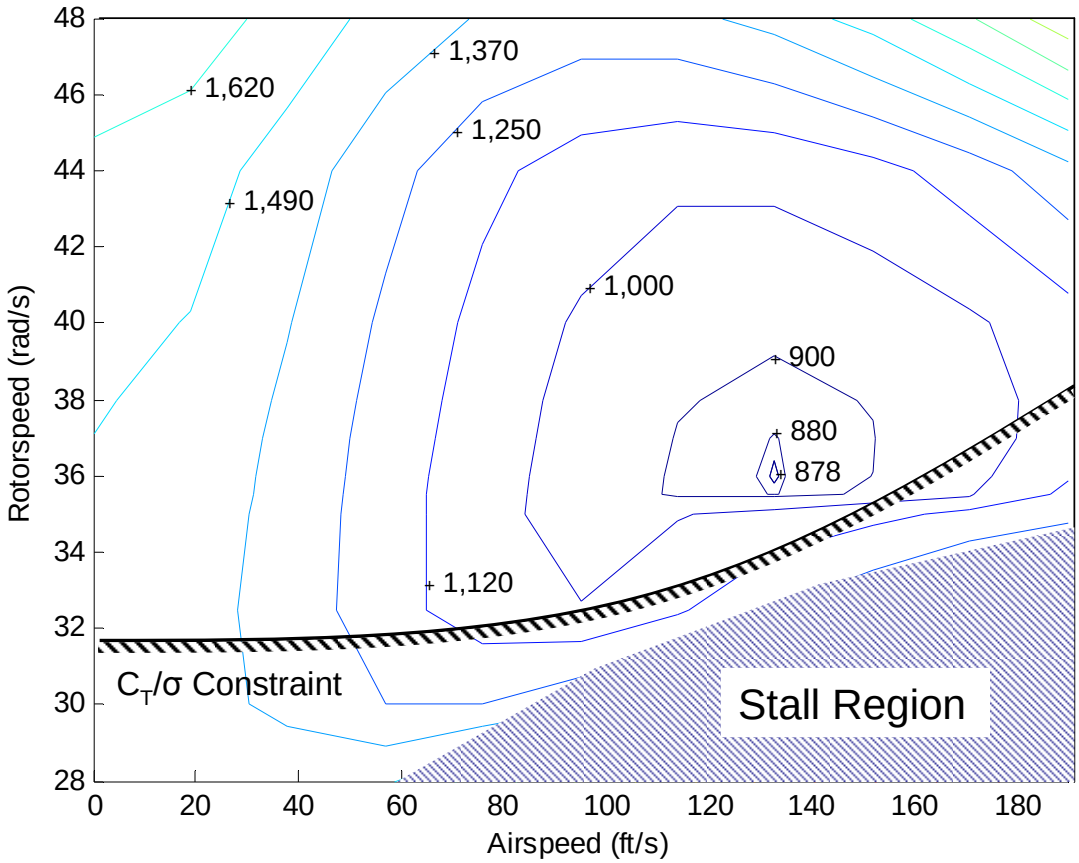

Figure 14: Helicopter Power Map (HP)

The forward flight optimal trim case is run without and with the C_T/σ constraint to demonstrate its capability. With no constraint on C_T/σ, the lower limit of the rotor speed is set such that the non converging stall region is excluded from the trim solution space, with a lower limit of 35 rad/s. The optimal trim problem is set up and listed in Equations 3.10 and 3.11, with the addition of airspeed as an independent control variable subject to the limits listed in Equation 3.29. Tables 6 - 8 each show the progressive trim optimization results from various arbitrary initial independent variable values within their specified ranges. Figure 15 graphically shows the convergence of the optimum power for each line search iteration. The results show that the minimum power value of approximately 875 HP is located near 130 ft/s and 35.5 rad/s. The optimizer has no difficulty locating the minimum and satisfying all 6 equality constraints.

Subject to: $0 \le X_{1I} \le 190$ **3.29**

$$35 \le X_{2I} \le 48$$

$$\vec{X}_D = [\theta_0, \theta_{1s}, \theta_{1c}, \alpha, \phi, \theta_{TR}];\ \vec{X}_I = [V, \Omega] \qquad \textbf{3.30}$$

Table 6: Forward Flight X^O=[0, 40]

Iteration	*Power*	X_{1I}	X_{2I}	X_{1D}	X_{2D}	X_{3D}	X_{4D}	X_{5D}	X_{6D}	*delta*	*Function*
0	1,527.00	0.00	40.20	9.29	-0.52	0.63	23.61	-4.63	4.11	---	---
1	881.13	126.25	35.00	9.48	2.31	-3.73	13.11	-1.97	2.24	645.85	168
2	877.21	134.25	35.81	9.07	2.21	-3.70	12.50	-1.96	2.01	3.92	252
3	876.42	134.21	35.84	9.05	2.20	-3.70	12.49	-1.95	2.01	0.79	358

Table 7: Forward Flight X^O=[135, 35]

Iteration	*Power*	X_{1I}	X_{2I}	X_{1D}	X_{2D}	X_{3D}	X_{4D}	X_{5D}	X_{6D}	*delta*	*Function*
0	884.98	135.00	35.20	9.43	2.26	-3.98	12.71	-1.98	1.99	---	---
1	876.59	127.77	35.96	8.94	2.21	-3.43	12.72	-1.94	2.19	8.39	44
2	876.35	127.86	35.96	8.94	2.21	-3.43	12.71	-1.94	2.19	0.25	130
3	876.06	127.86	35.96	8.94	2.21	-3.43	12.71	-1.94	2.19	0.29	177
4	875.65	129.86	35.89	8.99	2.21	-3.53	12.65	-1.94	2.13	0.41	239

Table 8: Forward Flight X^O=[165, 48]

Iteration	*Power*	X_{1I}	X_{2I}	X_{1D}	X_{2D}	X_{3D}	X_{4D}	X_{5D}	X_{6D}	*delta*	*Function*
0	1,664.80	165.00	48.20	5.55	1.26	-1.89	15.03	-3.50	-0.75	---	---
1	915.75	108.21	37.71	8.15	2.15	-2.40	13.46	-1.94	2.70	749.00	94
2	879.13	134.43	37.02	8.44	2.11	-3.31	12.18	-1.91	2.00	36.62	145
3	877.60	132.43	36.93	8.47	2.12	-3.27	12.28	-1.91	2.06	1.53	201
4	877.26	128.43	36.56	8.64	2.16	-3.26	12.54	-1.92	2.18	0.34	274
5	875.84	132.38	36.23	8.82	2.17	-3.49	12.45	-1.93	2.06	1.43	349

Next, the C_T/σ inequality constraint is included in the trim optimization as listed in Equation 3.26 and the lower limit of the rotor speed variable is reduced to 28 rad/s. The inequality is handled in two different ways for this problem. The first method is the slack variable method discussed in the previous section, which requires rotor speed to become an independent variable, $X_{7D,}$ driven by the Ct/σ constraint value. The second method is to keep rotor speed in the independent variable category and add a penalty function to the objective

$$P(\vec{X}) = \left\{ \max\left[0, \left(\frac{C_T}{\sigma} - \frac{C_T}{\sigma}_{\max} \right) \right] \right\}^2 \qquad \textbf{3.31}$$

The two inequality constraint methods are applied to the optimal trim helicopter problem with an initial condition of zero forward speed and rotor speed of 40 rad/s. Line search step-size, radius of convergence and all other parameters are kept at the same values for the two inequality constraint methods. The results of the two methods are listed in Table 9 and Table 10 with the objective reduction for the cases shown graphically in Figure 16. For the slack variable technique, the slack variable X_{11} remains zero during the first line search, which indicates the constraint is active, but in the remaining line searches, the finite value indicates the optimum is off of the constraint. Eventually the slack variable method terminates before converging at the optimum solution. The penalty function method has no problem finding the minimum.

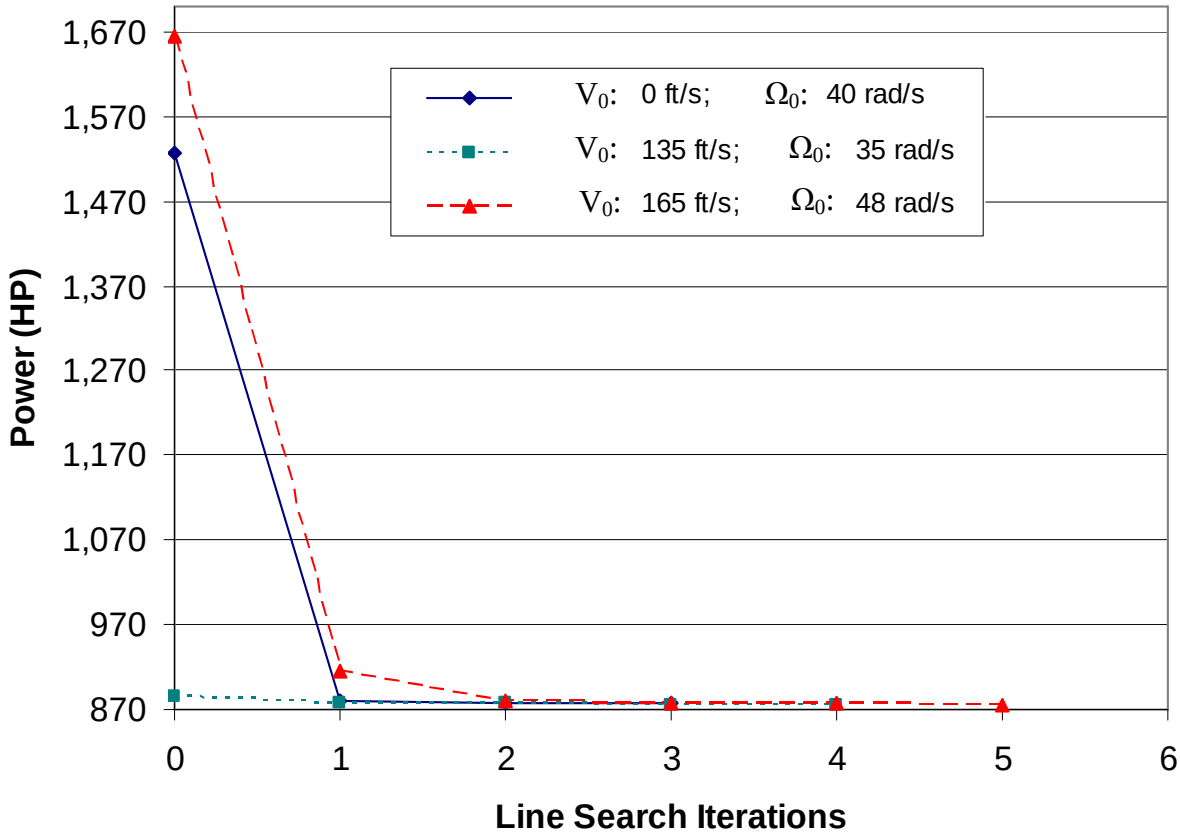

Figure 15: Optimal Trim Convergence: 2 Independent Control Variables

Table 9: Inequality Constrained Forward Flight X^O=[0, 40]; Dependent Ω

Iteration	*Objective*	X_{1I}	X_{2I}	X_{1D}	X_{2D}	X_{3D}	X_{4D}	X_{5D}	X_{6D}	X_{7D}	*delta*	*Function*
0	1,467.6	0.000	0.00	12.15	-0.71	0.70	25.41	-0.09	0.07	34.11	---	---
1	1,023.9	0.000	84.00	11.49	2.47	-3.08	17.70	-0.05	0.05	32.38	443.73	179
2	969.1	0.025	90.18	9.10	2.22	-2.23	15.34	-0.04	0.05	36.11	54.71	406
3	953.5	0.013	93.18	10.19	2.39	-2.85	15.69	-0.04	0.05	34.03	16.03	709
4	942.3	0.025	96.18	9.07	2.25	-2.43	14.73	-0.04	0.05	35.98	11.13	1251

Table 10: Inequality Constrained Forward Flight X^O=[0, 40]; Independent Ω

Iteration	*Objective*	X_{1I}	X_{2I}	X_{1D}	X_{2D}	X_{3D}	X_{4D}	X_{5D}	X_{6D}	*delta*	*Function*
0	1,527.00	0.00	40.00	9.31	-0.52	0.63	23.62	-0.08	0.07	---	---
1	1,004.30	84.00	33.00	11.01	2.40	-2.82	17.20	-0.04	0.05	522.68	130
2	884.47	132.44	34.94	9.57	2.29	-3.99	12.92	-0.03	0.04	119.82	226
3	880.48	125.57	35.20	9.36	2.29	-3.62	13.06	-0.03	0.04	4.00	270
4	876.16	133.56	35.86	9.03	2.20	-3.66	12.51	-0.03	0.04	4.31	315
5	876.02	133.56	35.86	9.03	2.20	-3.66	12.51	-0.03	0.04	0.14	389

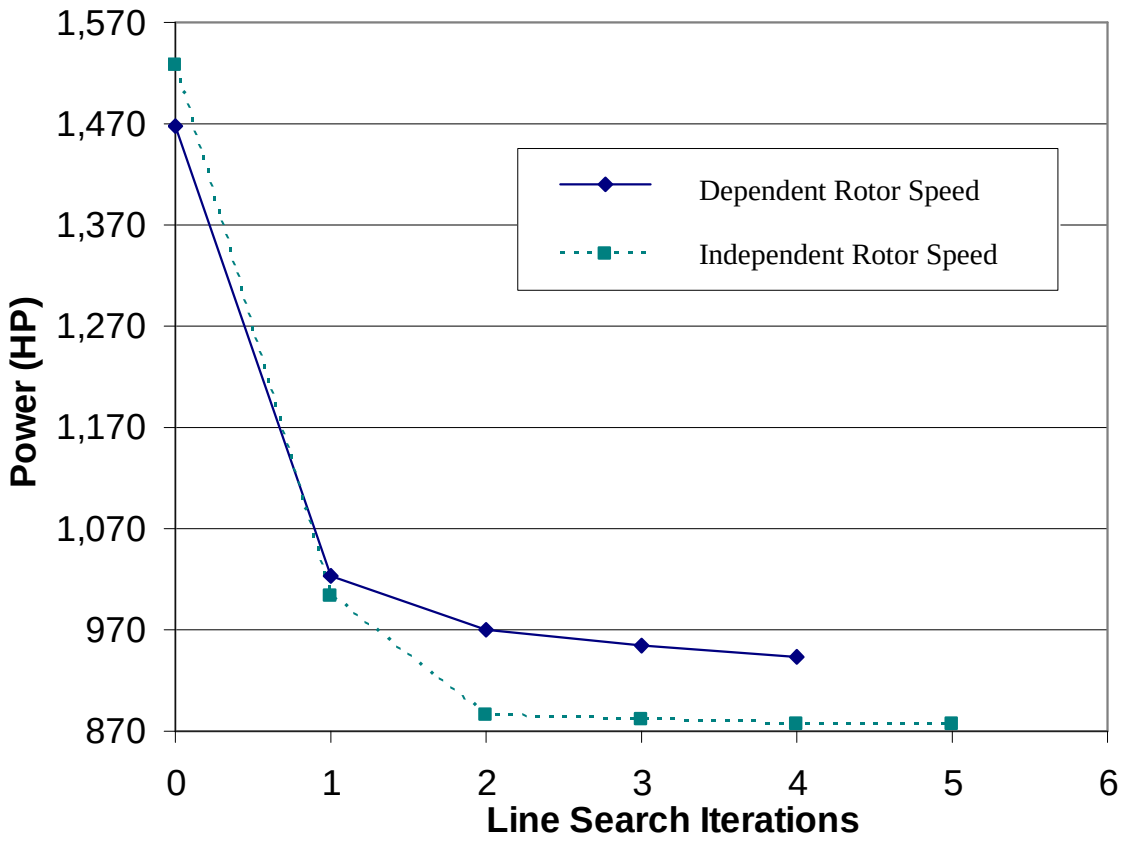

Figure 16: Optimal Trim Convergence: Dependent vs. Independent Rotor Speed

The results listed in Table 9 and Table 10 show an interesting trend in the number of total function calls required in seeking the optimum. The method which treats rotor speed as a dependent variable requires several times the number of total function calls compared to the method with rotor speed as an independent variable. Table 11 shows the total function call number for two additional initial conditions for the two inequality constraint methods. The trend remains that rotor speed treated as an independent variable requires fewer function calls by several times; a substantial savings. In addition to the case shown in Figure 16, another case failed to converge also where the initial independent variable values were far from the constraint, the dependent variable constraints could not converge before the optimization began. The apparent reason for this difference in the two methods is first, the use of a slack variable increases the number of independent variables and dependant variables. Secondly, the rotor speed may influence the periodicity of the system and therefore the local nonlinearity of the system. The change in nonlinearity due to the introduction of variable rotor speed may drive up the number of N-R iterations for dependent variable convergence. This fact alone would be a major reason to utilize methods that keep rotor speed as an independent variable in optimal trim problems with variable rotor speed.

Table 11: Total Function Calls for Inequality Constrained Optimization

Initial Coordinate	Dependent Rotor speed	Independent Rotor speed
[0,40]	1251 (no convergence)	389
[135,35]	245	89
[165,48]	51 (no convergence)	360

3.3.3 Optimal Trim Results Discussion

The results of the two optimal trim validation cases clearly indicate the method's capability to find the minimum power trim solution. Therefore, these results may be extended to more complex configurations for the application of general optimal trim solutions where the solution space topology is more complex and unknown; this is purpose of Chapter 6. Results also indicate the convergence tolerance significantly affects the total number of function calls. As the objective reduction rate decreases, the

function call rate increases. Therefore care should be used when determining the convergence tolerance.

Several factors impact the rate of convergence of the optimal trim solution in each iteration such as the line-search step-size length, equality constraint convergence limits and the independent variable radii of convergence, the latter factor being the most significant factor. Recall that after each line search step, the dependent variables are adjusted through a N-R iterative process to maintain feasibility. If too large a step size is taken, the equality constraints will not converge. Precise knowledge of the radius of convergence is difficult to ascertain because it is dependent on the nonlinearity of the local trim space topography and the topography changes with the independent variable values. In the helicopter example given, the radius of convergence for the airspeed variable is about 20 to 30 ft/s at low airspeeds, but decreases to only 5 to 10 ft/s at higher airspeeds. The radius of convergence for the rotor speed variable is approximately 10 rad/s at low speed, and reduces to only 1 to 2 rad/s at higher airspeeds. These limits affect the line search step size. Of course a large step size is desired if the starting position is far from the optimum, but a small step size is favorable near the optimum. Note in Table 10 that a relatively small reduction in the rotor power of about 11 HP required over 500 function calls, more function calls than the first two line searches combined. This is because the default step size fails to have equality constraint convergence, and must reduce the step length repetitively, generating a large number of function calls.

In the optimal trim algorithm implementation, the user specifies a maximum radius of convergence for each variable. If the step-size is such that it violates the limit, the search direction $\vec{S}^k$ is modified to conform to the specified limits. The resulting search direction therefore modifies the search direction determined by the conjugate gradient. The impact of this search direction modification on convergence efficiency is not known. Future research on optimal trim would benefit from methods that optimize the search direction and step size under radius of convergence constraints. This would most likely

require a combination of a quasi-Newton search direction and better initial step size, such as a hybrid GRG-SQP method [37].

3.4 Chapter Summary

An optimal trim algorithm is developed based on the nonlinear programming technique of the Generalized Reduced Gradient (GRG) and is encoded into the comprehensive rotorcraft analysis code RCAS. The conjugate (reduced) gradient search direction method is modified for radii of convergence of the various independent variables in a novel manner. The optimal trim algorithm is then applied to a series of increasing complexity helicopter power minimization problems, progressing from 1 independent variable 6 DOF trimmed hover to 2 independent variable inequality constrained 6 DOF trimmed forward flight. Inequality rotor C_T/σ constraints are fulfilled by both slack variable and external penalty function methods. Results suggest that treating rotor speed as an independent variable reduces system nonlinearity and results in more efficient optimal solution convergence compared to treating rotor speed as a dependent variable. The optimal trim algorithm quickly converges on the independent variable values which produce the minimum power solution, as determined from a parametric mapping of the solution space. These results affirm the hypothesis to the primary research question in that *an optimal trim solution can be systematically found through the use NLP methods, namely the Generalized Reduced Gradient method.*

CHAPTER 4
AUTOROTATIVE TRIM WITH VARIABLE ROTOR SPEED

An object of this thesis is to contribute to the analytical techniques required to model and analyze rotors in the mode of autorotation. The specific capability to be developed is an analytical method that allows rotor speed to vary in trim for comprehensive rotorcraft numerical simulations. This chapter discusses the physical aspects of autorotation including autorotative stability and rotor speed variation. Next a method that allows rotor speed to vary based on numerical iterative techniques is developed. The method is correlated with autorotative test data of an isolated wind tunnel rotor and a small gyroplane trimmed in 6 DOF. Finally, some possibilities of trim optimization are discussed relative to autorotation.

4.1 Physics of Autorotation

For an aerodynamic segment of the rotor in autorotational equilibrium the inflow angle must be such that there is no net in-plane force and, therefore, no contribution to rotor torque. In this condition the in-plane component of lift cancels the in-plane component of drag,

$$dQ = \left(D\cos\phi - L\sin\phi\right)r dr = 0 \qquad \textbf{4.1}$$

From Figure 17 it can be seen that three factors affect the inplane forces of the segment in autorotative equilibrium: the inflow angle (ϕ), geometric pitch (θ) and the airfoil drag to lift ratio (C_d/C_l). With the assumption of uniform (up) inflow over the rotor disk and axial symmetry (vertical descent), the induced angle of attack (AOA) at a blade element is

$$\phi = \frac{\text{Upflow Velocity}}{\text{Inplane Velocity}} = \tan^{-1}\left(\frac{\left|V_C - v_i\right|}{\Omega r}\right) \qquad \textbf{4.2}$$

The geometric angle θ is determined by the blade twist and collective setting and the airfoil lift-to-drag ratio is a function of the airfoil 2-D cross-sectional geometry. From inspection of Figure 17 it can be seen that the inflow angle of an element may be expressed as a function of the geometric angle or, assuming small angles, as a function of the airfoil drag-to-lift ratio as follows,

$$\phi = \alpha - \theta = \frac{C_d}{C_l}. \qquad \textbf{4.3}$$

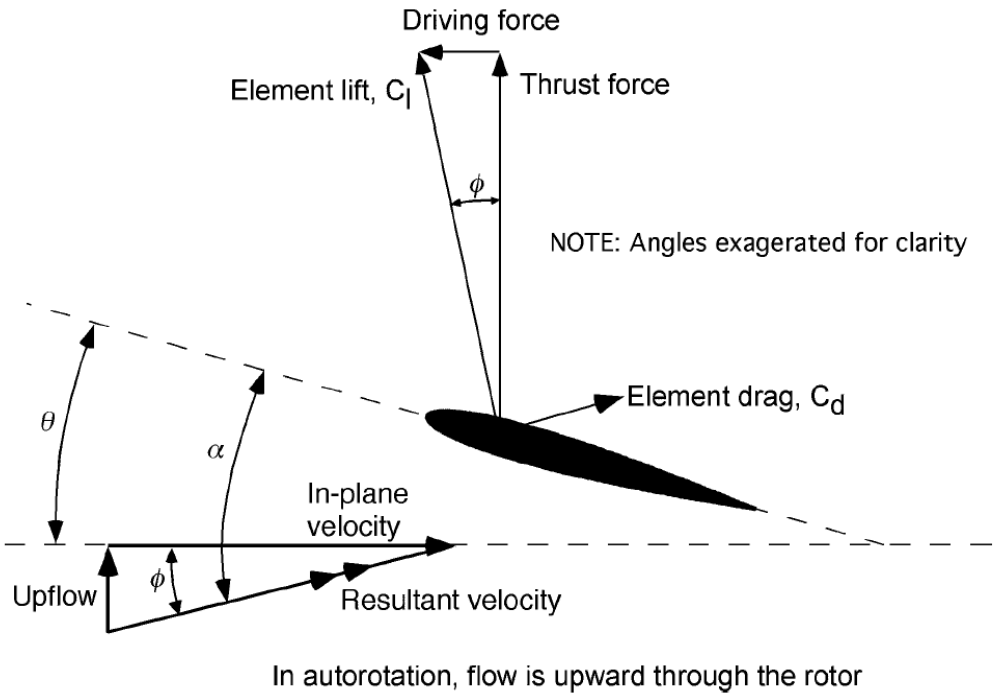

Figure 17: Detailed Blade Element Flow in Autorotation [38]

In the fully established autorotational state, an element will seek to find an equilibrium velocity such that the net force becomes zero. This phenomenon is illustrated with a plot that shows the 2-D airfoil ratio of C_d/C_l versus angle of attack, shown in Figure 18. This representation is referred to as an autorotational diagram, and provides insight into the relation between collective setting and inplane forces [68]. Recall the section equilibrium requirements from Equation 5.3, which for a given θ is a line at 45° on the C_d/C_l versus α plane. The intersection of this line with the curve of the airfoil drag-to-lift ratio

determines the angle of attack for which equilibrium is achieved. If the blade section operates in the concave region of the curve (point a) the angle ϕ is greater than C_d/C_l, then the forward component of the lift vector is greater than the drag force causing the blade to accelerate. If the blade section operates in the convex side of the curve (point c), then the angle ϕ is less than C_d/C_l and the drag force is greater than the forward component of the lift vector and the blade decelerates. The autorotation diagram is for a single element, however a complete rotor blade and the integrated forces along the span exhibit the same behavior; Ω will self adjust until zero torque equilibrium is obtained.

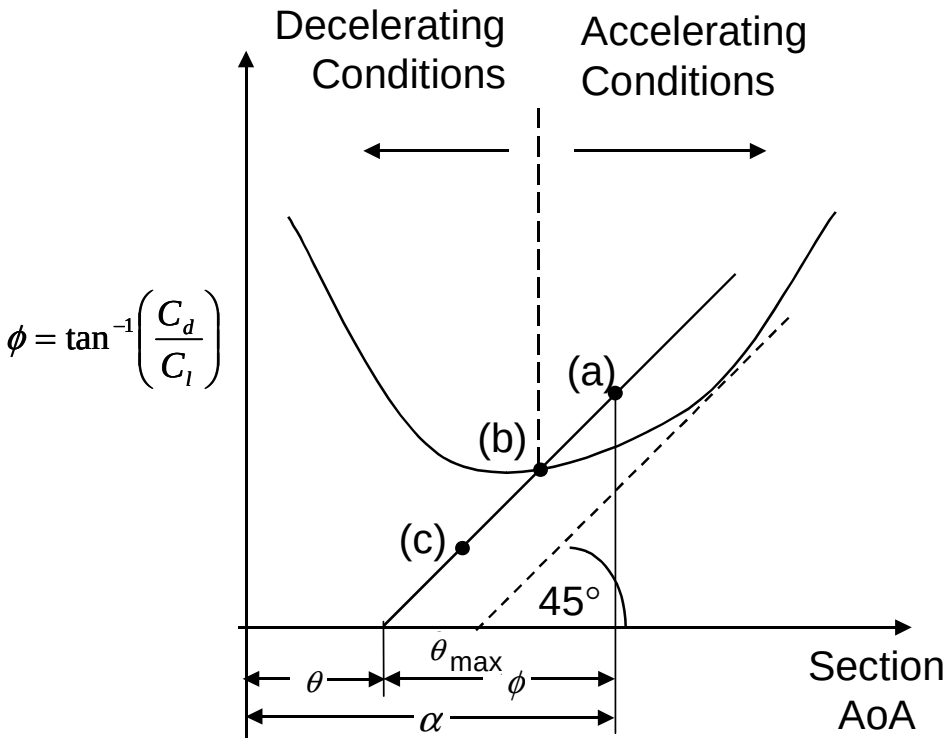

Figure 18: Autorotational Diagram

The autorotation diagram shows that there is a maximum collective pitch angle θ_{max}, above which equilibrium is not possible. When the angle of attack is high because of the high collective, the rotor stalls and not enough lift becomes available to balance the decelerating torque created by the high drag. The tangent to the curve represents a discontinuity; any point above or below the point would result in the rotor quickly decelerating to a stop. In helicopter engine out conditions, the pilot must quickly

decrease the collective to move from the right side of the tangent, where autorotation can not occur, to the left side for a safe recovery. Reference [69] explored the autorotative stability of a rotor in the presence of gusts and showed that a rotor operating close to the tangent point on the curve, when subject to a gust or some other type of disturbance, can penetrate the region where autorotation discontinues, causing a disastrous decay of rotor speed. Therefore, some limit less than θ_{max} must be placed on the practical collective setting to allow for such disturbances and maintain stable operation. Reference [70] found the value of approximately 4˚ collective to provide such margin.

In general, autorotational equilibrium is a condition that exists at only one or two radial locations. Some portions of the rotor absorb power from the free stream and other portions will consume power in such a way that the net torque at the rotor shaft is zero. i.e. $\int_0^R dQ = 0$ [71]. In autorotational equilibrium the induced angles of attack over the inboard portions of the blade are relatively high due to low Ωr. Conversely, the induced angles of attack near the outboard portion of the blade are relatively low as Ωr grows large. The higher induced angle of attack at the inboard portion of the blade yields a forward inclination of the lift vector providing a propulsive component greater than the profile drag. Therefore the inboard region has a net driving torque that is said to generate power. Toward the tip of the blade where ϕ is lower, the rotor sections consume power because the small values of ϕ result in a lift vector that has a forward component less than the profile drag component. In this region a dragging torque is produced; the rotor is driven. See Figure 19.

4.2 Numerical Method for Variable Rotor speed

Rotor speed in forward flight is determined by the torque equilibrium of the entire rotor as the blades rotate around the azimuth. At any given instant, the time rate of change of rotor angular momentum is the sum of the moments integrated on all the blades.

$$I_R\dot{\Omega} = \sum_{i=1}^{B}\int_0^R (L\cos\phi - D\sin\phi)rdr \qquad \textbf{4.4}$$

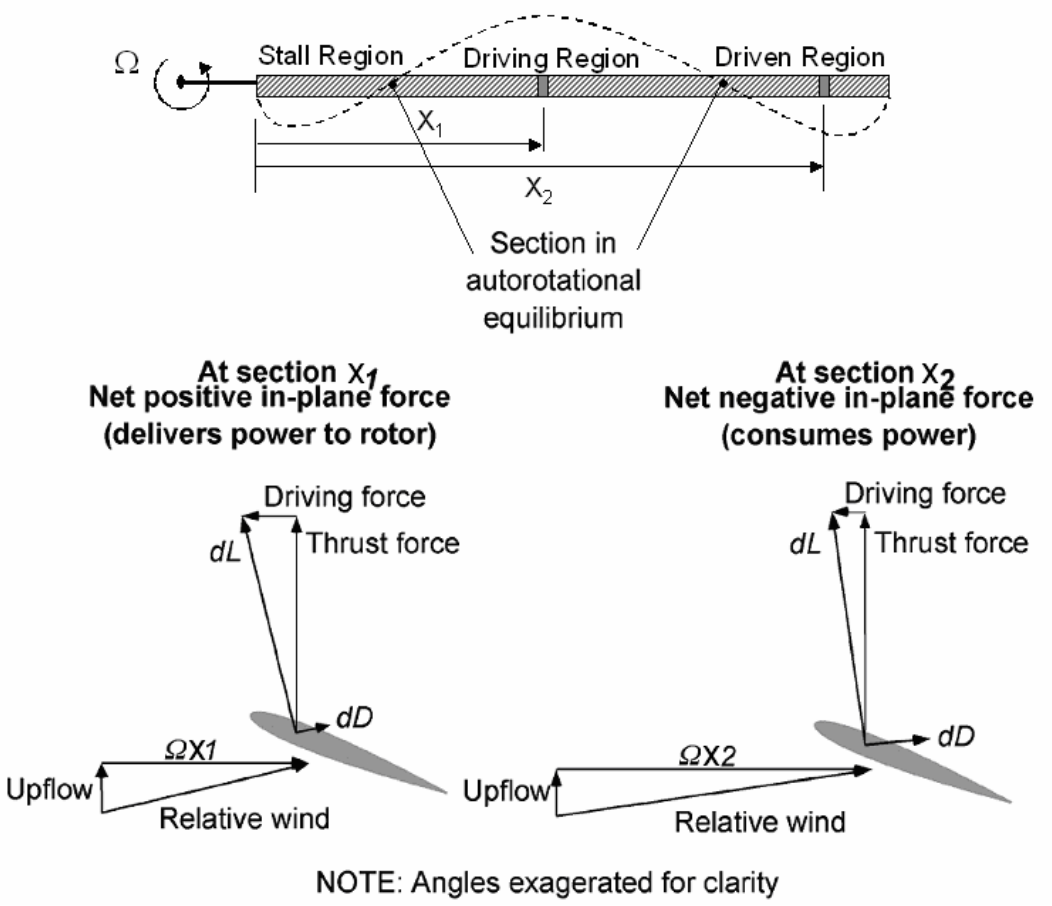

Figure 19: Driving and Driven Regions [38]

Computation of the integrated forces along the blade span at their respective azimuth locations in forward flight is much more complex than vertical flight due to the stall, normal and reverse flow regions. Numerical methods are best suited for the inclusion of all the flow regions including non-uniform inflow and unsteady effects. The methods used to achieve a trim solution for numerical rotorcraft methods are discussed briefly in 2.1. The trim constraints (for any method) are discussed in 1.1.4, and are re-presented for reference.

$$h_m = \frac{1}{T}\int_0^T \bar{h}_m(x_j, X_n)dt + \hat{h}_m(x_j, X_n) \qquad \textbf{4.5}$$

The constraint is on the average, or the zero order harmonic of some state from the model, usually a force or moment. By observation of Equation 4.5 it is obvious that the value of the period (T) must be known to determine the value of the constraint, and thus determine if the trim conditions are satisfied. Most trim methods perform a direct computation of Equation 5.6 to compute the residual for a type N-R iteration. The autopilot method requires an indirect computation of 5.6, typically through some type of error signal filtering to minimize an oscillatory error signal, usually a type of Fourier method which requires the period to be specified. For a helicopter where the rotor or engine speed is fixed as a design parameter, the period is known. However, the rotor speed in autorotative flight is not known a priori, and some changes are required of the trim methodology to accommodate variable and unknown rotor speed.

An approach that is a fairly simple adaptation of any trim method employing a N-R type iterative method is to use the rotor speed as a trim control parameter. Recall from Equation 1.5 that by definition, a trim control variable does not change with time. A constant rotor speed can define the shaft 'boundary condition' as

$$\dot{\psi} = \Omega \qquad \textbf{4.6}$$

$$\psi_i = \psi_{i-1} + \Omega \Delta t \, .$$

The rotor speed Ω can be used as a trim control variable, X_i, in Equation 1.1. The trim constraint is that the average torque vanishes.

$$\sum_{i=1}^{B} \int_0^T \int_0^R (L\cos\phi - D\sin\phi) r dr \, dt = 0 \qquad \textbf{4.7}$$

Therefore, because Ω is specified for each periodic solution, the period T is known and the computation of the constraints can be accomplished. Over the trim iterative process, the rotor speed is varied in a controlled manner until the zero average torque condition is satisfied, along with other trim conditions which may exist.

One particular advantage of this approach is that if the user specifies initial conditions that are in the region where autorotation can not exist, see Figure 18, rotor speed will not rapidly decay; rotor speed is driven and the torque is a fall out. However, if collective control is set too high for autorotation a zero torque solution is not physically possible and the N-R method will never converge to satisfy all the constraints. Nonetheless, when collective is fixed at some value that does allow autorotation, the rotor speed controlled to zero average torque method is quite effective.

One caveat must be mentioned about the trim solution arrived at when using this approach. That is the *average* torque is zero, but the *instantaneous* torque may not be zero. Rotor speed is controlled as a constant value for each time step, which is an artificial 'boundary condition.' Observation of Equation 5.4 indicates that in fact the rotor speed can be non-constant for a fixed period of operation. Therefore, when the relatively small rotor speed oscillations are unimportant, as in the computation of rotor forces and moments, this approach is adequate. However, when rotor loads, especially blade chordwise moments and forces, are sought from the trim solution, the values may not be accurate for the controlled rotor speed method. In this case, a two part trim can be utilized that first trims the average torque to zero with a specified rotational constraint and then adds additional drive-train degree of freedom once the period is known. An example of this is provided in the next section.

4.3 Rotor Speed Correlation

To validate that the autorotative trim method accurately reflects the rotor speed variation, two trim correlation cases are presented which compare the analytical prediction of rotor speed to test data. A search of the literature to identify data for correlation proved that indeed data on autorotating rotors is sparse. Nonetheless, two data sets were identified, one from 1935 and the other from 2003. The first is an isolated rotor with data from a wind tunnel test. The second is a full gyroplane vehicle with data from flight test.

4.3.1 Isolated Rotor Trim

The first validation effort correlates model predictions using the rotor speed as a control variable with test data from 'Wind-Tunnel Tests of a 10-foot-Diameter Gyroplane Rotor' [72]. The reference contains data from a 10 foot diameter autorotating rotor from zero advance ratio to 0.80 advance ratio and includes thrust coefficient, cyclic control, and shaft tilt. The rotor physical parameters are listed in Table 12. The rotor is of the rigid type, that is to say it does not have articulated blades with flapping hinges. Rather, it has a system of cams that feather the rotor cyclic to trim out the moments, essentially a different incarnation of a modern swash plate. The rotor cam system only has feathering capability for the roll axis, and after the lateral roll moment is trimmed out a pitching moment still exists. Collective pitch was obtained with shims inserted between the hub forks and blade butts, with a collective range from 0 to 6 degrees. At high collective settings the feathering motion required for zero roll moment at advance ratios greater than 0.45 is reported to exceed the mechanism capability. At lower advance ratios, below 0.10, the rolling moment was reported to be unsteady (most likely due to turbulence as the rotor operated in the turbulent vortex ring state), and the feathering control could not be effectively employed. For these reasons, the test data between advance ratios of 0.15 and 0.45 is believed to be the best set for model validation; only data over this range is used for correlation.

Table 12: 10 Foot Diameter Wind Tunnel Rotor Properties

Parameter	Wind Tunnel Rotor
Diameter	10.04 (ft)
No. Blades	4
Twist	0 (deg)
Chord	6.28 (in)
Airfoil	NACA 0015
RPM	550 (ft/s)

A model of the rotor was constructed in RCAS consisting of rigid blades and θ_{1s} cyclic. Rotor airfoil data for the NACA 0015 rotor was obtained from Reference [73]. The rotor inflow used was a dynamic model developed by Peters and He [74], and validated for

application in autorotation for advance ratios above 0.10 by Houston and Brown in Reference [75]. The inflow model consisted of 15 inflow states with the intent of capturing effects from inflow non-uniformities over the rotor disk.

The method used to gather data from the test rotor was such that the rotor speed was held constant. That is for a given tunnel wind speed and collective setting, the shaft was tilted and feathering adjusted such that the rotor speed obtained the desired 550 rpm, in addition to zero roll moment. The intent of this correlation was to use the measured shaft angle and cyclic feathering input to correlate the predicted rotor speed with test value of 550 rpm. This method proved difficult for two reasons. First, the precise shaft angle was difficult to determine from the report at certain advance ratios due to low resolution plots and many data curves overlaid in the same vicinity as shown in Figure 20. And second, the rotor speed is highly sensitive to shaft tilt angle. Therefore, the correlation was carried out in the following two step method. First, a two variable trim was conducted using lateral cyclic and shaft tilt as trim variables to achieve a zero shaft torque and zero roll moment condition at 550 rpm, essentially duplicating the trim method of the wind tunnel test. Second, at a particular advance ratio and collective setting, the shaft angle from the first step was fixed, and rotor speed and cyclic were used to trim for zero torque and roll moment; initial rotor speed was set to be ± 20% of the target 550 rpm.

The trimmed shaft angle from the model is presented in Figure 21 for the collective settings from 0˚ to 6˚. From visual inspection of the test shaft trim angles in Figure 20, the model captures the essential behavior of the test data. The 6˚ collective case failed to reach a converged solution for $\mu \geq 0.275$. The test report states that high collective cases could not be trimmed as the rest due to cyclic feathering mechanism limitations, with the effect most likely manifest in 6˚ collective model results. The trimmed cyclic control value is also compared to the test values for the range of collective settings shown in Figure 22. These results in general show an excellent correlation, indicating the model captures the cyclic trim quite well. The model thrust coefficient results are compared with test data in Figure 24. In general the model captures the rotor thrust trend. The

higher collective conditions are slightly under predicted by the model as are the low advance ratio condition for all collective settings.

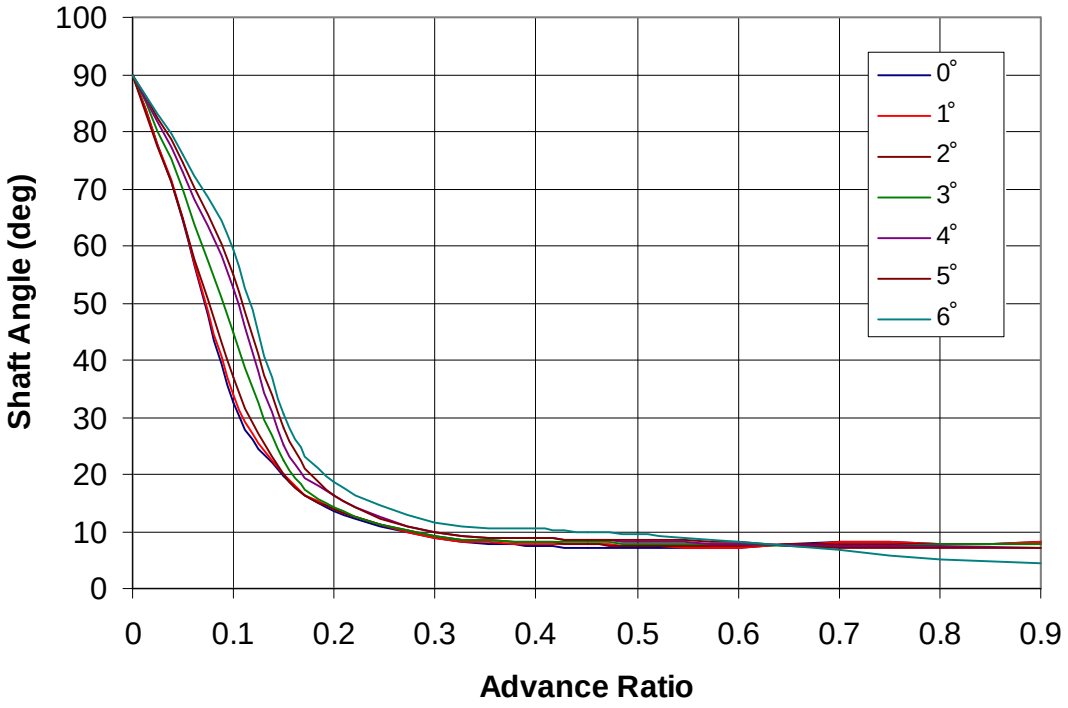

Figure 20: Isolated Rotor Shaft Angle vs. Advance Ratio Test Resluts

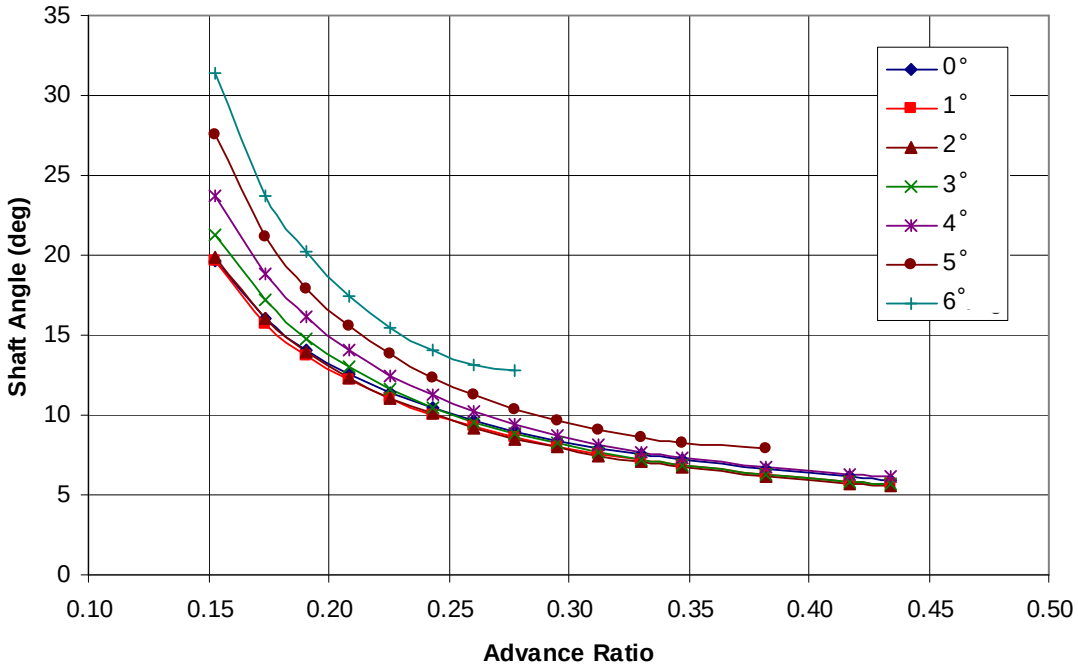

Figure 21: Isolated Rotor Shaft Angle Model Prediction

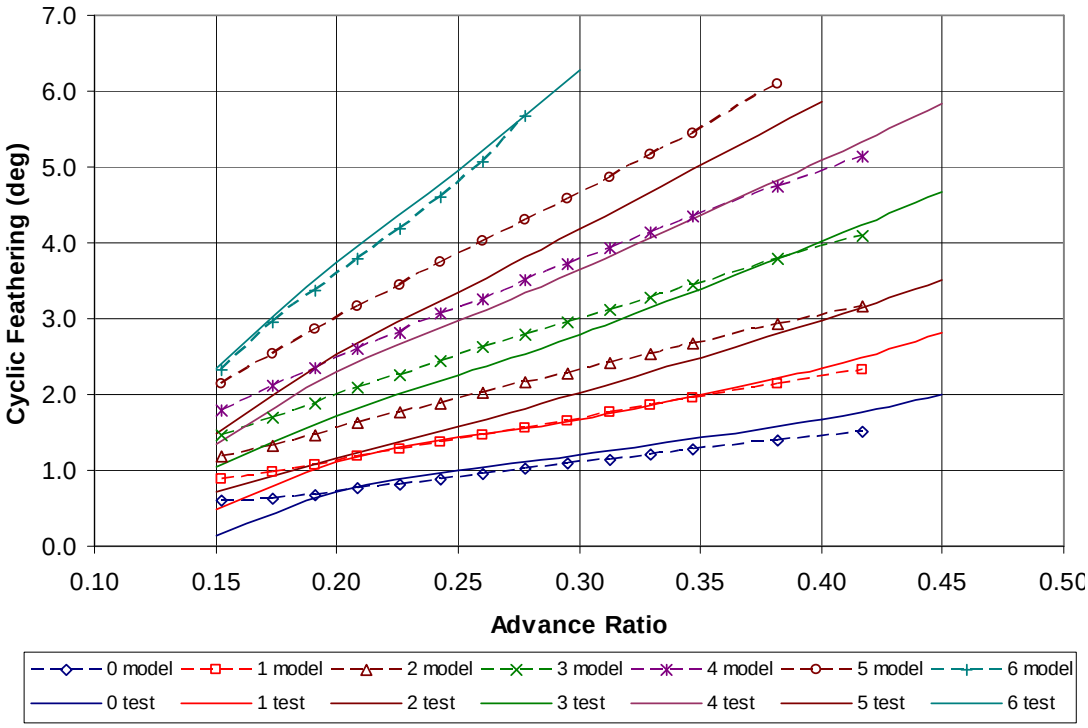

Figure 22: Isolated Rotor θ_{1s} Correlation

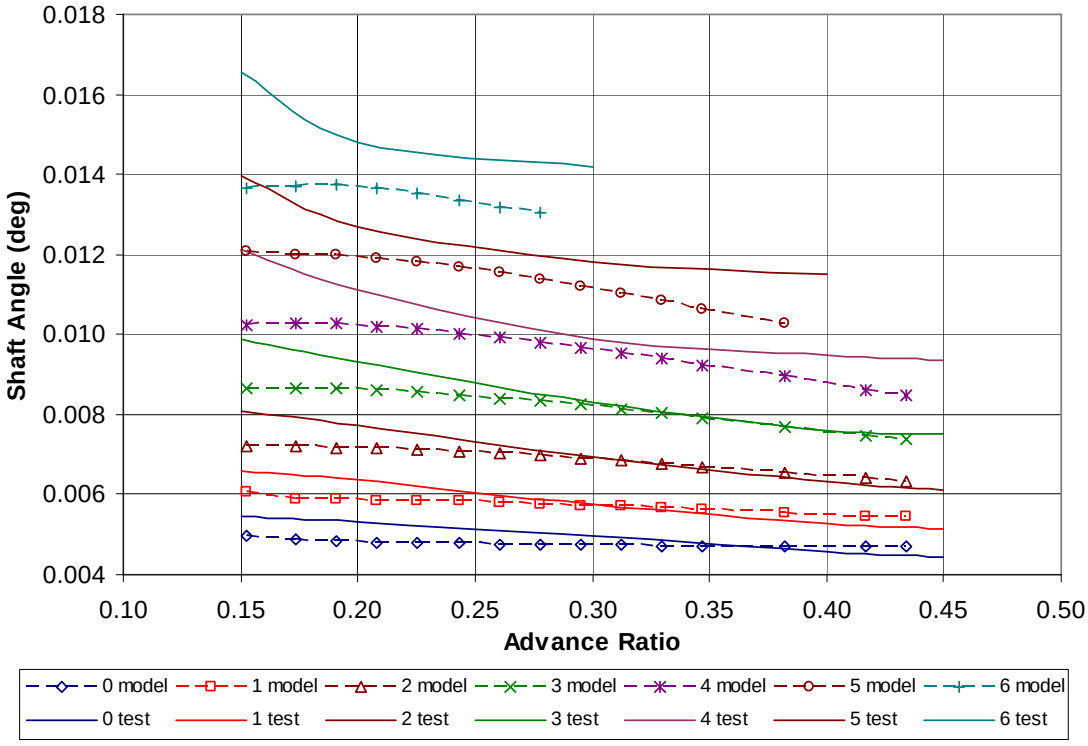

Figure 23: Isolated Rotor Thrust Coefficient Correlation

The rotor speed trim results for all collective settings are presented in Figure 24. The test rotor speed was 550 rpm and the chart shows the 0 collective setting at 550 rpm with each collective setting offset by 10˚ to avoid data overlap. In general, the results show the trimmed rotor speed to be within 10 rpm of the test value, indicating the method captures the variable rotor speed physical behavior within 3%. The report lists the accuracy of measured parameters to be within ± 3% to 4%, approximately the same accuracy as the model results.

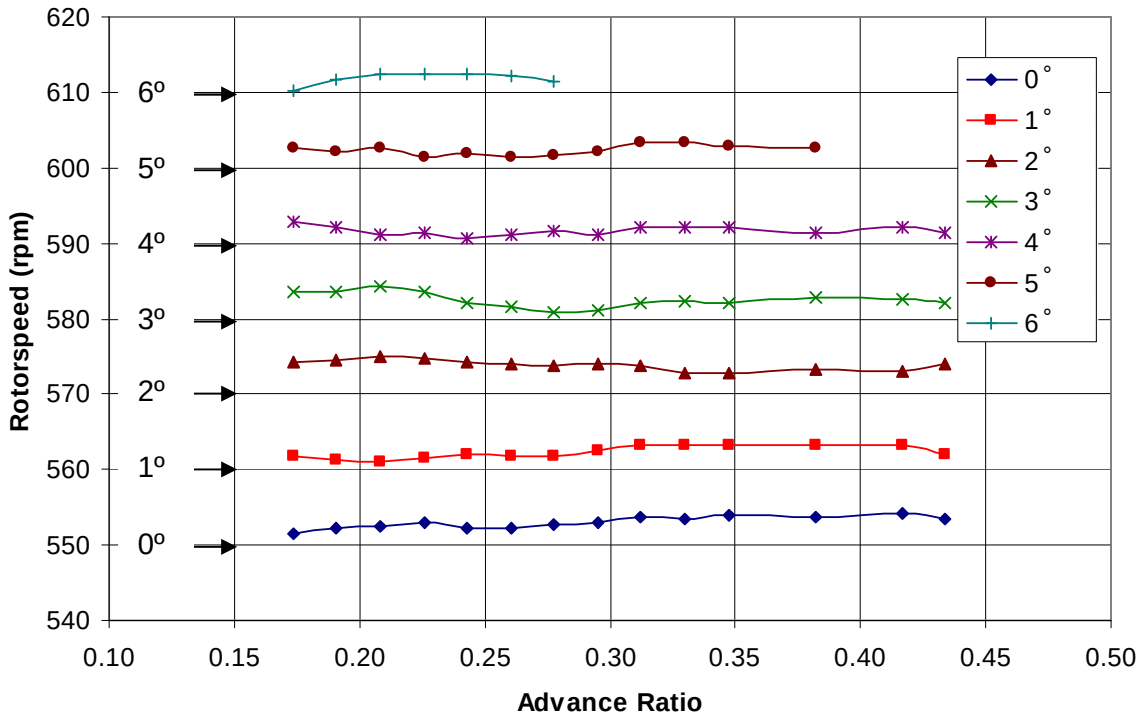

Figure 24: Trimmed Rotor Speed Model Resluts

The initial rotor speed was set to ± 20% of the target rotor speed for all cases to verify the method works for both high and low rotor speed initial conditions. Figure 25 and Figure 26 show the rotor speed and rotor torque respectively as a function of N-R trim iterations at $\mu = 0.29$ when initial rotor speed is above the zero torque speed. Likewise Figure 27 and Figure 28 show the same results when the initial rotor speed is lower than the autorotative condition. Again, these results indicate that utilizing rotor speed as a trim control is quite effective in reaching autorotative trim, as shown by correlation to test data.

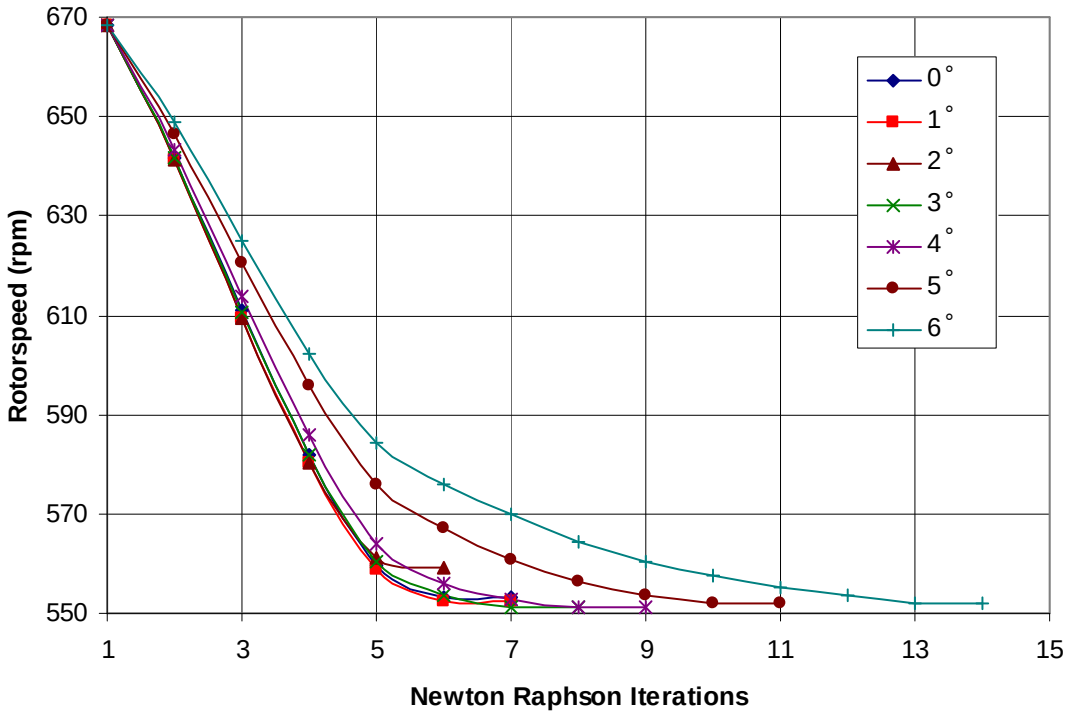

Figure 25: Rotor speed Convergence from 120% Nominal Rotor speed at μ = 0.29

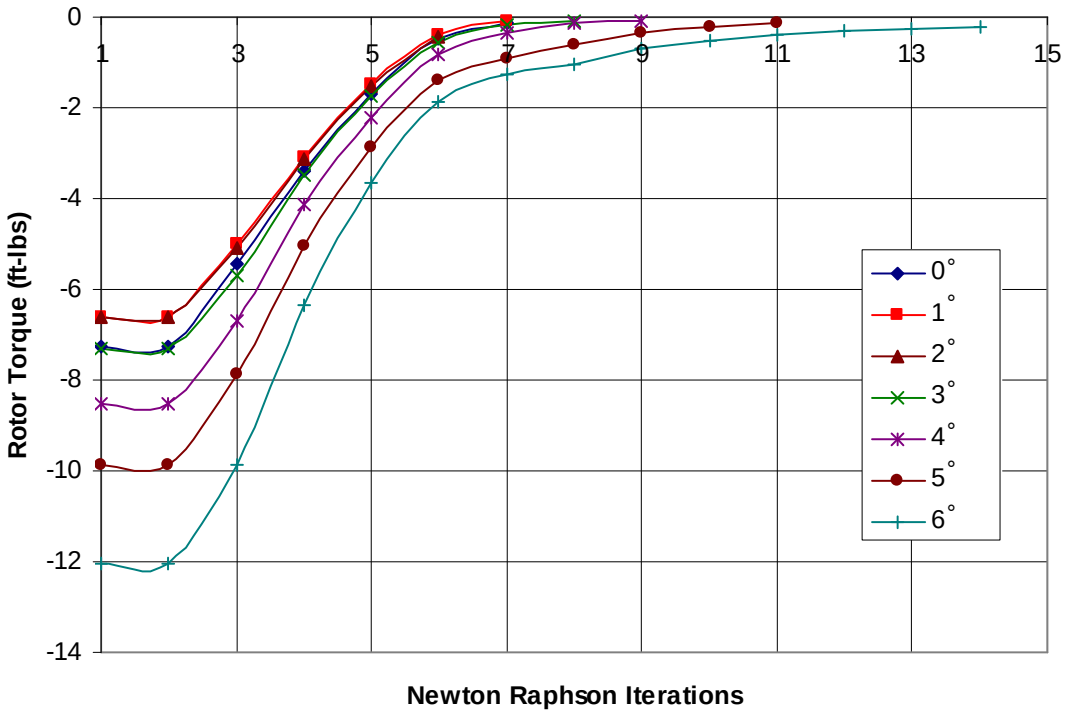

Figure 26: Rotor Torque Convergence from 120% Nominal Rotor speed at μ = 0.29

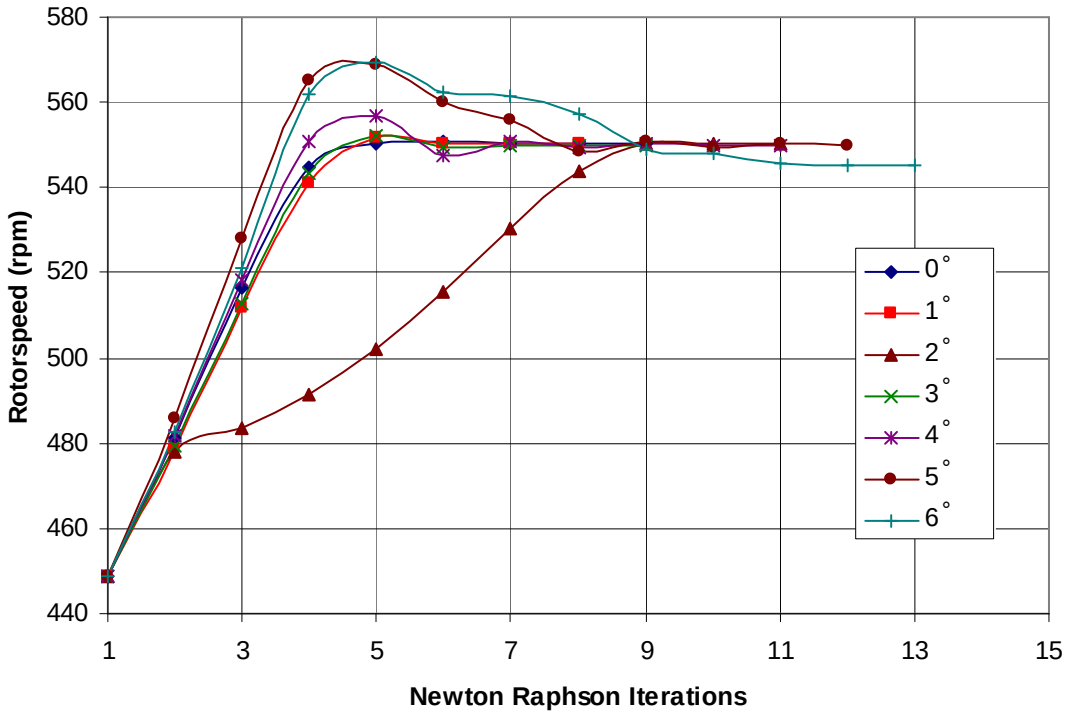

Figure 27: Rotor speed Convergence from 80% Nominal Rotor speed at μ = 0.29

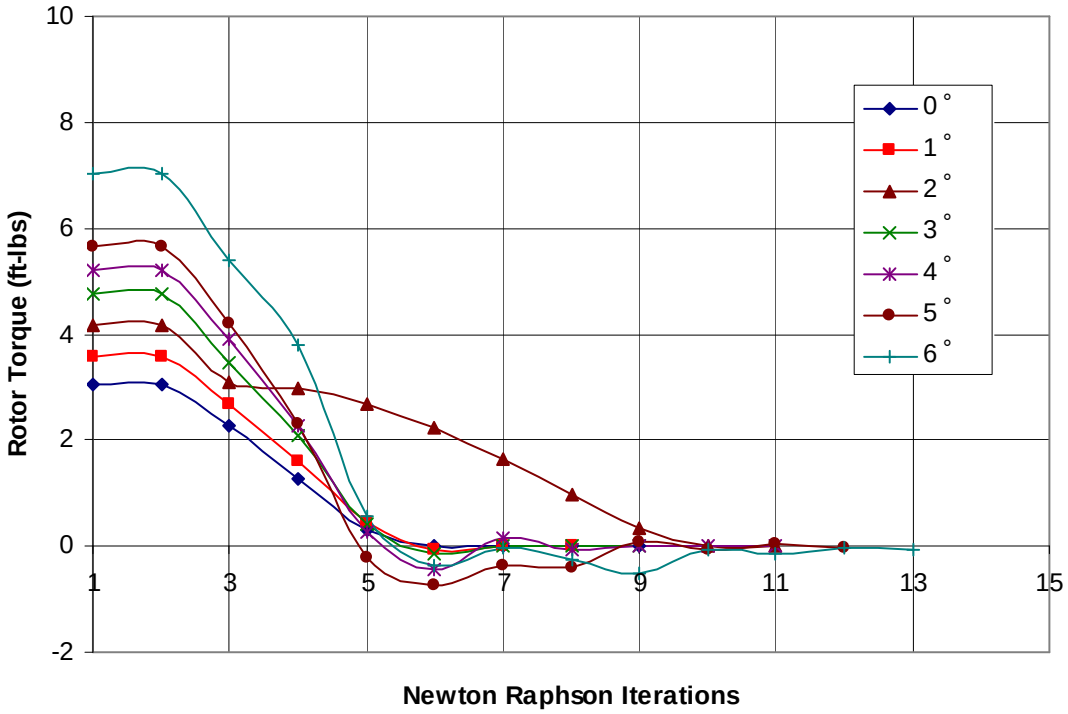

Figure 28: Rotor Torque Convergence from 80% Nominal Rotor speed at μ = 0.29

The model inplane force (pounds) distribution of the trimmed autorotative rotor is shown at four advance ratios: 0.15 through 0.42 in Figure 29. These figures are given to visually show the driving and driven regions and the change of these regions with advance ratio. As is typical for a rotor in autorotation, the driving region starts to shift to the retreating side of the disk and the driven region starts to shift to the right. The stall region also shifts left, remaining inside the driving region. The progression becomes more pronounced with advance ratio, until at an advance ratio of 0.41, almost the entire advancing side is driven. The retreating side is dominated by stall on the inner portion and driven region elsewhere. One other noticeable trend with the inplane force distribution is the development of a strong driving region near 180 degrees and a weaker driven region near 0 degrees azimuth. These regions are most likely due to the fact that the rotor was not trimmed for zero pitch, only zero roll. Therefore the asymmetric aerodynamic forces also manifest themselves in this inplane force distribution pattern.

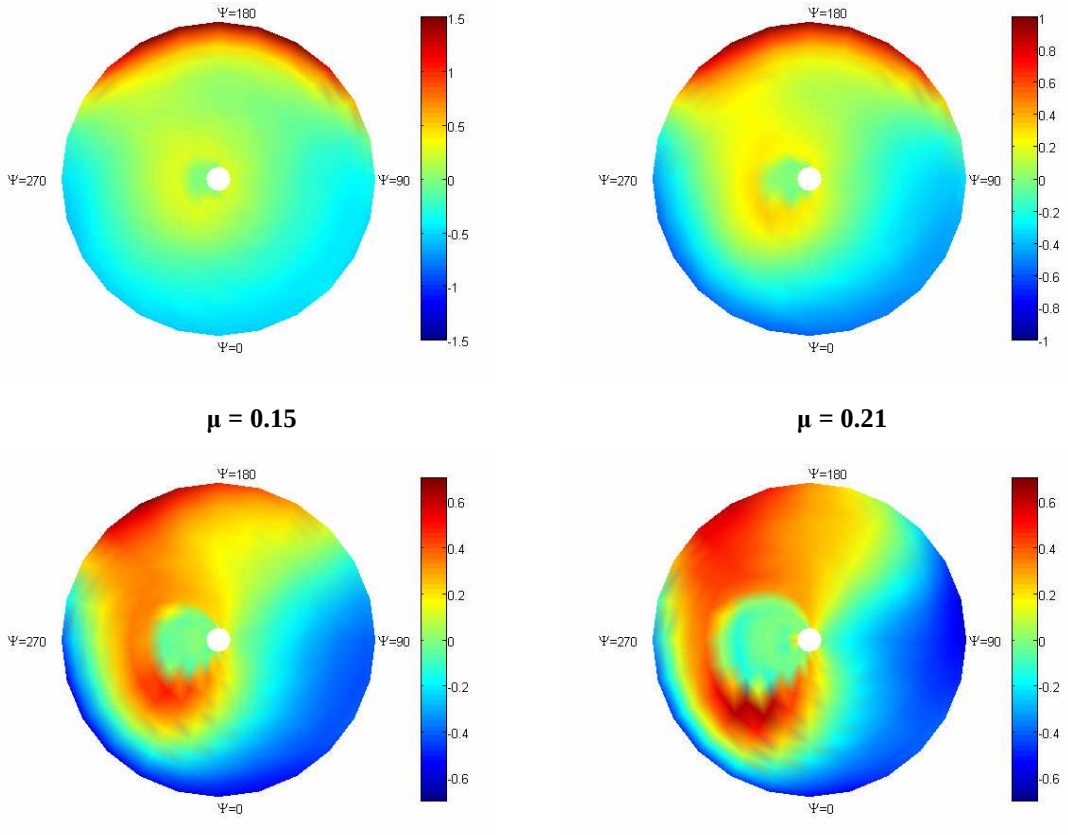

μ = 0.15 **μ = 0.21**

μ = 0.31 **μ = 0.42**

Figure 29: Inplane Force (lbs) Distribution at Advance Ratios 0.15 through 0.42

Finally, recall that treating the rotor speed as a trim control parameter trims to an average torque value. Because the rotor speed is constrained to a constant value, rotor speed dynamics are suppressed and shaft torque at various points around the azimuth is non-zero. The effect of using a constant rotor speed with average torque on the accuracy of the rotor forces and moments is negligible. However, it will impact the accuracy of certain loads. Figure 30 shows the periodic torque with two drive-train constraints, one with constant, controlled rotor speed and another with an additional variable in the drive-train model, with no external torque input. The periodic torque varies when rotor speed is constant, but is zero for the additional degree of freedom. For forces and moments that are sensitive to the periodic torque, such as inplane 1-D beam loads, a two-step trim process may be required.

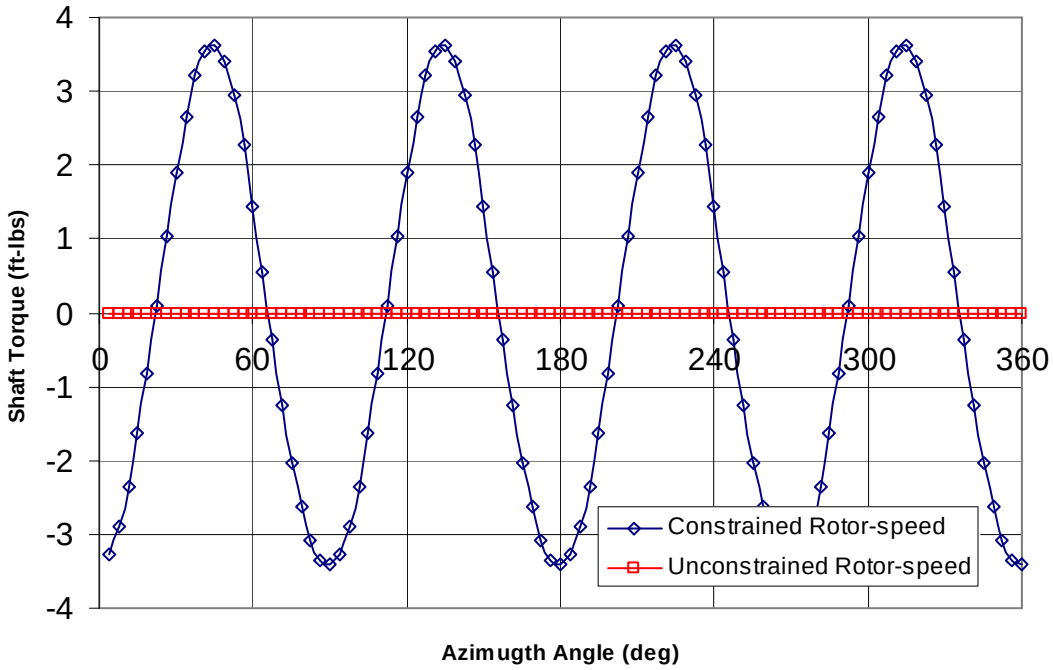

Figure 30: Periodic Shaft Torque with Two Shaft Boundary Conditions

4.3.2 6 DOF Vehicle Trim

A second full vehicle 6 DOF trim was also correlated against flight test data from a small two place recreational gyroplane, a VPM M16 shown in Figure 31. The flight testing was done to investigate the dynamic stability and control characteristics of the aircraft,

specifically investigating the influence of the rotor speed degree of freedom on stability [76,77,78]. Steady level flight data was obtained and recorded with on-board data acquisition sensors and recording equipment. Pitch attitude, flight speed, control positions and rotor speed were recorded. The significant design parameters are given in the references and are listed in Table 13.

Table 13: VPM M16 Properties

Parameter	VPM M16
Empty Weight	595 (lbs)
Gross Weight	992 (lbs)
No. Blades	2
Radius	14 (ft)
Twist	0 (deg)
Chord	.728 (ft)
Airfoil	NACA 8-H-12
Hub	Direct tilt, teetering

Figure 31: University of Glasgow Instrumented Gyroplane

A model of the VPM M16 was constructed in RCAS utilizing the published data. The airfoil data for the NACA 8-H-12 was obtained from Reference [79]. The fuselage aerodynamic characteristics of the VPM M16 were obtained from a wind tunnel test in Reference [80] and were incorporated into the model. The two-blade rotor is of the

teetering type. The teeter hinge is modeled as a revolute joint with the two blades rigidly attached to it. In this manner, the equations reflect the physical condition of the blades being attached at the teeter axis, such that as one blade flaps up, the other simultaneously flaps down. No elastic properties for the blade were provided and the blades were therefore assumed to be rigid in the model. The hub control configuration was of the direct tilt type. The pilot controls directly tilt the hub axis of rotation for and aft or side to side in the fixed frame, rather than input cyclic control through a swash plate into the rotating frame. The collective pitch is fixed; the pilot can not change it on the ground or in flight. The inflow model consisted of 15 states, capturing radial and azimuthal variations in the induced velocity.

Analysis results are compared against test data in Figure 32 and Figure 33. Test data of the parameters were collected for two gross weights, however the data points are not specifically identified which gross weight they reflect. The model prediction results are shown for the maximum weight condition. The model pitch attitude results correlate within reasonable uncertainty to the pitch attitude data. Additional data from test included lateral and longitudinal stick position. The general slope trends from the model matched the data, but the maximum and minimum stick positions were not given in absolute angles, and the data could not be directly correlated to the model output. The rotor speed trend also shows good correlation to the data, with the exception of a reduced slope as a function of forward speed. This difference may stem from two sources. First, elastic effects of the rotor are neglected in the model and may be significant. More likely is the fact that the airfoil data used was not reflective of the Mach numbers experienced in flight. The data used from the reference provided 2-D airfoil data for only a single Reynolds number condition. In forward flight, the advancing tip portion of the rotor disk experiences Mach number conditions in the range of 0.55 and the 2-D airfoil coefficients are modified, namely the drag coefficient increases, which would tend to drive up the resulting rotor speed. The difference between the data and the model prediction increases slightly with airspeed. Therefore, the difference is believed to be the limited 2-D airfoil data for the NACA 8-H-12 airfoil. However, the rotor speed trim method still captures the variable rotor speed quite well, validating the method.

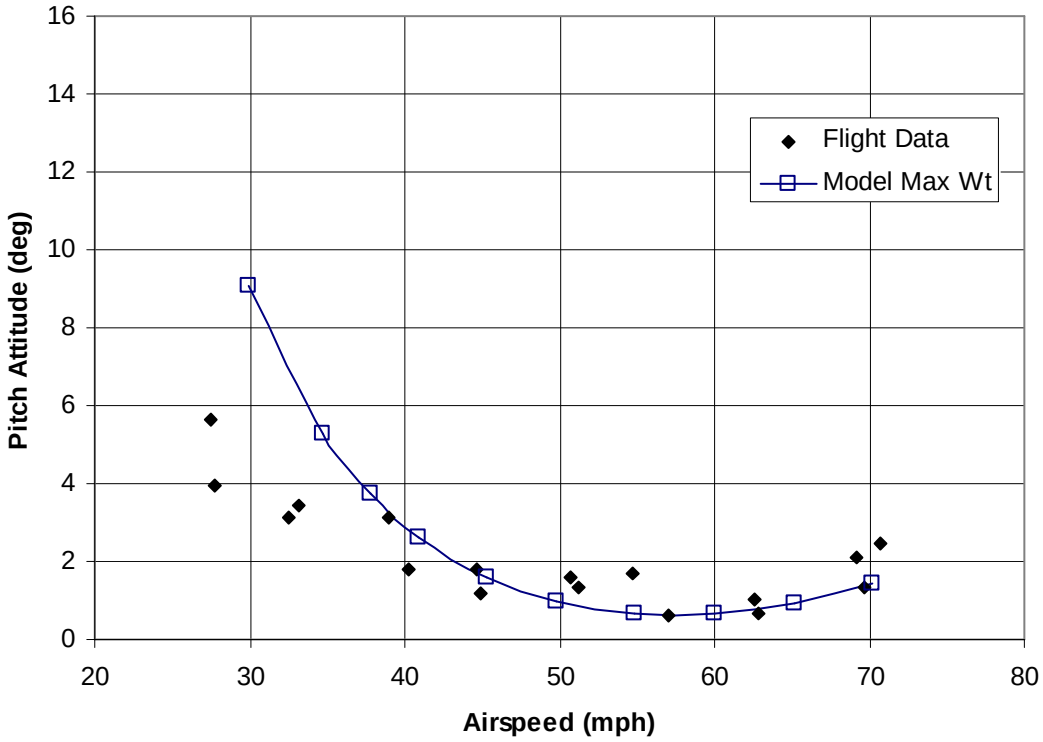

Figure 32: Pitch Attitude Correlation of Flight Test and Model

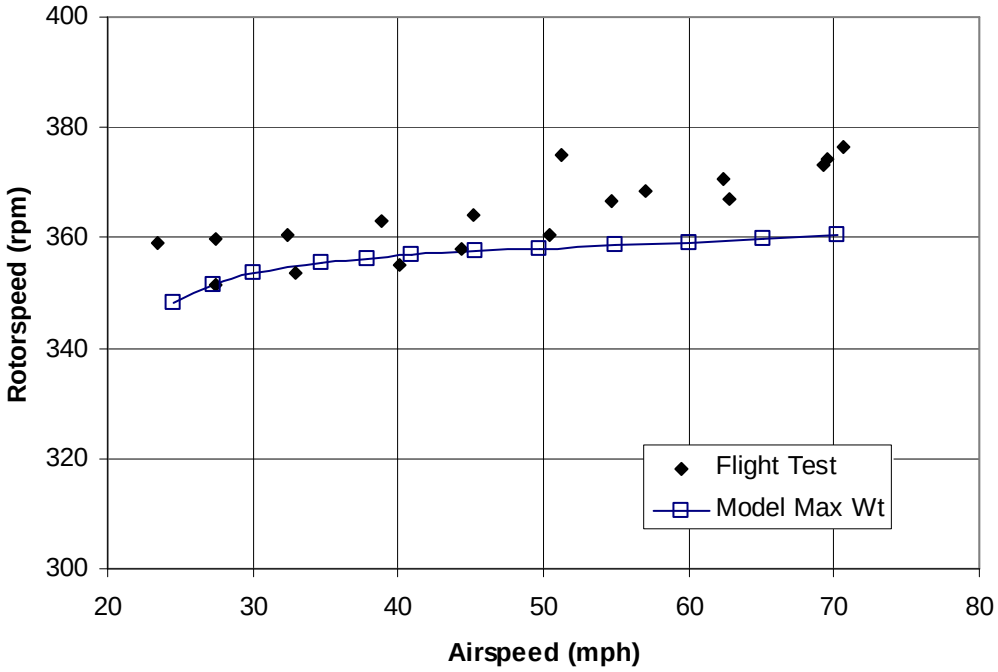

Figure 33: Rotor speed Correlation of Flight Test and Model

4.4 Optimal Trim Application to Autorotation

The trim solution space is nonlinear, and multiple trim solutions are possible. The solution for zero torque autorotative trim is an example of a trim problem with multiple solutions. Figure 34 shows the shaft torque of the wind tunnel rotor from section 4.3.1 at constant rotor speed plotted against shaft angle. The collective setting is -1 degree, airspeed is 200 ft/s, and the roll moment is trimmed to zero as before. In the figure positive torque means power is extracted from the flow, while negative torque requires power in. The nonlinearity of the trim space becomes obvious as the torque crosses zero at two locations. Note at one zero lift is positive, approximately 50 pounds; and at the other zero lift is negative, at 40 pounds. These solutions represent the physical condition that rotors can autorotate with either positive or negative lift, depending on the inflow direction. The solution space is nonlinear and the converged solutions of typical trim processes depend highly on the initial conditions. For example, if the initial shaft-tilt setting is too low (yet positive), the final trim solution may converge to a negative rotor lift condition. If positive lift is required, the initial conditions will require adjustment, and larger initial shaft tilt will converge at positive lift.

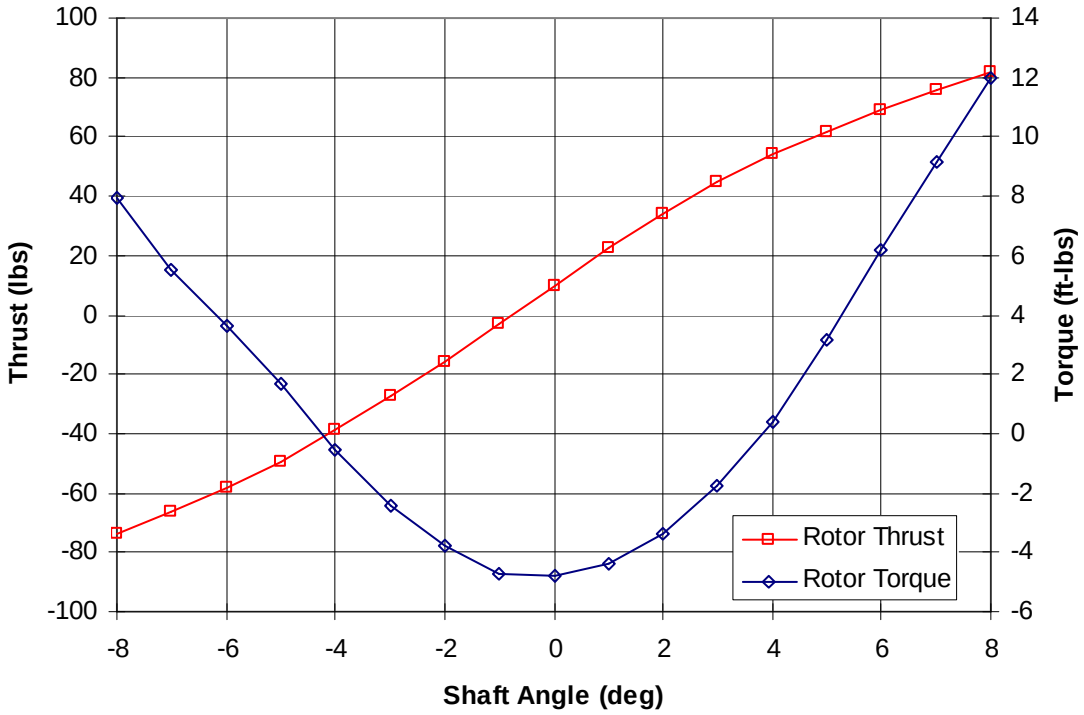

Figure 34: Rotor Torque and Lift vs. Shaft Angle

Typically, the autorotation condition that is sought is the one where lift is positive on the rotor; however, the convergence to this particular solution is entirely dependent on the initial conditions. Initial conditions that guarantee a particular trim solution when more than one exists are unknown. Using optimal trim, the converged solution can allow a favorable solution when multiple solutions exist, however the solution space must be continuous. The solution space in Figure 34 is not continuous, only two point solutions exist for the fixed rotor speed condition. If the rotor speed is not constrained, as in free autorotation, a continuous solution exists. Figure 35 shows the rotor thrust and rotor speed for the same rotor and airspeed as Figure 34, however every point across the range is a zero torque, autorotation solution. Therefore, since the solution is continuous, the trim solution can be optimized in a number of ways. For the wind tunnel rotor at this airspeed condition, the rotor lift-to-drag was maximized, guaranteeing positive lift. The optimum lift-to-drag ratio results in a value of 8.8 at a shaft tilt angle of 4.29 degrees.

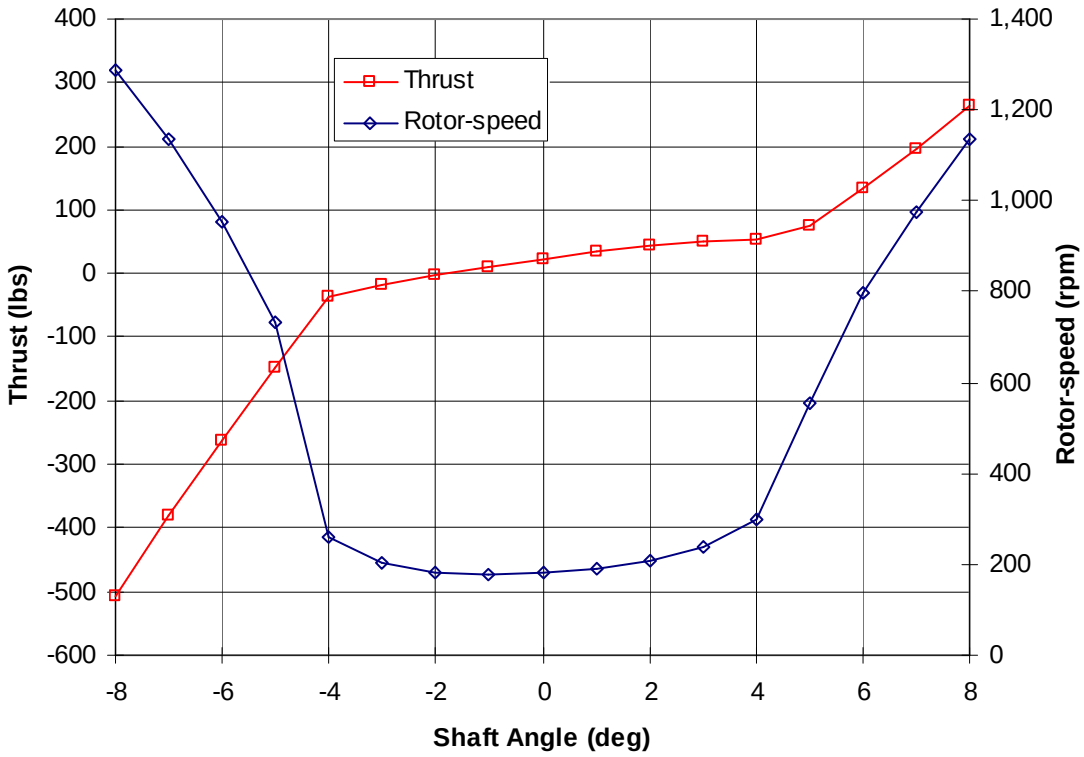

Figure 35: Rotor speed and Lift vs. Shaft Angle

4.5 Chapter Summary

The phenomenon of autorotation is discussed with specific reference to the fact that rotor speed varies as steady flight conditions change and its value is not known a priori. A method is developed which captures rotor speed variation by controlling rotor speed as a trim control parameter in a Newton-Raphson iterative method. The method is validated against isolated wind tunnel rotor data and steady level flight of a small gyroplane. Application of the optimal trim method allows rotor speed to vary as an independent variable rather than a dependent variable and still satisfy the requirement of zero average torque in conditions where multiple zero torque solutions exist. These results affirm the hypothesis to supporting question 1 in that *rotor speed treated as a trim control parameter allows the rotor speed to be known during each trim iteration, yet vary between iterations until autorotative equilibrium is reached.*

CHAPTER 5
SURROGATE BLADE STRESS AND STRAIN

In conventional helicopter flight operations, the rotor speed is designed to operate at a fixed value. A constant rotor speed is chosen to avoid a host of dynamic conditions that would increase rotor vibration and blade loads. Rotors that operate over a wider range of angular velocities will surely encounter more diverse dynamic conditions as changes in centrifugal stiffening modify blade structural mode frequencies and increase (hingeless) bending moments. While the design of the rotor must account for the dynamic conditions, there may still exist in the flight envelope dynamic conditions that result in unacceptable loads. An example of one such condition is resonance when rotor primary or secondary structural modes operate in close proximity to multiples of the rotor frequency. Given that rotor blade design information is available, the blade stress/strain values themselves provide the best indication if loads are unacceptably high. A method that can determine the blade stress/strain values from the trim model is desired, where the values themselves relative to material limits become constraints that limit the trim solution space.

This chapter presents a method of capturing blade stress and strain in the trim process to guarantee the optimal trim solution does not exceed stress or strain constraints. The current framework for rotor blade stress/strain recovery is reviewed which shows the aeroelastic rotor loads recovery process to entail a structural domain and a dynamic/aeroelastic domain. A novel concept is introduced which allows the stress/strain to be captured in a surrogate model and computed in time scales that are equal to or less than those required in the dynamic/aeroelastic domain. This chapter concludes by applying the surrogate stress/strain recovery process to a composite rotor blade cross-section where the stress/strain loads are recovered using the VAM tool VABS directly and by the surrogate method, the latter method showing several orders of magnitude reduction in computational time while maintaining sufficient accuracy.

5.1 Rotor Aeroelastic and Structural Analysis Framework

Current rotorcraft aeroelastic analysis frameworks have evolved into two major analysis domains including a structural domain and dynamic/aeroelastic domain as illustrated in Figure 36. The structural component utilizes the dimensional reduction method of VABS and provides sectional mass and stiffness information. The dynamic/aeroelastic analysis is multidisciplinary in nature and includes structures (1-D beam analysis), aerodynamics (3-D inflow and 2-D lifting theory), dynamics (multi-body formulations, trim solutions, stability analysis, etc.) and control disciplines. The 1-D beam analysis utilizes the mass and stiffness information to compute the blade displacements, shear forces and moments which are fed back to the structural tool to recover the 3-D displacement, stress and strain fields. For the application of optimal trim with structural constraints, the recovered stress/strain loads feed back to the trim solution (shown with a dashed line) to ensure the solution does not violate structural constraints, as illustrated in Figure 36.

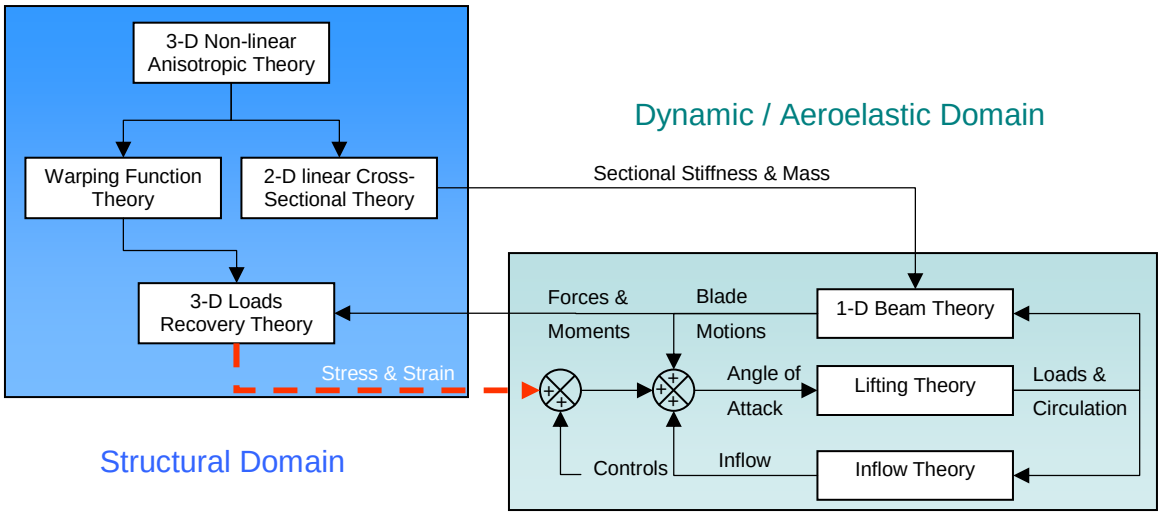

Figure 36: Rotorcraft Aeroelastic Loads Framework

This framework is comprehensive in the sense that it captures the various disciplines in rotorcraft analysis with mathematical formulations that are of appropriate level of fidelity and computationally efficient. The coupling of the structural and dynamic/aeroelastic domains, however, presents some challenges in the feedback required for the trim

solution stress/strain constraints. In particular the computation of stress/strain for the constraint feed forward is not accomplished in time scales that are compatible with dynamic trim solutions. For example, the computation of the 1-D beam analysis generally requires computational time on the order of milliseconds to seconds for each time step, where the 3-D loads recovery generally requires computational time on the order of minutes for each cross-section. A blade typically has multiple cross-sections, potentially driving the structural analysis computational time several orders of magnitude greater than the dynamic analysis. Therefore, from the standpoint of computational time, the structural analysis is incompatible with the beam analysis for real-time feedback for optimal trim. A method that reduces the computation time of the structural analysis of all cross-sections to be on the same order as the 1-D beam analysis is required for real-time feedback for optimal trim. Two additional requirements of such a method are first, the accuracy of the structural analysis is maintained and second, the analysis be performed in the dynamics/aeroelastic tool to eliminate the feedback loops required between multiple tools.

5.2 Surrogate Stress/Strain Method

A novel method is proposed and applied which creates an approximation or surrogate of the recovered 3-D cross-sectional stress/strains that is fed forward from the structural tool to the dynamic/aeroelastic tool (similar to the mass and stiffness information) see Figure 37. The method is based on the concept of surrogate models, where for a given range of input variable values, one or multiple responses can be captured in simple mathematical form for rapid computation. Surrogate models of the analysis problem offer a way to shift the burden from the integration of large interconnected computer programs to the problem of constructing approximations. The models are obtained by sampled numerical experiments over the solution space, using more analysis cases than regression coefficients, thereby over-fitting the regression model using the theory of design of experiments. Surrogate model methods have found wide scale application to numerous fields [81,82,83] in addition to the multidisciplinary rotorcraft problem [84,85].

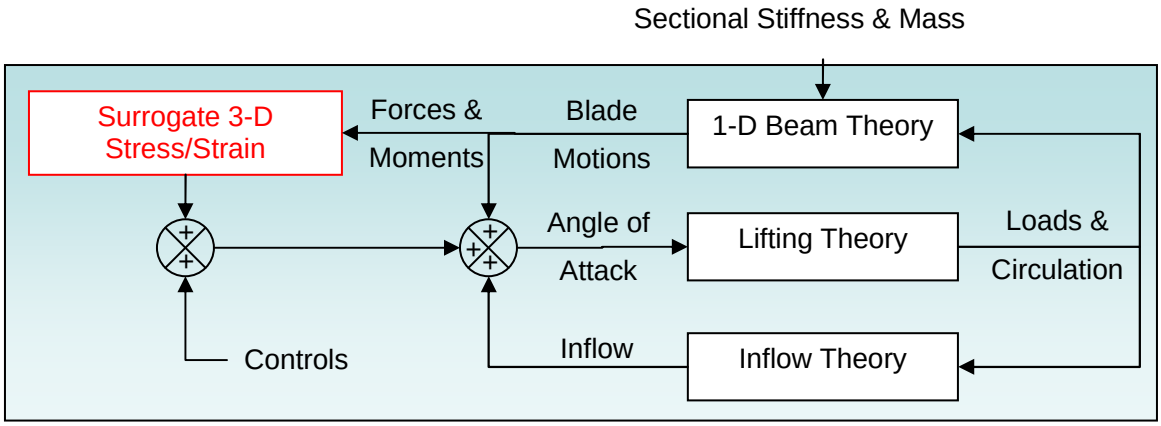

Figure 37: Surrogate Stress/Strain Feedback

In the VAM stress/strain recovery problem, the cross-sectional stress/strain field for a particular spanwise location is primarily defined by six parameters from the 1-D beam analysis: the axial force, two transverse shear forces, axial torsion moment and two bending moments. Therefore, these six parameters become the inputs for the surrogate and define the response. VABS can actually take other secondary effects into account, however, the three forces and three moments listed dominate. The output of the 3-D structural recovery is six stress and strain components at each Gauss point in the 2-D cross-sectional finite element mesh. The number of actual Gauss points therefore depends on the mesh size, which may range from several thousand to greater than 100,000 per cross section. Therefore, a logical subset of the actual Gauss point stress and strain components will generally be required to capture the surrogate response to the force and moment inputs.

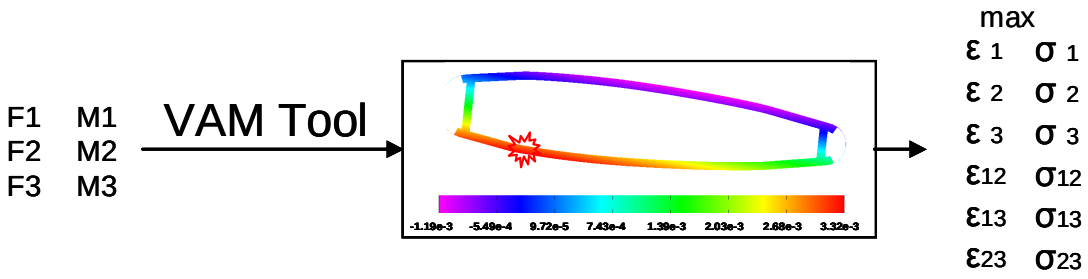

Figure 38: Stress/Strain Field vs. Response Subset

Thus the use of a surrogate produces a loss of fidelity of the full 3-D strain field of a cross-section. Therefore, one must decide what piece, or pieces of information are essential to be captured. Generally, the largest stress or strain values of a cross section are of high importance, as they determine endurance limit or structural failure criteria limit. This is the case for load recovery for structural constrains in trim and for fatigue analysis. If higher detail than a single stress or strain parameter for an entire cross section is desired, the section can be divided into multiple sections or responses as required. This may be particularly useful for applications which are sensitive to the location of the maximum stress/strain in the cross section. An example of this case is the estimation of cumulative damage for fatigue life analysis. The cumulative damage may by overestimated by a single maximum strain response if the maximum strain jumps to different locations in the cross-section. Tracking the strains from multiple responses in different cross-sectional locations will provide a better estimation of actual fatigue damage accumulated throughout a given time loading sequence. The cost to develop multiple responses per cross section will of course have to be weighed against the benefits of such.

The surrogate load recovery method proposed herein captures the stress/strain response of a beam structure as computed by the dimensional reduction process, specifically that computed by VABS. The surrogate loads model, once created, is therefore valid for the cross-section as long as the design remains unchanged. Since the surrogate is an approximation of the load response of the specific geometry, material, lay-up scheme, etc. any changes will require a new surrogate be created. This of course implies that if multiple cross sections are to be analyzed along the blade span, as many surrogates are required to be generated when the blade design varies spanwise. This fact, however, does not detract from the usefulness of the method in its intended use. Generally, once a blade design is mature enough to require aeroelastic analysis in trimmed flight (as is used in the optimal trim method) the frequency of design changes reduces to a manageable level.

Different classes of surrogate models have been applied to capture the response(s) of high fidelity analysis for use as approximations including response surface polynomials and

neural networks. For nonlinear systems in particular, neural networks have shown specific aptitude to capture complex behavior with relative simplicity while maintaining accurate predictive capability. This attribute is important for application to stress/strain, especially for responses that capture the maximum load of a cross-section. As mentioned previously, the maximum stress/strain value is dependant on the material properties, cross-sectional geometry, fiber orientation, matrix properties, etc. in addition, the maximum stress/strain location may jump around in a given cross-section as the time loads vary. This potentially produces nonlinear behavior in the maximum cross-sectional stress/strain values. Therefore, neural networks are used as the surrogate method of choice for this thesis effort.

5.3 Neural Networks

Neural Networks are a type of surrogate model that map a set of input variables to a set of responses through a set of filters, called the hidden layer(s) [86]. The hidden layer(s) may consist of one or more parallel node sets connected to defined inputs and outputs which form a network of interconnected nodes as illustrated in Figure 39. The benefit of this architecture is the ability to exhibit complex global behavior determined by the connections between the processing elements and element parameters. The original inspiration for the technique was developed in the 1940's to mimic the process of the human brain's ability to process information through a network of neurons, hence the name neural networks [87]. In the network, each node receives the signal from the input links and computes an activation level that is sent to the next layer along the output links. Networks that obtain input signals from only connections upstream are referred to as feed forward networks and are most commonly used for prediction, pattern recognition, and nonlinear function fitting. Networks that contain feedback connection loops are called recurrent networks and are used for time-series prediction, dynamic system modeling, and control system application. The surrogate loads method presented herein uses feed forward neural networks.

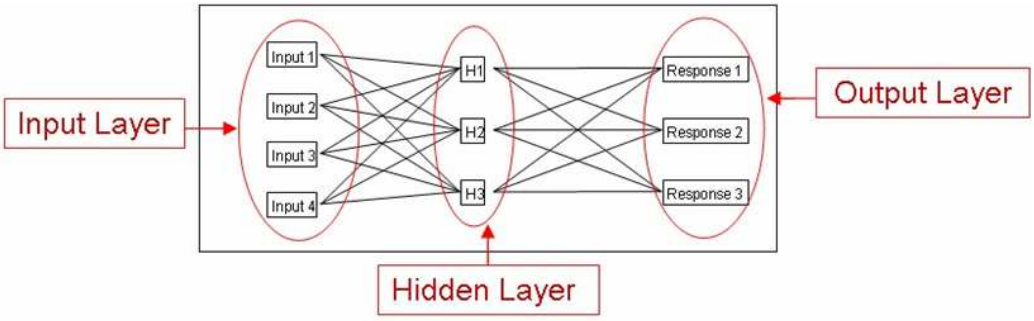

Figure 39: Neural Network Conceptual Diagram

The nodal unit in the network is the basic computational unit of the system. The node receives input from external sources (input layer) or from other nodes, see Figure 40, depending on the number of hidden layers. Each input has an associated weight b_i, which can be adjusted so as to model synaptic learning. The node H_q computes some function f of the weighted sum of its $\hat{N}$ inputs and an offset value a_q.

$$H_q = a_q + \sum_{i=1}^{\hat{N}} \left(b_{iq} X_i \right) \qquad \textbf{5.1}$$

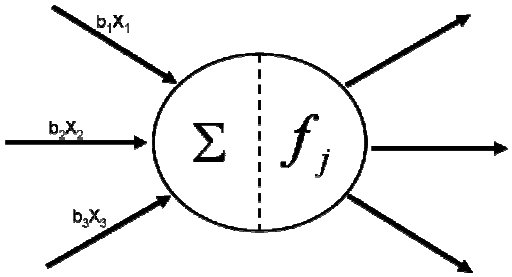

Figure 40: Nodal Output(s) as a Function of Weighted Inputs

The nonlinear response $\hat{R}_k$ in the output layer, similar to the nodal response in the hidden layer(s), is also a function of the weighted nodal inputs H_q, as shown in
5.2 where q_{jk} is again a weighting and e_k an offset, each adjusted for the synaptic learning.

$$\hat{R}_k = e_k + \sum_{q=1}^{N_H} \left(f_{qk} H_q \right) \qquad \textbf{5.2}$$

The precise benefit of the neural network system is that it is not programmed to solve a specific problem in an algorithmic way. Just as humans apply knowledge gained from past experience to new problems, neural networks are 'trained' against a set of data which is used to build a system of neurons that learn how to solve a new problem by changing the nature and the intensity of the input links. For this reason, the training phase is fundamental, and it generally consists of two main stages; the learning phase and the validation phase. In the first phase, the neural network learns to reproduce a specific problem only through the knowledge of a certain number of inputs and outputs, called a training set. In this way, the neural networks look for patterns in training sets of data, learn these patterns, and develop the ability to classify correctly a new pattern or to make forecasts and predictions. Training is conducted through a process termed error back-propagation, where the basic goal of the leaning process is to obtain values for all the weighting and offset parameters (b_{ij}, a_j, f_{jk}, and e_k) which minimize the difference between the neural net predictions and the training data. The process consists of a design space search for the set of parameter values which minimize some cost function. The definition of the cost function typically is a statistical measure of the minimum error between the training data and predictions, such as the mean square error or sum square error.

$$E = \sum \left(f(x_i) - R_i \right)^2 \qquad \textbf{5.3}$$

The design space search process draws from the same nonlinear mathematical programming methods discussed in the optimal trim section 1.2.2, complete with search direction determination, typically based on the design variable vector gradient, and a number of 1-D line searches. In addition, the search process may progress through a range of hidden layer node values and make a determination of the best number of nodes (as this value is not known a priori) based on the best cost function value.

In the second phase of the training process, the neural network's capabilities are assessed in terms of the generalized predictive capability through a certain number of validation

cases for the test sets; the validation set is not used for the training process. The choice of cases for training and test sets are very important because they qualify the final performances of the neural networks. Typically, validation cases may consist of randomly chosen values for the input/design variable within the limits. The error of the predictions quantifies the goodness of the neural network's capability to reflect the actual function value. Once the error is considered acceptable, the neural network can be used as a surrogate for the actual complex function with the benefit that it is a simple equation and can be solved with extreme speed.

5.4 Blade Surrogate Strain Model Validation

This section outlines the surrogate model development methodology and applies it to an example anisotropic, composite rotor blade cross-section subject to external loads with the objective of recovering the internal strains. The general methodology for constructing a surrogate model is covered in detail in Reference [88]. A summary of the method is given below with a discussion of specific issues in the following sections as they apply to the recovery of internal loads.

Surrogate Model Development Methodology

1. Identify input variables and their ranges
2. Sample the solution space
3. Fit the responses to create the surrogate model
4. Check the surrogate model for goodness of fit

The example beam used for the surrogate strain model validation is a hingeless rotor blade shown in Figure 41. The critical stress/strain values generally occur at the spanwise location where the bending moment is highest. For articulated rotors this around the blade mid-span and for hingeless rotors this occurs at the blade root. The example rotor is hingeless and the maximum strain does occur in the root region, where the flex beam transitions into the aerodynamic portion of the blade. In this region, the geometry of the blade changes and so do the number of composite plies from the clamped

root. Figure 41 shows a picture of the blade with the spanwise location determined to experience the highest strain values which is radial station (RSTA) 69.75 (inches). The blade structure is composed of multiple carbon fiber laminates of various thickness and orientation. As such, it is an anisotropic, complex three-dimensional composite beam structure. Analysis of the structure as multiple 2-D cross-sections and a 1-D beam is performed by the dimensional reduction process shown in Figure 6. A two dimensional cross-section model is built for the critical spanwise station and imported into VABS, from which the stiffness and mass matrices are generated in addition to warping function files that are needed to recover the 3-D stress/strain. The mesh size of the cross section is fairly small, resulting in a relatively high fidelity model of the section: 59,752 elements. From this model, VABS generates the distributed 3-D stress and strain field across the cross-section for a given set of three forces and three bending moments. The computational time required to recover the stress and strain field for each section for a given set of force and moment inputs is on the order of 2 minutes.

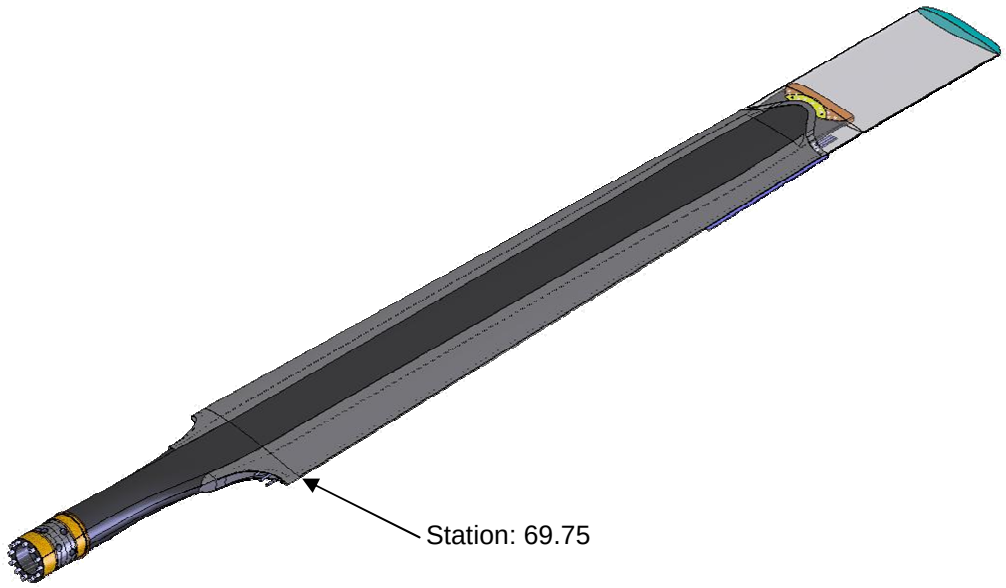

Figure 41: Rotor Critical Strain Spanwise Location (in.)

Table 14: RSTA 69.75 Cross-Section Properties

Material	Carbon Fiber (IM7)
Matrix	BMI
Ply Number	50
Ply Orientation	± 30˚ ± 20˚ ± 60˚

5.4.1 Identify Input Variables and Ranges

The first step in the surrogate development process is to determine the significant variables that affect the response. As stated previously, according to the VAM utilized by VABS, the 3-D strains recovered in the cross-section are defined by the primary forces and moments from the 1-D beam analysis. Therefore, the resulting loads are defined by six parameters: three forces and three moments. The range of the forces and moments experienced at a particular cross section is a function of the magnitude and location of the external loads, and also the properties of the internal structure (the mass and stiffness matrices). The limits of the design variables are important because they determine the ranges over which inputs will generate a valid, accurate response. Responses should not be extrapolated beyond the limits of the parameters; the accuracy of such results will be unknown. On the other hand, if the limits are chosen over too large a range, the number of training cases required for a given model accuracy grows large and this situation is not desirable either. This presents somewhat of a challenge for the surrogate stress/strain model because the limits of the 3 forces and moments are not necessarily known a priori; they are dependent on the external beam loads, the beam cross-sectional geometry, material properties, lay-up angles, etc. Therefore, an initial estimate of the force and moment limits must be made when developing the model, and subsequent refinement of the limits may be necessary if the 1-D beam analysis yields values beyond the initial estimate. In this way, the process is somewhat iterative.

A dynamic model of the rotor blade is constructed in the multi-body rotorcraft simulation code RCAS using 10 nonlinear finite beam elements. The model is set up to reflect the beam boundary conditions of a hingeless blade; fixed displacement and slope at the root and free at the tip. Distributed spanwise 1-D beam cross sectional properties are generated in VABS for 22 radial stations which consist of 6x6 element mass and stiffness matrices, and four 4x4 warping matrices. As is illustrated in Figure 36 this information is required for accurate modeling of the anisotropic, coupled behavior of the composite beam and recovery of the 3-D strains. Multiple aeroelastic simulations of the blade model are run with resulting 1-D beam forces and moments for the blade cross-section of interest. The maximum and minimum forces and moments can be observed from the simulations to gage the limits for the six parameters. In surrogate strain model problems such as this, the ranges are not known prior to the 1-D beam analysis for all external loading conditions and some iteration of the maximum and minimum values may be required. For this problem, an initial set of ranges was chosen based on simulations over a broad range on conditions. This initial set produced an unsatisfactory fit and certain parameters limits had to be narrowed to get a more acceptable model fit. The final limits of the parameter ranges are listed in Table 15.

Table 15: Design Variable Input Ranges

PARAMETER	MINIMUM	MAXIMUM
F_1	4,000	50,000
F_2	-10,000	10,000
F_3	-3,000	4,000
M_1	-8,000	8,000
M_2	-50,000	50,000
M_3	-100,000	100,000

5.4.2 Sample Solution Space

Response Surface Methods (RSM) have a well defined set of experimental designs that are commonly used to sample the solution space in a systematic way. Neural networks have no such design sets, and thus care must be exercised in selecting a method that covers the solution space in a manner consistent with the variable ranges. Neural

network training typically requires more training cases than a response surface and needs a large sample of the entire space. A common practice suggested by Reference [88] is to use a Latin Hyper Cube (LHC) design, as it breaks the design space into any specified number of even segments, assuring coverage of the entire solution space. Additionally, some tools such as MatLAB have built-in algorithms that optimize the distance between each of the segments within the specified design cases. The Central Composite Design (CCD) DOE assures that the corners of the solution space are covered. When used in combination, the LHC and CCD offer the potential to cover the entire solution space, including the corners and midpoints. This CCD LHC combination is utilized for the composite rotor strain recovery example. The CCD with 6 design variables generates 44 cases. For the LHC design, a total of 1000 LHC combinatory cases are used. Additionally, an extra 300 cases are generated where the 6 parameter values are randomly chosen between their limits. These cases are used for validation after the neural network training is complete, to quantify the goodness of the model fit.

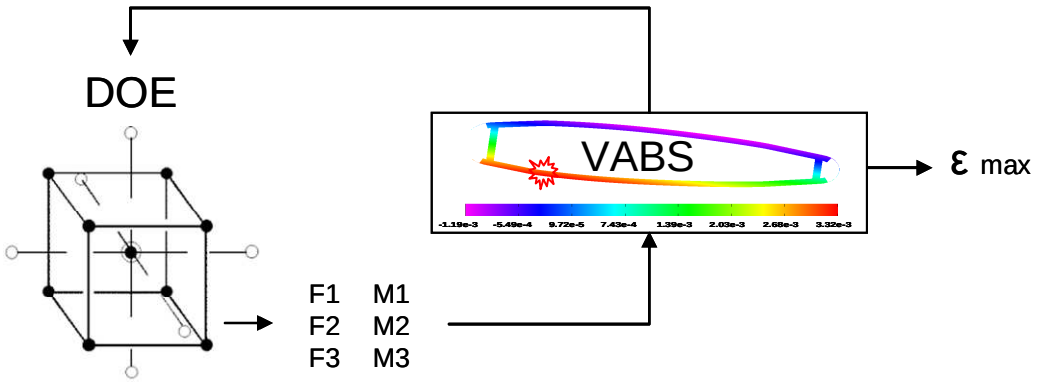

Figure 42: Cross-sectional Strain Solution Space Sampling

A script is written that reads the design variable values for each combinatory case, writes them into a VABS input file, executes the VABS program to recover the maximum 3-D strain value for each of the six strain components, then writes the values to a results file. The captured responses for each combination of the three forces and moments are the maximum of each of the six cross-sectional strain components. The force and moment values and the corresponding six strain responses are used as training data for the neural net model. This process is illustrated in Figure 42.

The responses captured from the example blade cross-section are the maximum values of the six strain components and also the maximum equivalent strain or von Mises strain

$$\varepsilon_{vm} = \sqrt{\frac{1}{2}\left[\left(\varepsilon_{xx} - \varepsilon_{yy}\right)^2 + \left(\varepsilon_{yy} - \varepsilon_{zz}\right)^2 + \left(\varepsilon_{xx} - \varepsilon_{zz}\right)^2\right] - \frac{3}{4}\left(\varepsilon_{yz}^2 + \varepsilon_{xz}^2 + \varepsilon_{xy}^2\right)}. \tag{5.4}$$

This formulation is a type of strain invariant, that is to say its magnitude remains unchanged with coordinate system transformation [89]. Strain invariant failure theory (SIFT) uses mechanical and thermo-mechanical amplification factors extracted from unit cell finite element micro-mechanical models to determine the strain of homogeneous finite element solutions for composites at the macro-mechanical level [90]. The invariant strain value is a useful quantity in determining composite structure cumulative damage for fatigue life assessment. Typically an endurance limit value is established; loads generating invariant strain values beyond this limit reduce the life of the structure. It is not desirable to use up structure life in steady level flight, therefore the endurance strain limit can be used as a constraint in trim solution.

5.4.3 Model Goodness of Fit

The model goodness of fit quantifies the model's predicative capability and is principally determined from two metrics. The first is the error between the training data and the predicted values, termed model fit error. The second is the error between the randomly generated test data set and the predicted values, called the validation error. The model fit error is typically smaller than the validation error, but should not be significantly smaller. The error of the test set is important because it shows the error for cases not used to train the network. The distribution of both error sets should be normally distributed about zero and the standard deviation of the error distribution quantifies the fit. Results of the model von Mises strain fit for the sample rotor blade cross-section are presented in Figure 43. Both error distributions are normal and centered about zero. The standard deviation of the model fit error and model representation error is 38.92 and 42.87 respectively. This

indicates that 95.4 percent of the model predictions are within approximately ±86 micro-strain. Further model accuracy information is indicated in the residual by predicted plot. The plot shows that there is larger variation in the error at lower values of the von Mises strain response. Therefore the larger the strain response value, the greater the predictive accuracy of the surrogate model. The endurance limit of the material has been determined to be approximately 3,800 micro-strain, therefore strain values at and above endurance limits will be more accurate.

The residual by predicted plots for each of the maximum strain component values are shown in Figure 44. These plots reveal some interesting characteristics of the strain response behavior of the composite cross-section. First, the total range of the various model errors is significantly different for the strain components, the shear strain error range ε_{13} is an order of magnitude larger than the axial strain ε_{11}. Second, the model error decreases with total strain magnitude for several strain components, specifically ε_{12} and ε_{13}. The von Mises strain exhibits a similar behavior to a lesser degree as it is composed of these component strains. The reason for this behavior is due to the mechanics that cause the strains. From a basic mechanics of materials approach, longitudinal strain for an isotropic beam is fundamentally a function of the axial force and bending moments, other affects are of a higher order. For the shear strains, an area moment of inertia cross-sectional warping function is of the same order of magnitude as the external load effects [91]. Thus, there is more variability in the shear and transverse strains compared to the longitudinal strain. The same effect is in play for composites, only to a higher degree due to anisotropic properties. This variability is observed in the results, indicating the accuracy of these parameters is more sensitive to their range values. A summary of the strain response fits is listed in Table 16 and also includes the number of hidden nodes in each of the surrogate models.

5.4.4 Surrogate Strain Validation Results

In this section the surrogate models are exercised on two different time loads sets and the

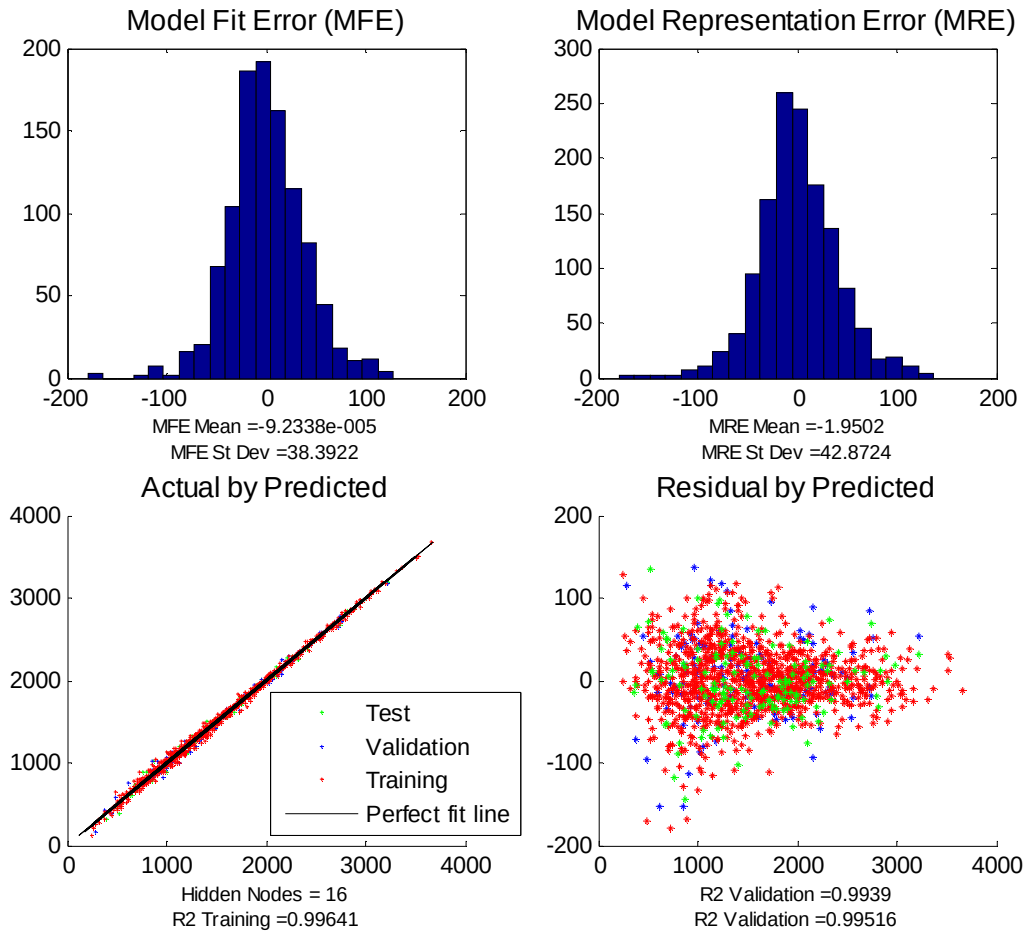

Figure 43: Cross Sectional Surrogate ε_{vm} Model Fit

Table 16: Surrogate Model Goodness of Fit Summary

RESPONSE PARAMETER	HIDDEN NODES	MODEL FIT ERROR STD (micro-strain)	MODEL OVERAL ERROR STD (micro-strain)
ε_{vm}	16	38.39	42.87
ε_{11}	16	0.644	1.634
ε_{12}	17	31.533	35.601
ε_{13}	16	61.701	73.721
ε_{22}	17	17.299	26.778
ε_{23}	17	25.262	28.424
ε_{33}	17	22.168	29.448

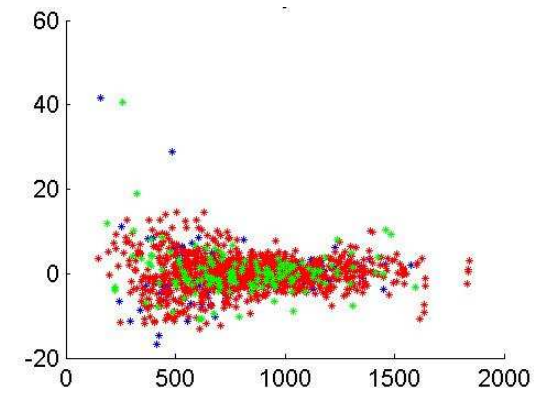

ε_{11}

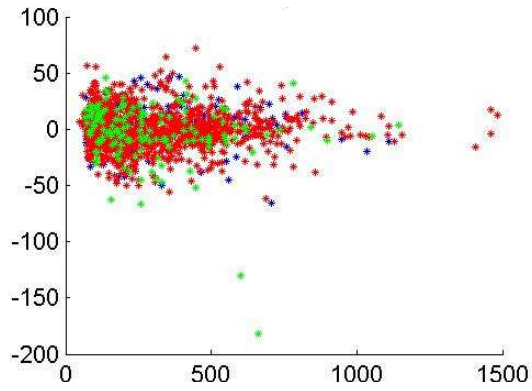

ε_{22}

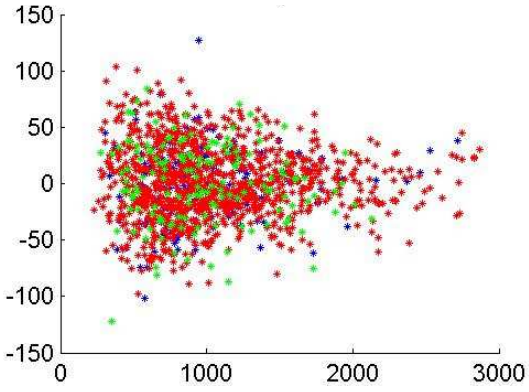

ε_{12}

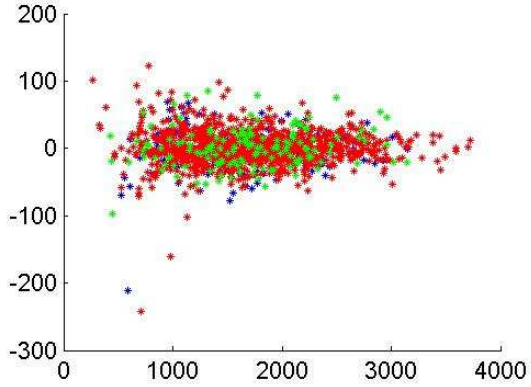

ε_{23}

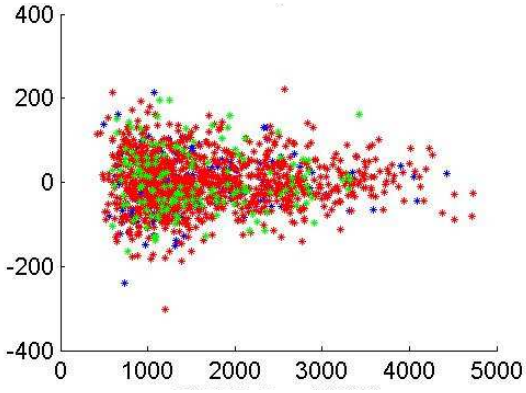

ε_{13}

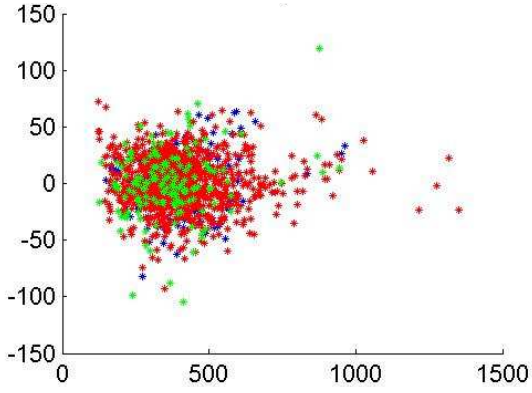

ε_{33}

Figure 44: Cross-Sectional Strain Components Residual by Predicted (micro-strain)

strain response values and computation time are compared to the same as computed by VABS. The two loads sets are obtained from the sample rotor blade as it is applied to a high speed compound rotary wing aircraft which is detailed in the following chapter. The loads are generated from two separate control configurations of the aircraft subjected to a vertical gust. In one control configuration, the hingeless rotor carries a moment and is loads referred to as case 1, in the other, no moment is present and is referred to as loads case 2. The data set from the rotor that carries a moment is in the mid region of the response region while the set from the rotor with no moment is at the low end of the response region. A comparison of the time dependent strain values (between VABS and the surrogate) of these two load sets allows another way to view the model accuracy.

A nonlinear aeroelastic simulation is performed with the elastic blade and vehicle in free flight. In the analyses, the vehicles are initially in steady cruise at the maximum weight condition. From trim, a vertical gust of 30 ft/s second is simulated for a period of less than 2 seconds as defined in Reference [92]. The gust profile has a 1-cosine type build up over a 200 ms span, the simulation profile of which is given in Figure 45. The complete vehicle is allowed to respond to the gust in 6 degrees of freedom along with the full elastic response of the four individual rotor blades. The simulation is performed over a 5 second interval with a time step size of 0.005 seconds, therefore a total of 1,000 time steps are generated.

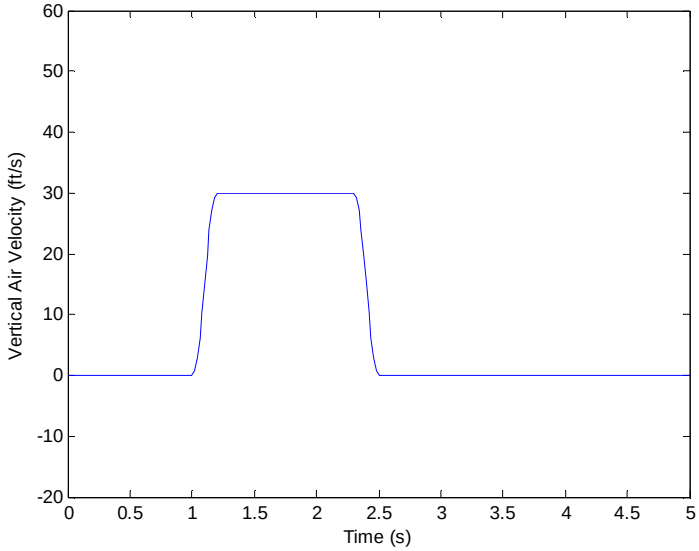

Figure 45: Vertical Gust Velocity Profile

The nonlinear gust simulation case 1 loads for station 69.75 are shown in Figure 46. The axial force (F1) is much larger than the two transverse shear forces (F3 and F3). Also note that for the moments, the chordwise moment (M3) is much larger than the torsion and flap moments (M1 and M2). The large chordwise moments are due to the fact that the rotor is stiff-inplane, and carries a moment from cyclic flapping. The gust generally causes increased flapping and therefore drives the chordwise loads higher due to Coriolis effects. Figure 47 shows the maximum von Mises strain as computed by the neural net surrogate and also as recovered by VABS. Figures 48 through 53 show the results of the surrogate and VABS for the individual strain components. The general correlation between the two methods is good with exception of the two shear strain values ε_{12} and ε_{13} at the lower strain response range. This behavior is somewhat expected from the model fit results exhibited in Figure 44 and is reflected to some degree in the von Mises strain correlation of Figure 47.

The nonlinear gust simulation case 2 loads are shown in Figure 54. Note that the maximum chordwise bending moment is nearly an order of magnitude less when the hub moment is zeroed. Therefore the magnitude of the strain would be expected to be lower than the previous cases, with a lower degree of correlation between the surrogate and VABS values due to the model fit behavior. Figure 55 shows the maximum von Mises strain as computed by the neural net surrogate and also as recovered by VABS. Figures 56 through 61 show the results of the surrogate and VABS for the individual strain components. Note the discrepancy of the shear and transverse strain values, specifically at the lower strain values. Again, this discrepancy becomes somewhat evident in the maximum von Mises strain as shown in Figure 55. However, the total difference between the maximum von Mises strains of two methods is on the order of 5%, and is not particularly significant in the low strain region.

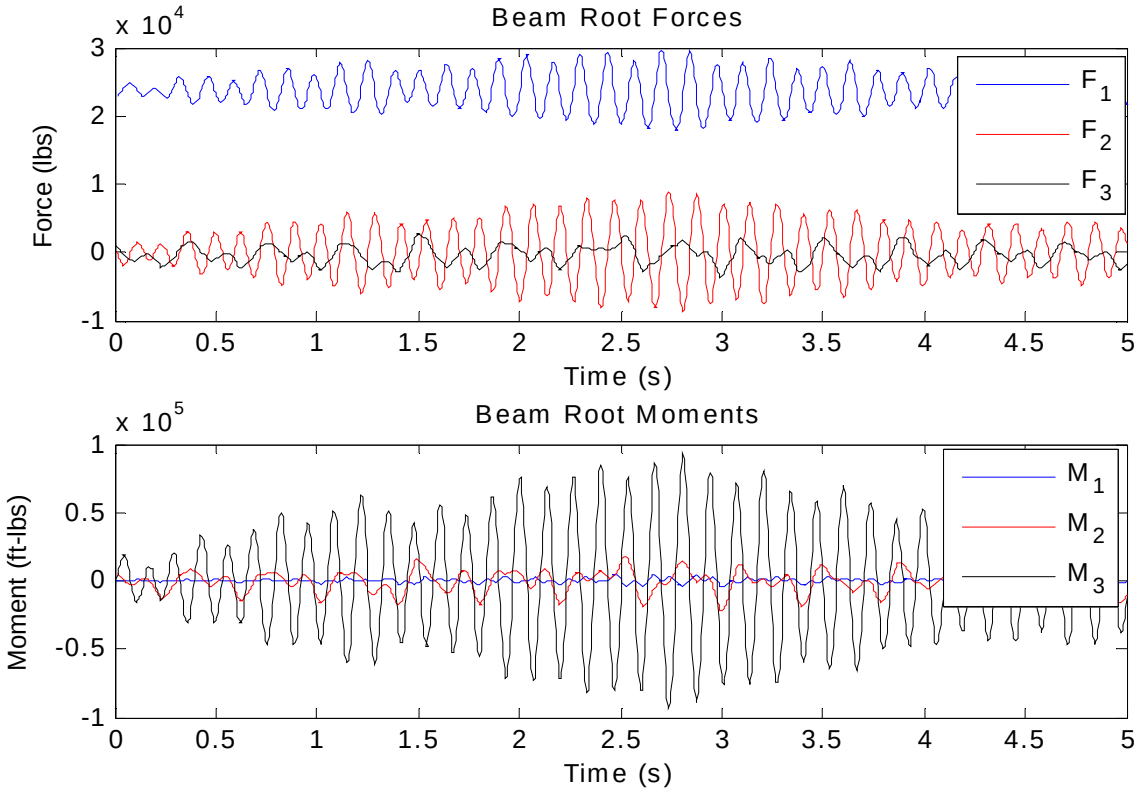

Figure 46: Case 1 Gust Response RSTA 69.75 Forces and Moments

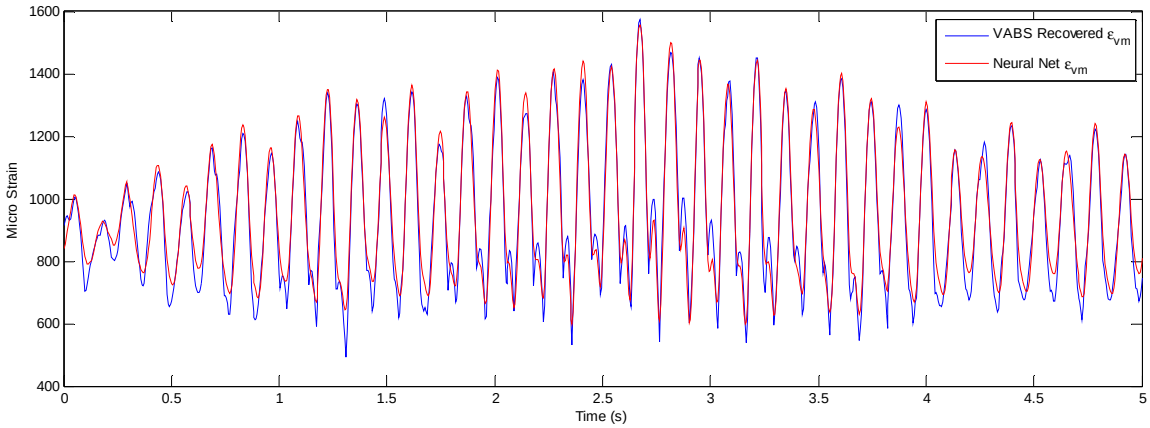

Figure 47: Case 1 Time Dependent Max ε_{vm}

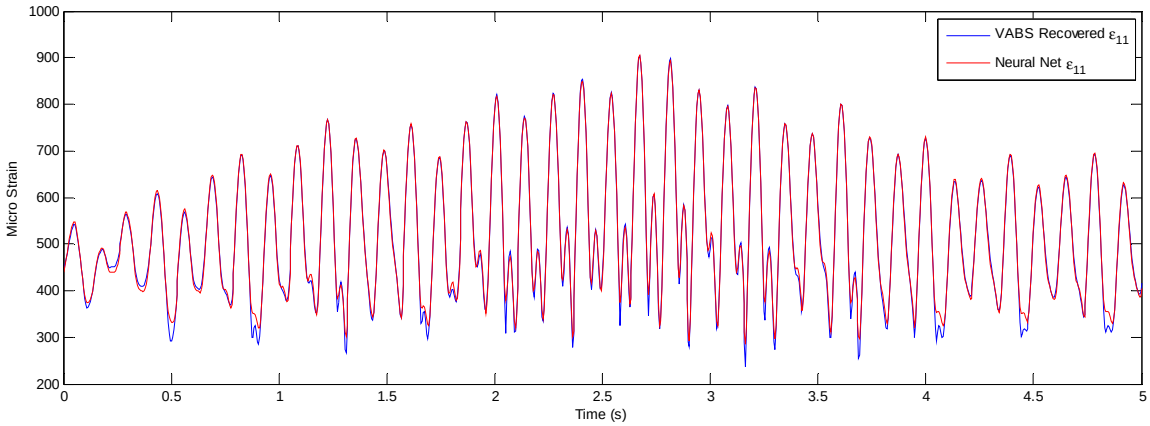

Figure 48: Case 1 Time Dependent Max ε_{11}

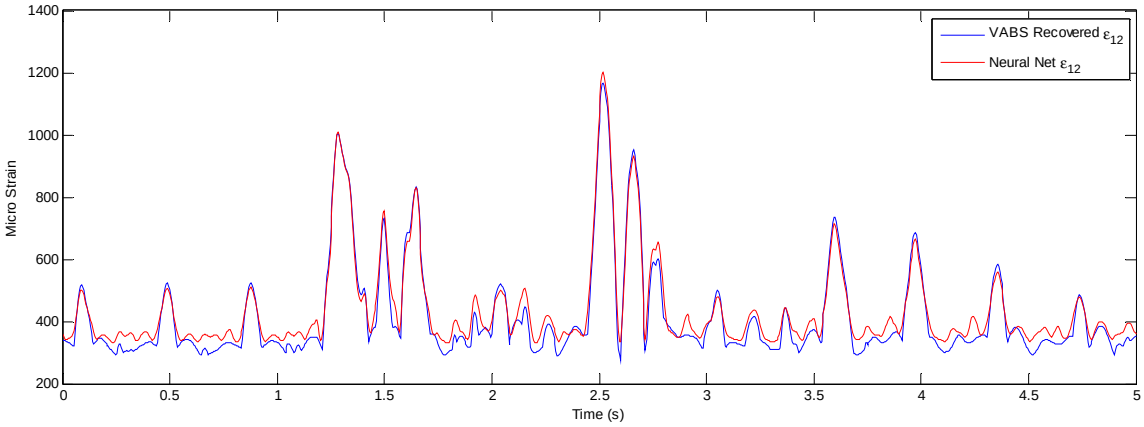

Figure 49: Case 1 Time Dependent Max ε_{12}

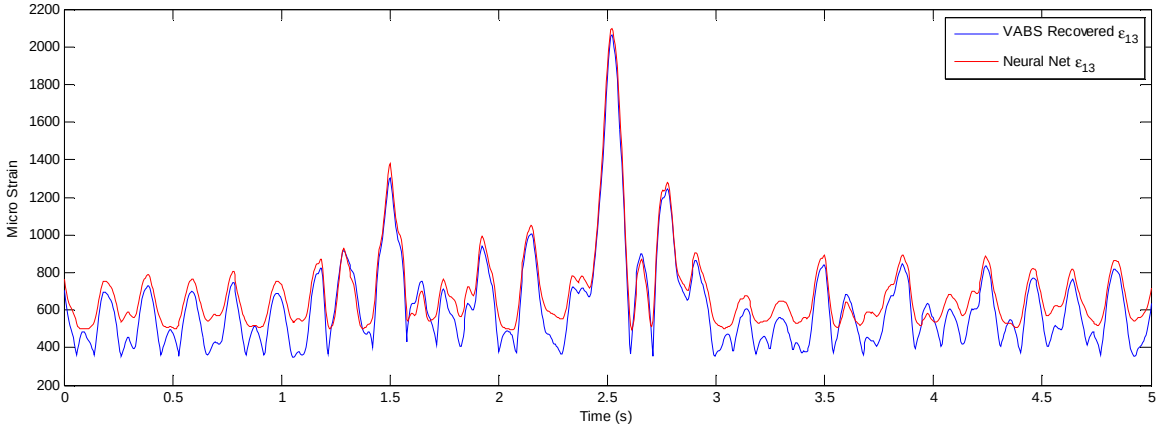

Figure 50: Case 1 Time Dependent Max ε_{13}

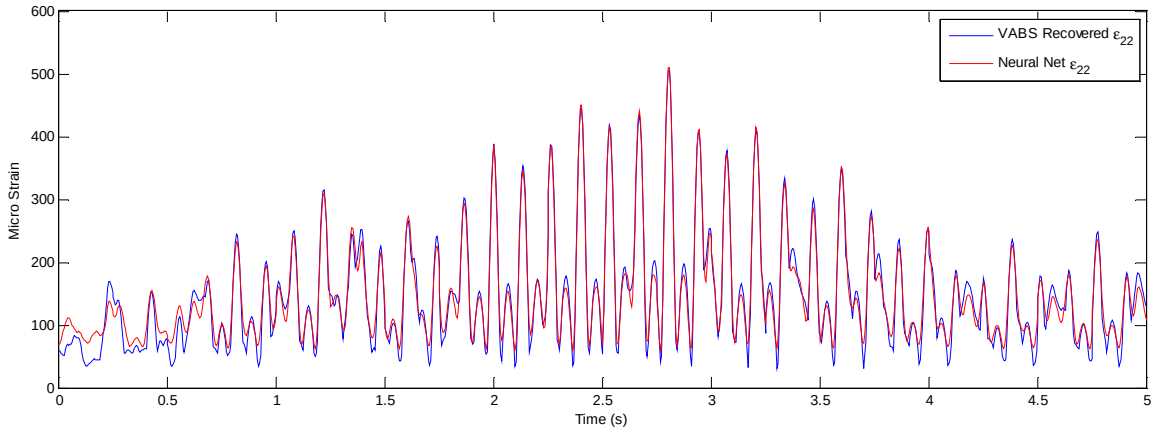

Figure 51: Case 1 Time Dependent Max ε_{22}

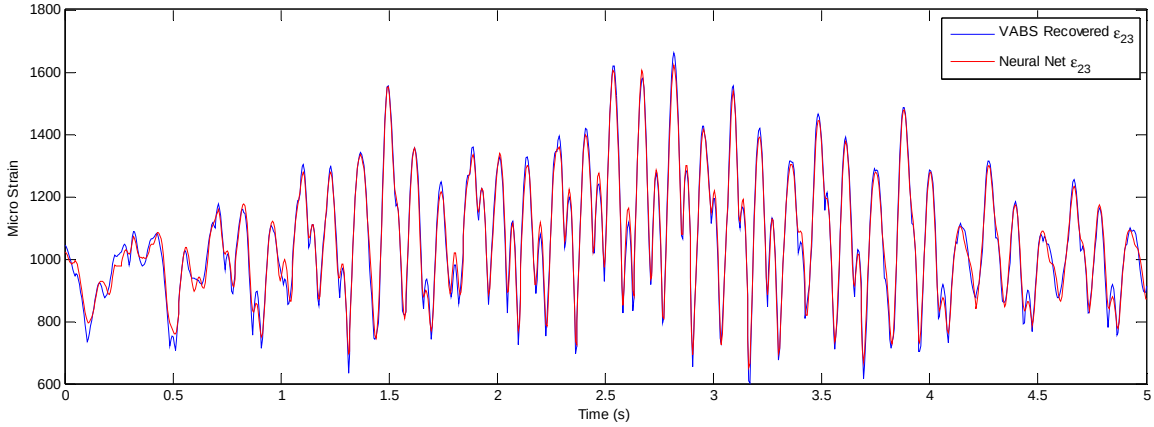

Figure 52: Case 1 Time Dependent Max ε_{23}

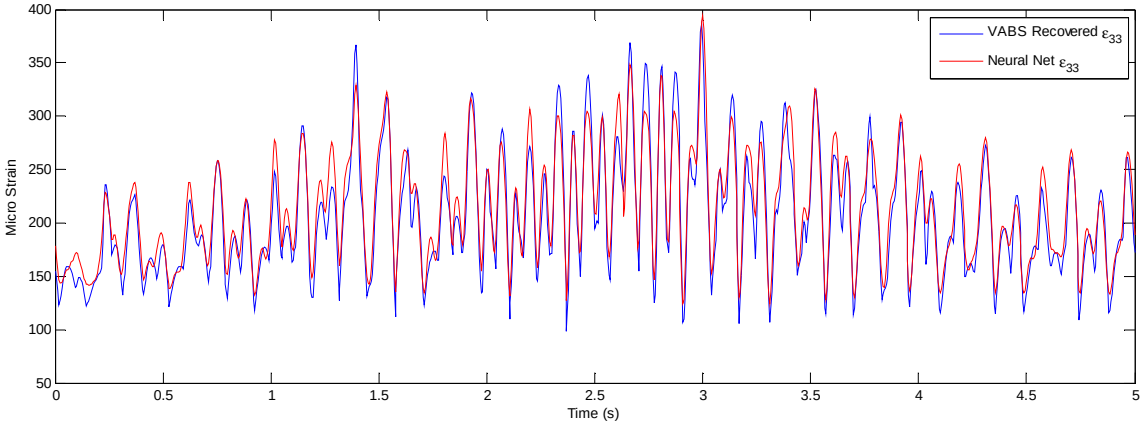

Figure 53: Case 1 Time Dependent Max ε_{33}

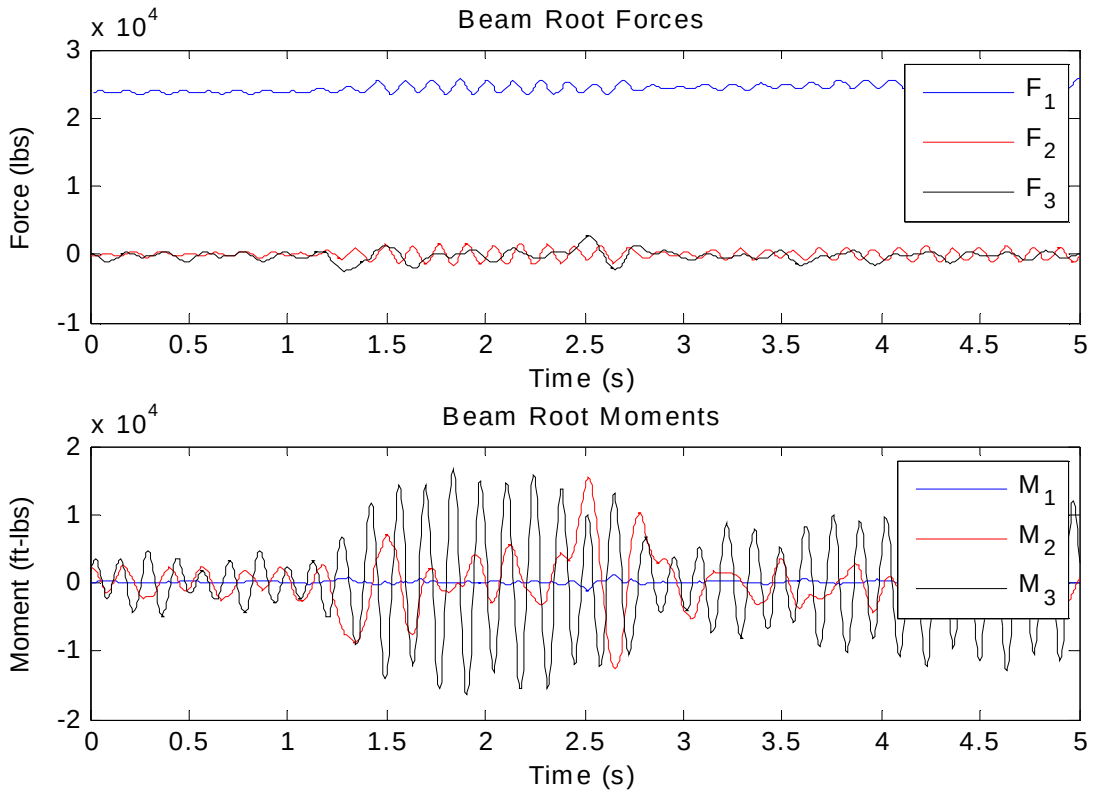

Figure 54: Case 2 Gust Response RSTA 69.75 Forces and Moments

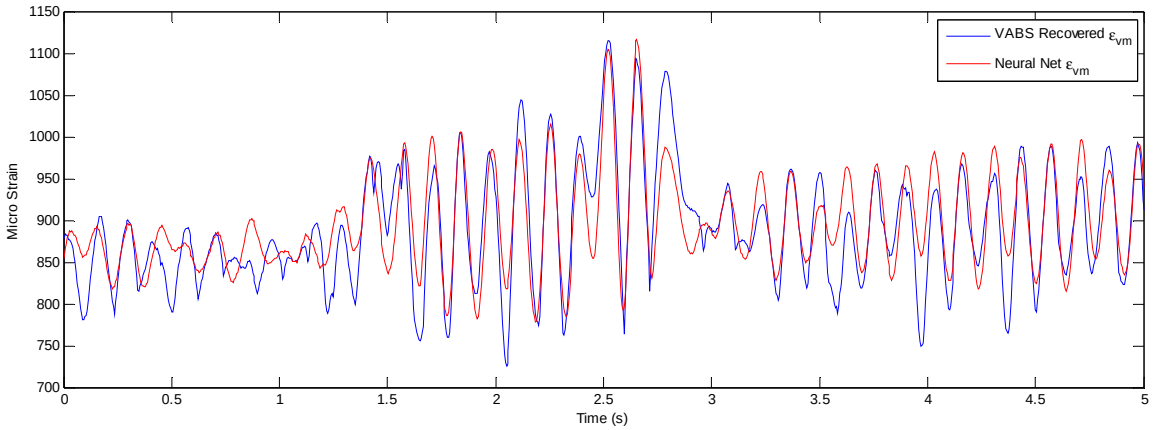

Figure 55: Case 2 Time Dependent Max ε_{vm}

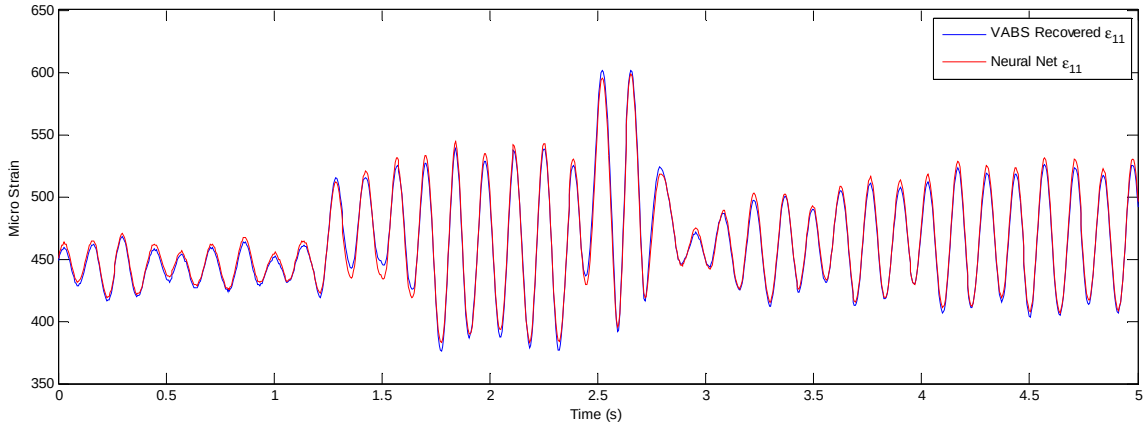

Figure 56: Case 2 Time Dependent Max ε_{11}

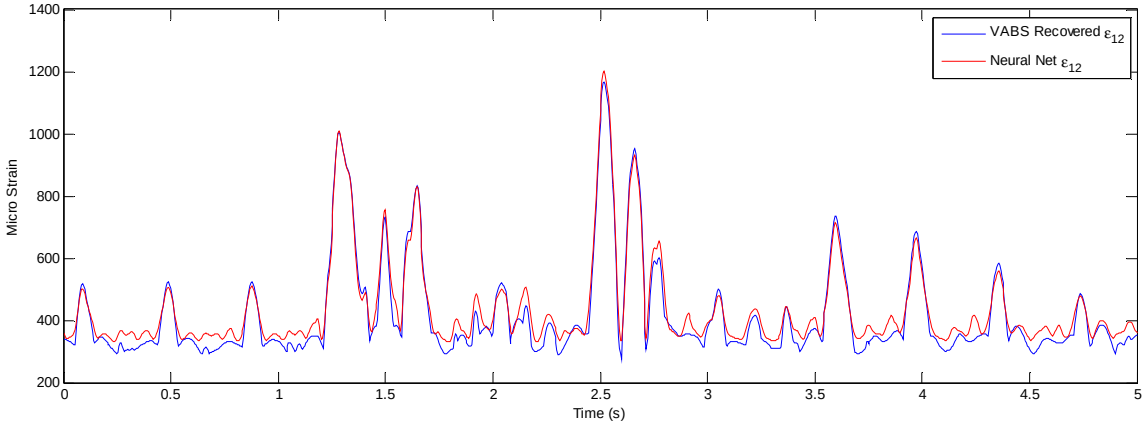

Figure 57: Case 2 Time Dependent Max ε_{12}

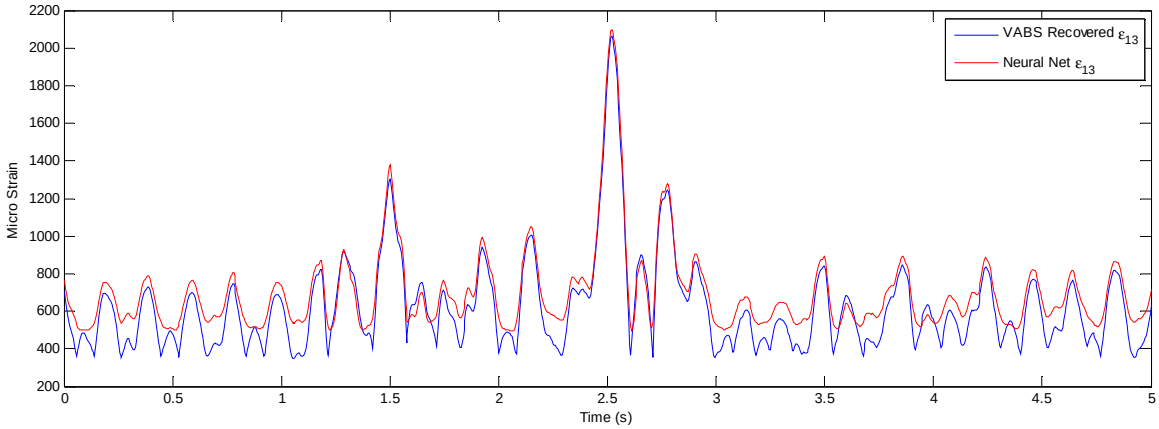

Figure 58: Case 2 Time Dependent Max ε_{13}

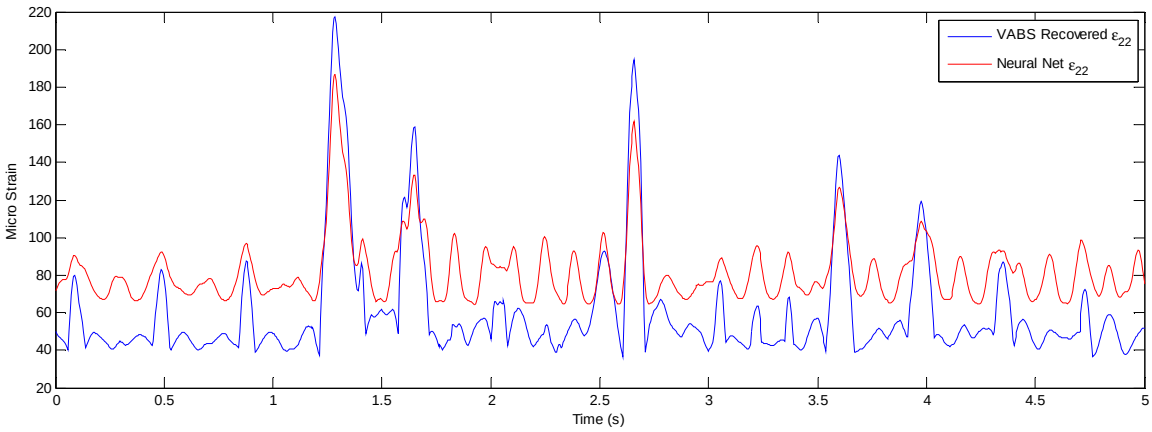

Figure 59: Case 2 Time Dependent Max ε_{22}

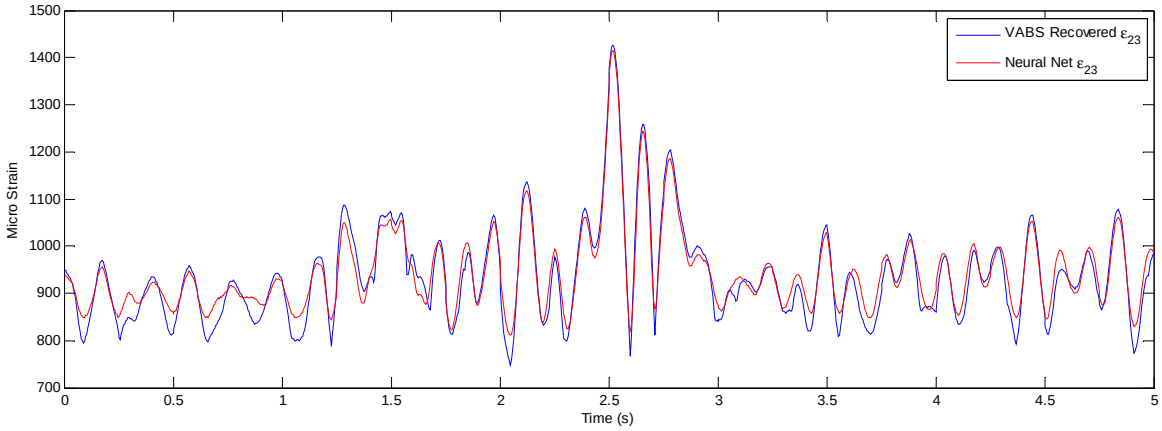

Figure 60: Case 2 Time Dependent Max ε_{23}

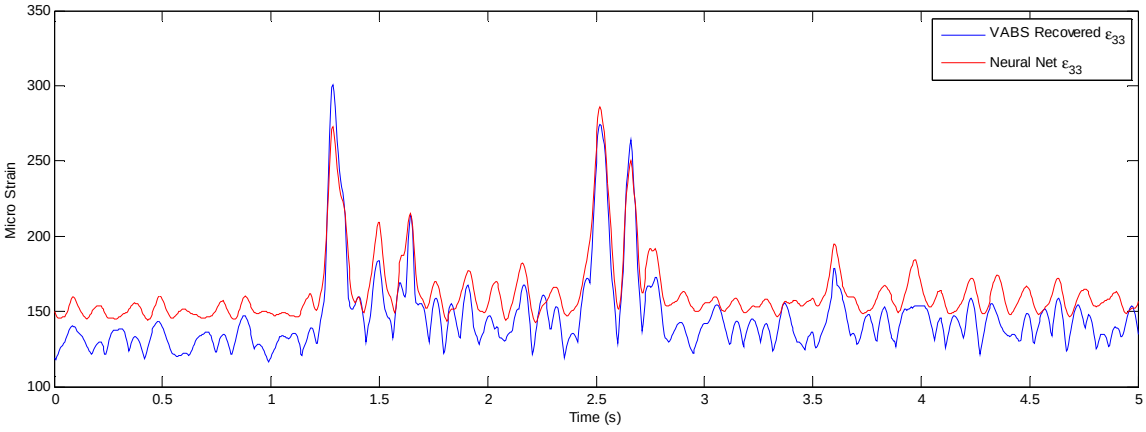

Figure 61: Case 2 Time Dependent Max ε_{33}

Table 17: Strain Recovery Time Summary

MAX STRAIN RECOVERY METHOD	TOTAL RECOVERY TIME
Loads Case 1	
VABS	7.579 (hours)
(VABS) Neural Net Surrogate	1.069 (seconds)
Loads Case 2	
VABS	7.549 (hours)
(VABS) Neural Net Surrogate	1.071 (seconds)

Table 17 lists the computational time to recover the maximum strain values from VABS and from the neural net surrogates for all six strain components and the von Mises strain. It is significant to point out that the computational time reduction of the surrogate model is greater than two orders of magnitude compared to VABS. The (VABS) neural net surrogate method requires about a second, and VABS directly requires over seven hours. The validated accuracy and significantly reduced strain recovery computational times will allow rotor blade cross-sectional strain to be computed in time scales that are compatible with dynamic/aeroelastic simulations. Therefore, these strain values can be used as constraints in the trim process and will be demonstrated in the following chapter. The surrogate stress/strain recovery method is useful to other applications in addition to trim solution constraints. One such application is in the life determination of any beam structure. To quantify the life degradation, the time stress/strains must be known somewhat precisely as the mean and oscillatory stress/strains influence the cumulative damage. For example, the determination of the life of a helicopter blade is made by the cumulative damage assessment of the rotor blade subject to a number of maneuvers, gusts, over speed conditions etc. The determination of the maximum stress/strain over lengthy simulations is computationally expensive. Using the surrogate loads method, it has been demonstrated that the computational cost for examining the loads of extensive time simulations can be significantly reduced.

It must be pointed out that the significant strain computational cost saving comes at the expense of constructing the surrogate to degree of accuracy required. The creation of the

surrogate model for this example required 1,344 VABS cases, and is therefore slightly larger in time cost (in terms of VABS function calls for a given cross-section) than a single gust simulation. The refinement of the surrogate input parameter limits (forces and moments) required two iterations in the surrogate training data generation, for a total of approximately 20 hours of VABS computational time. The two gust cases for the fixed and titling shaft configuration required just over 15 hours of computation time. Generally a number of nonlinear loads simulations are run for gusts at multiple flight envelope conditions and for maneuvers, etc. Therefore, the time cost of the surrogate creation, even with multiple iterations, roughly seems to pay for itself after one or two stress/strain recovery simulations.

Typically the analysis of complex (composite) structures requires 3-D finite element methods and yields the stress/strain field of the entire structure. The development of dimensional reduction utilizing VAM significantly reduces the computational time over 3-D FEA by approximately a couple orders of magnitude. Of course VAM methods are applied to spanwise beam 2-D cross-sections and more limited information is available compared to 3-D FEA. Finally the surrogate stress/strain method developed in this work shows computational cost reductions by approximately another couple orders of magnitude compared to VAM. The surrogate method is not an alternative approach to compute the 3-D stress/strain as VAM is compared to FEA, rather it is a new concept in approximating the maximum stress/strain for vary fast results. The cost of the surrogate method is, once again, less information than the full cross-sectional 3-D stress/strain field. However, for certain applications such as trim solution constraints and cumulative damage assessment, the surrogate stress/strain method provides fast stress and strain computation capability.

5.5 Chapter Summary

This chapter presents the current framework for aeroelastic trim and loads analysis. A novel method to rapidly approximate elastic rotor blade stress/strain in aeroelastic analyses is developed which decouples the dynamic load feedback loop between multiple analysis codes for certain types of stress/strain constrained applications. The method

captures the maximum cross-sectional stress/strain loads based on the trained response of an artificial neural network (ANN) surrogate as a function of 1-D beam forces and moments. The method is validated by comparison of the surrogate predicted loads against the VABS recovered loads for a complex, anisotropic beam cross-section loaded in time. A comparison of the individual strain component values from the surrogate and VABS for the time loading shows good correlation. However, the surrogate model computed the same strains in a time span two orders of magnitude less than VABS. This innovation opens the door for analyses that require stress/strain information in a reduced time span. These results confirm the first hypothesis to supporting question 2 in that *stresses and strains can be captured by a surrogate model as a function of the 1-D beam forces and moments.*

CHAPTER 6
CONSTRAINED OPTIMAL TRIM APPLICATION

This chapter applies the optimal trim algorithm that has been integrated into the rotorcraft comprehensive code RCAS to an advanced, high-speed compound gyroplane configuration. The concepts of variable rotor speed trim developed in Chapter 4 and surrogate strain developed in Chapter 5 are also applied to the example problem. A description of the vehicle configuration and the rotor system design is provided. An optimal trim analysis of the vehicle is performed in the high speed range with the purpose of maximizing the vehicle cruise efficiency while maintaining rotor blade strain below endurance limit values. The application of the optimal trim method to the high speed compound gyroplane configuration demonstrates the utility of optimal trim for an advanced rotorcraft vehicle that has multiple constrained trim solutions.

6.1 Example Compound Gyroplane

Recently, interest in expanding the envelope of vertical-lift-vehicles has increased, particularly in terms of speed, altitude and range [93]. Increased range allows military rescue vehicles to reach further from their bases. Additional speed and altitude capability increases the survivability of military vehicles and cost efficiency of civilian aircraft. Two rotorcraft configurations that offer potentially higher speed and range than conventional helicopters are the compound helicopter and compound gyroplane. These configurations provide STOL and VTOL capability, but are capable of higher speeds than conventional helicopters because the rotor does not provide the propulsive force, or at high speed, the vehicle lift. The drawback is that redundant lift and/or propulsion add weight and drag. For high speeds to be achieved, an edgewise rotor must be slowed to avoid compressibility effects on the advancing blade. The potential advantage of the compound gyroplane is that there is no need for a variable speed transmission, since its rotor is powered from the free-stream in autorotation. The potential reduction of the propulsion system complexity and weight is significant. One such compound gyroplane

has been proposed for a long-range rescue mission application [3], and is shown in Figure 62. The main purpose of this chapter is to demonstrate the utility of the optimal trim method developed in Chapter 3, with the variable rotor speed method of Chapter 4 and surrogate strain method of Chapter 5 with application to this example high speed gyroplane.

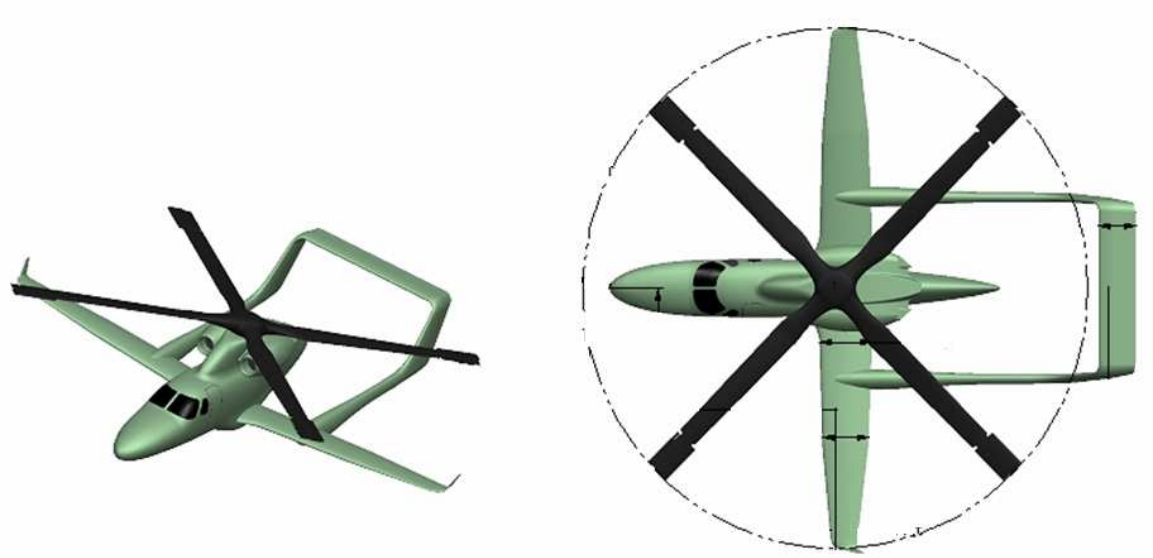

Figure 62: High Speed Compound Gyroplane

For the rescue mission, the vehicle is required to have a maximum dash speed of 350 knots. The combination of high speed and slowed rotational (rotor) speed results in high advance ratio conditions. Advance ratio is the ratio (μ) of forward speed to rotor tip speed and characterizes the portion of reverse velocity airflow on the retreating side. Typically helicopters operate at advance ratios of less than 0.45. The compound gyroplane will operate at a maximum advance ratio of 2.4 to keep the advancing tip below Mach 0.85 at 30,000 ft altitude. Figure 63 shows the relation between tip speed, true airspeed, advancing tip Mach number and advance ratio at 30,000 ft altitude. Both analysis and test have shown articulated rotors to be susceptible to unstable flapping motion at high advance ratio conditions [94,95,96,97]. One approach to avoid flapping instability is to elastically restrain flapping with a structural flex beam, i.e. hingeless rotors. Analysis has shown that for proper combinations of rotor inertial Lock number and flap stiffness (quantified as non-dimensional flap frequency) the rotor will always

retain stable flapping motion [98]. The flapwise stiff rotor is capable of producing very large bending moments that are desirable for control. However, rigid flapping must remain within limits to avoid exceeding structural endurance limit loads in trimmed flight and critical loads in gusts and maneuvers. Endurance limit flapping angels are on the order of a couple degrees for a rigid blade, much smaller than those routinely experience by articulate and teetering rotors.

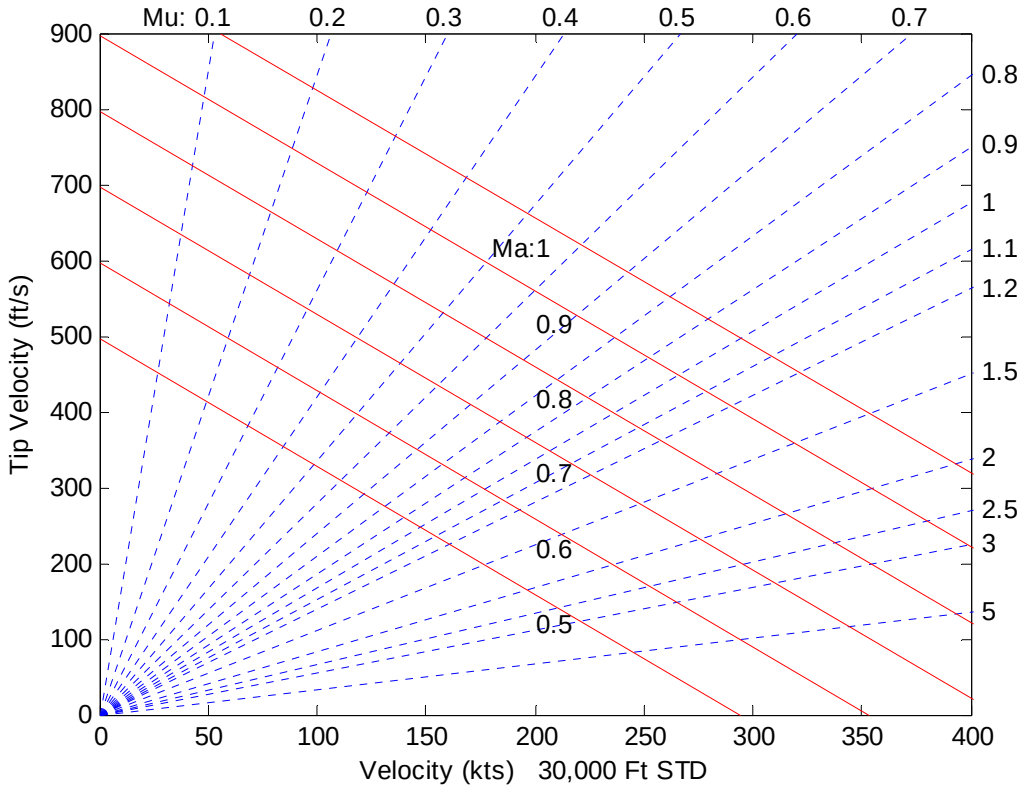

Figure 63: Rotor speed vs. Velocity Diagram (30,000 ft)

Aeroelastic trim analysis of the gyroplane for performance and loads is a complex undertaking due to the interdisciplinary couplings and a non-unique trim solution space from the multiple lifting, thrusting and controlling mechanisms. For example, should the rotor carry a moment or should it be controlled to zero moment. If a moment is carried, the rotor loads will be larger, but how will the overall vehicle performance be affected? In addition, the compound gyroplane rotor is not directly powered and must be controlled to operate in a zero average torque, autorotational state. Finally, the wide operational

rotor speed condition presents the challenge of load amplification when blade modal frequencies are in proximity to an n/rev multiple of the rotor speed. Figure 64 shows the rotor speeds at which the fundamental flap and lag modes cross the n/rev frequencies for the compound gyroplane rotor. This frequency coalescence is of particular concern for the fundamental lag mode, which for a siff-inplane rotor (such as the example gyroplane) can produce an undesirably high load build-up. Therefore, the problem of finding the most efficient way to fly the vehicle is non-trivial and requires a systematic way of finding the optimal trim solution with autorotation and structural constraints.

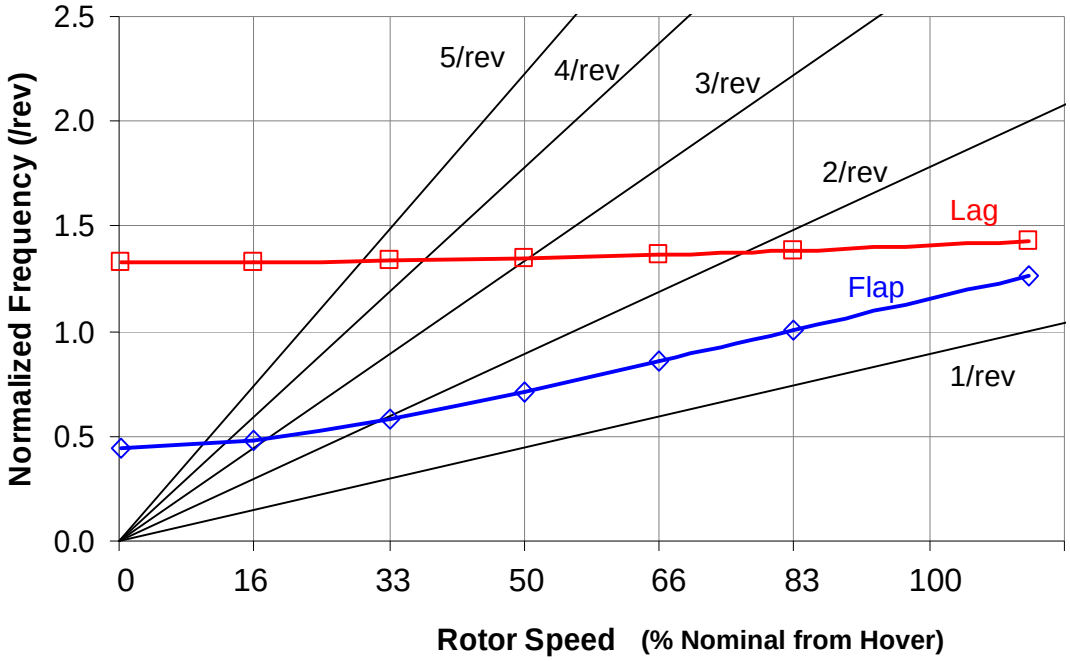

Figure 64: Compound Gyroplane Rotor Fundamental Frequencies vs. Rotor Speed

In this example problem, the compound gyroplane design is considered complete. The vehicle design parameters, such as wing span, area, rotor diameter, solidity, weight etc. are already determined from performance and sizing considerations. The rotor structural design is also fixed as the rotor design, specifically the flap stiffness, is driven primarily from the flapping stability consideration. Therefore, the problem at hand is to find the best way to fly the existing vehicle, considering rotor structural constraints. The problem is solved by developing a model of the example gyroplane in RCAS and then applying the optimal trim routine developed and validated in Chapter 3. The RCAS model

consists of a rigid fuselage, lifting and control surfaces in addition to 4 elastic blades. The vehicle structural representation from RCAS is shown in Figure 65. The elastic properties for the blade structure result from the blade cross-sectional geometry and material and are determined from VABS in the form of multiple spanwise stiffness and mass matrices. The elastic blade model was developed for use in Chapter 5 in conjunction with the blade surrogate strain validation. The fundamental blade elastic flap and lag frequencies are shown in Figure 64. The rotor airfoil is a NACA 0012 section, and qusi-steady aerodynamics in conjunction with a look up table are used to determine the lift, drag and pitching moment coefficients as functions of angle of attack and Mach number. Because the rotor is lightly loaded in the trim regions of interest, a uniform inflow is assumed.

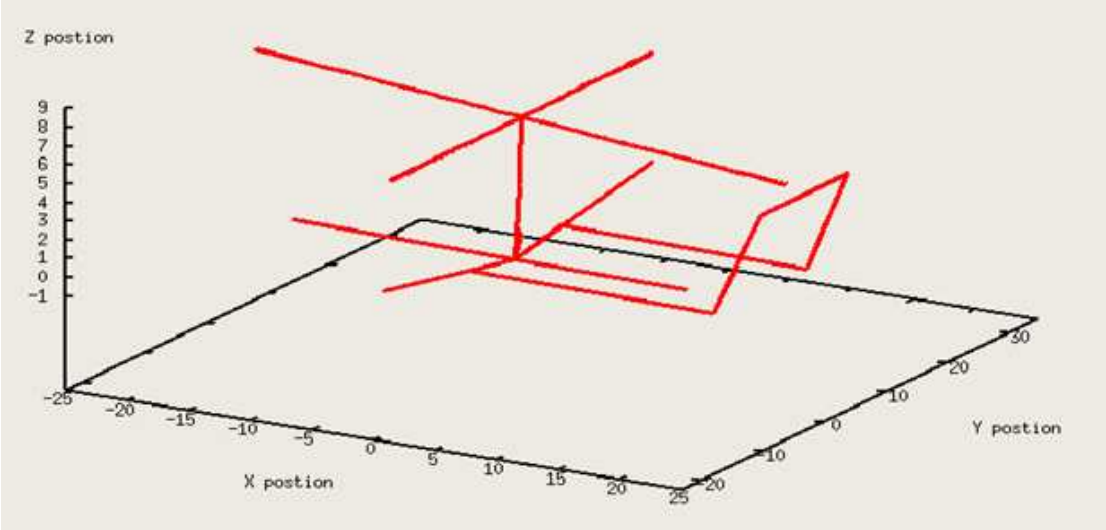

Figure 65: Compound Gyroplane Structural Model

6.2 Compound Gyroplane Optimal Aeroelastic Trim

The compound gyroplane shares lift between the rotor and wing in flight. This section considers the optimal distribution of lift between these two components during the high speed cruise of a long range mission by maximizing the vehicle lift-to-drag ratio. The compound gyroplane operates in steady autorotation during trimmed flight. As discussed in Chapter 4, the rotor disk must have a positive angle of attack relative to the free stream

as air flows up through the disk in autorotation. This can be accomplished indirectly by cyclic flapping or by directly tilting the rotor through shaft tilt. Many gyroplanes have a shaft tilting mechanism where practically all helicopters accomplish relative rotor disk incidence through cyclic flapping. A shaft tiling mechanism adds complexity to a physical aircraft, and a cyclic flapping solution is desirable. However, if the cyclic flapping magnitude is too large, blade fatigue life can be comprimized. The consideration of both methods is given herein and the details of their implementation in trim optimization are discussed in the next sections, followed by comparative optimal trim results.

6.2.1 Fixed Shaft Configuration

The fixed shaft, compound gyroplane configuration has a rotor shaft angle that is fixed with respect to the fuselage at 3º aft. This allows a positive rotor disk angle with respect to the freestream in normal flight conditions. The fixed shaft compound gyroplane achieves autorotation by a combination of blade cyclic flapping *and* fuselage tilt. The blade flapping is therefore controlled to reach the zero average torque condition through 1/rev cyclic input. The fuselage attitude is trimmed to zero the residual lift, which intern affects the inflow through the rotor, also affecting the cyclic flapping. It can be seen that the fixed shaft configuration has a complex, coupled trim solution. The optimization problem for the fixed shaft compound configuration is given as:

Problem Statement:

Maximize: Lift-to-Drag **6.1**

Subject to:

$$F_{Rx}(\vec{X}_D) = 0 \quad \textbf{6.2}$$

$$F_{Ry}(\vec{X}_D) = 0$$

$$F_{Rz}(\vec{X}_D) = 0$$

$$M_{HRx}(\vec{X}_D) = 0$$

$$M_{Ry}(\vec{X}_D) = 0$$

$$Q(\vec{X}_D) = 0$$

$$C_{L\max} \leq 1.0$$

$$\varepsilon_{vm\max} \le 3{,}500 \text{ micro-strain}$$

$$12 \le X_{2I} \le 25 \qquad \textbf{6.3}$$

$$\vec{X}_D = [T_E, \alpha, e, \phi, \theta_{1s}, \theta_{1c}]; \ \vec{X}_I = [V, \Omega] \qquad \textbf{6.4}$$

The first three constraints are the residual forces, followed by the residual hub roll moment and aircraft pitch moment and shaft torque constrained to be zero for autorotation. The last two constraints are the wing maximum lift coefficient and rotor maximum von Mises invariant strain at the critical cross section defined in Chapter 5. Dependant variables include engine thrust, aircraft body pitch and roll, elevator, and lateral and longitudinal cyclic. Independent variables include velocity and rotor speed.

Preliminary investigations show that the vehicle drag is predominately composed of body/hub parasite drag and interference drag between the rotor, hub and engine nacelle, even at low speed where lift induced drag typically dominates. The maximum lift-to-drag speed results in a wing lift coefficient that is too high (post stall) for the cambered airfoil. Therefore, a constraint is added to the optimal trim problem such that the wing lift coefficient must be less than 1.0. The wing maximum lift coefficient inequality constraint was converted to an equality constraint with the addition of a slack variable as outlined in sections 3.1.2. Rotor speed was set as a dependent variable to enforce the constraint. In the implementation of this scheme, the dependent variables failed to reach a converged solution. The reason was due to the apparent sensitivity of the other dependent parameters to rotor speed beside the wing lift coefficient. Specifically, the average shaft torque value was more sensitive to rotor speed than cyclic control, and the coupled solution tended to reduce rotor speed initially, and then fail. Apparently the addition of rotor speed in the dependent variable set in this problem changed the linearity of the system to such a degree than the solution could not converge from that set of initial conditions. A more robust approach is to keep rotor speed as an independent variable and add a penalty function to the objective as outlined in section 3.1.2. In this way, the optimal trim solution is found via a hybrid GRG/Penalty function method. The penalty function is

$$P_{C_L}(\vec{X}) = r_P\left(\max[0, C_{L_{Wing}} - C_{L_{Max}}]\right)^2 . \quad \textbf{6.5}$$

Results of a preliminary trim exploration for the fixed shaft configuration with a rigid rotor provide insight into the basic behavior of the flapping response with respect to rotor speed and airspeed in Figure 66. The rigid rotor blade model uses a spring restraint at the flapping hinge to simulate the elastic effects of the elastic blade. The flap spring value is chosen such that the rigid blade flapping frequency closely matches the fundamental flap mode of the elastic blade over the operational rotor speed range. A large component of the maximum forced response shown in Figure 66 is 2/rev in addition to the normal 1/rev flapping due to the relatively high flap stiffness of the rotor. The trends show that maximum rotor flapping angle increases with a reduction in rotor speed. The reduction in CF load and other resulting trim parameters cause the maximum flap angle to increase significantly. The question regarding rotor structural constrains is what is the limiting flap deflection before the endurance limit of the rigid rotor is exceeded. At high rotor speed conditions (hover), centrifugal stiffening causes the angular deflection to concentrate in the root section of the cantilevered beam. For lower rotor speed conditions, the angular deflection is distributed over a larger spanwise portion of the blade and larger total deflections can occur for equivalent strain levels. In hover, the maximum flap limit is 2 degrees, but at 40% hover speed, the maximum flap limit may more than double. Therefore, the limitation of blade loads as a function of flap angle or flap moment (from 1-D beam theory) do not truly capture what is needed. What is needed in the trim analysis is the actual blade stress and strain, especially where their limit values are exceeded. The inclusion of maximum strain as input to the optimal trim solution is discussed in detail in Chapter 5 and is accomplished via a surrogate model as a function of the 1-D beam forces and bending moments. The rotor strain constraint is included through the use of a penalty function in the objective, similar to the wing loading constraint.

$$P_{\varepsilon}(\vec{X}) = r_P\left(\max[0, \varepsilon_{vm} - \varepsilon_{vm\,\max}]\right)^2 \quad \textbf{6.6}$$

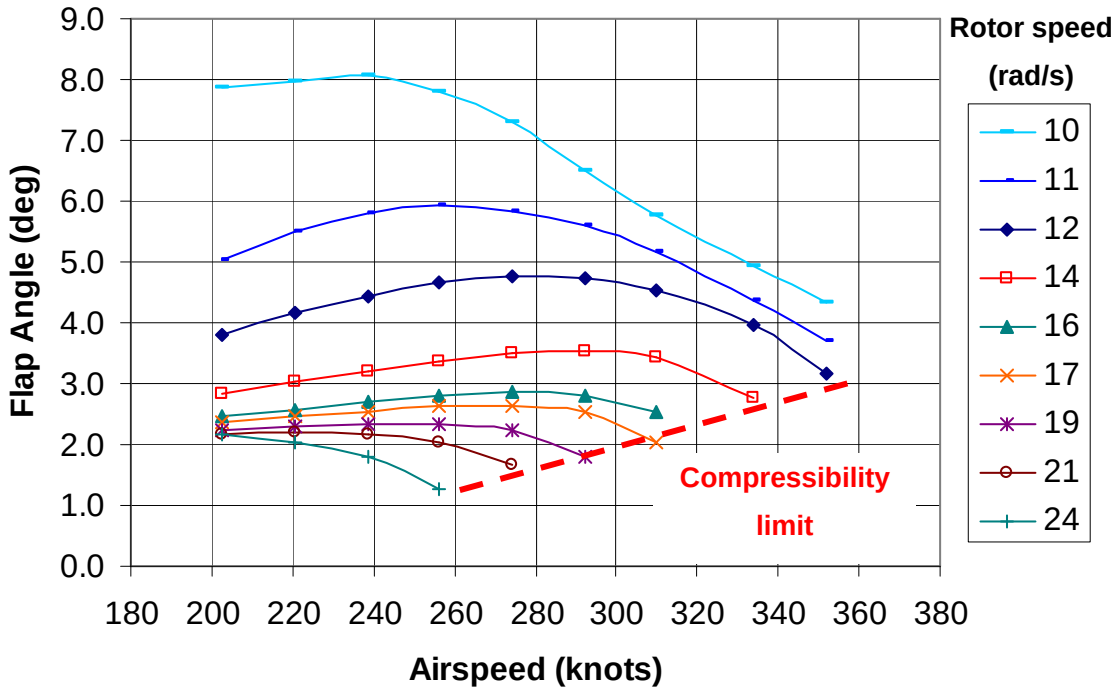

Figure 66: Rigid Blade Flapping at Reduced Rotor speeds

The final optimal trim problem for the fixed shaft compound gyroplane is conducted at 30,000 ft altitude and the limits for the independent variables are set at 12 to 25 rad/s and 200 to 350 knots for rotor speed and airspeed respectively.

6.2.2 Tilting Shaft Configuration

For the compound gyroplane with shaft tilt, a controlled revolute joint is added to the model where the mast connects to the fuselage as shown in Figure 62. The shaft tilting mechanism allows the effective disk incidence to be changed independent of the fuselage to obtain the controlled rotor speed value at zero shaft torque. With the shaft tilt, there is no need for cyclic flapping. In order to minimize loads and vibration, the rotor (average) pitch moment, in addition to the roll moment, is constrained to zero. Therefore, the trim optimization problem given in 6.2.1 has the following additional constraint and modified trim control parameter set:

Subject to:

$$M_{HRy}(\vec{X}_D) = 0 \qquad \textbf{6.7}$$

$$\vec{X}_D = [T_E, \alpha, e, \phi, \theta_{1s}, \theta_{1c}, \alpha_{shaft}]; \ \vec{X}_I = [V, \Omega]. \qquad \textbf{6.8}$$

The optimal trim problem for the tilting shaft configuration has seven dependant variables, the additional variable being shaft tilt, and two dependant variables. The analysis is conducted at 30,000 ft altitude with rotor speed side constraints the same as the fixed shaft problem. The inequality constraints for the wing lift coefficient and maximum blade strain are also implemented through the penalty function approach as before.

6.2.3 Trim Configuration Results

The optimal rotor speed solutions are shown in Figure 67 over a range of gross weights which bracket the maximum and minimum weight for the long range mission. This result shows an interesting contrast in the behavior of the optimal rotor speed with weight. The shaft tilting configuration starts at 16 rad/s and quickly drops down to the minimum rotor speed value of 12 rad/s. At heavier weight conditions, the rotor helps off-load the wing to meet the maximum lift coefficient constraint. Apparently a slight increase in rotor speed is more efficient than an increase in airspeed, a condition which is not initially obvious. However, as weight decreases, the rotor is less efficient than the wing and its speed is driven to the minimum allowable value. The fixed shaft configuration rotor speed also begins at approximately 16 rad/s at maximum weight, but increases as the weight is reduced. In the optimal trim history, the rotor speed initially decreases, but turns upward as the rotor strain value approach the constraint. Figure 68 shows the optimum airspeed trend for the two configurations. Both trends are approximately linear with a 15 to 20 knot difference between the two. The fixed shaft configuration also has a slightly increased slope, showing a reduction in optimal airspeed reduction rate over the shaft tilting configuration as fuel is burned. Finally, optimal lift-to-drag results from analysis are shown in Figure 69 for the fixed and tilting shaft compound gyroplane over the range of gross weights. The tilting shaft configuration has a higher lift-to-drag value over most of the gross weight range, except the last 500 lbs where the trend reverses to a

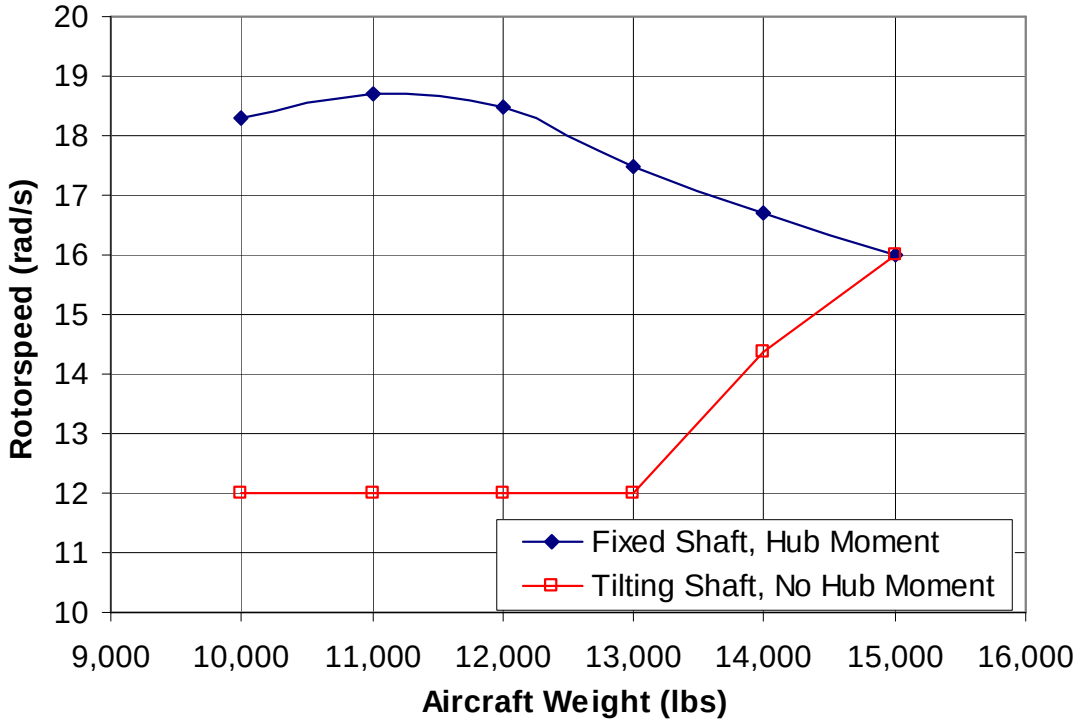

Figure 67: Compound Gyroplane Optimal Rotor Speed Trends

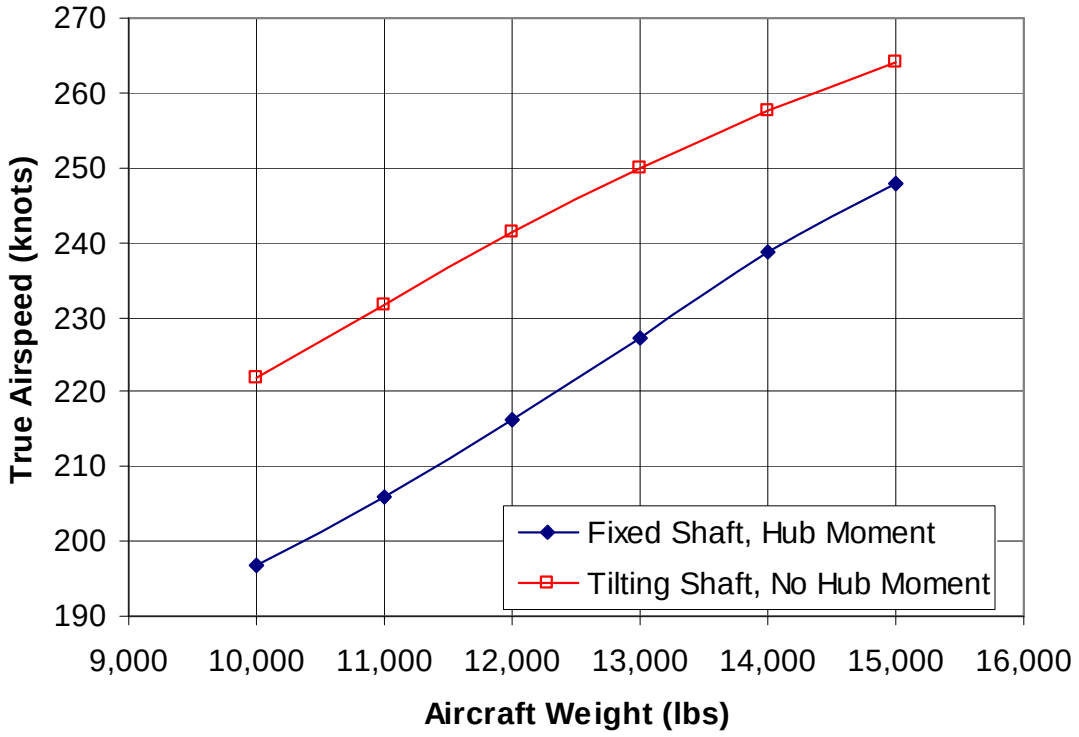

Figure 68: Compound Gyroplane Optimal Velocity Trends

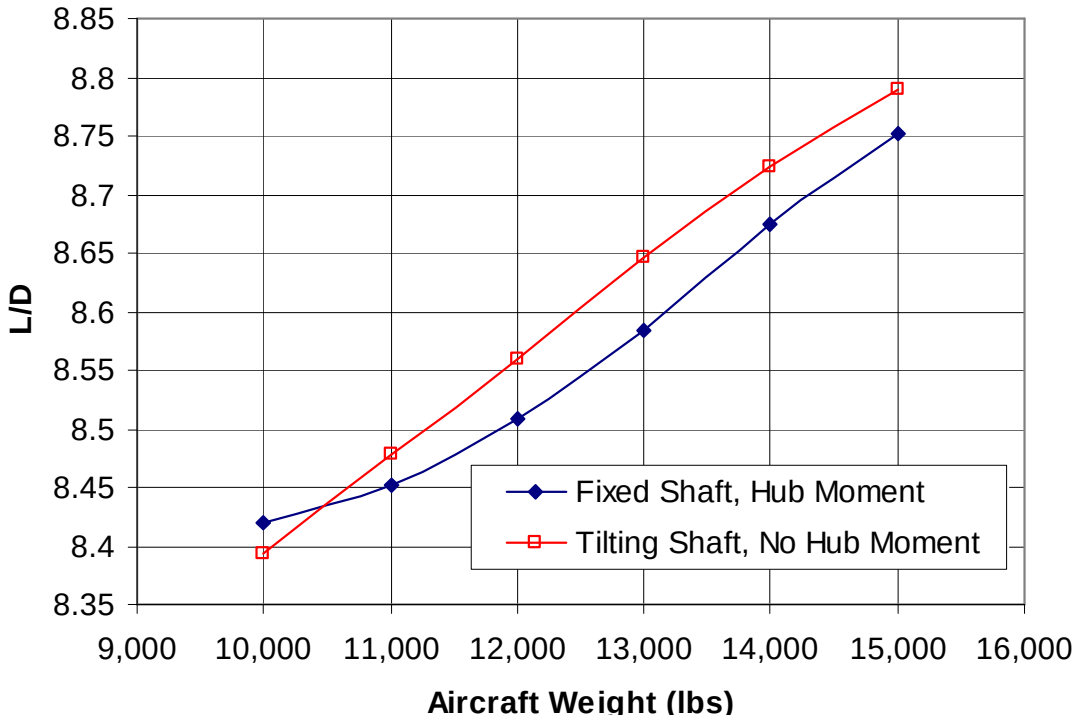

Figure 69: Compound Gyroplane Optimal Lift-to-Drag Trends

small degree. Therefore, the optimal aeroelastic trim results indicate that the tilting shaft configuration has better performance due to the lower loads allowing a lower rotor speed. The higher rotor speed produces a lower maximum vehicle efficiency (L/D) and lower optimal velocity.

6.2.4 Optimal Trim Purpose

The ultimate goal of an optimal trim solution is to guide the designer and controls engineer to the best way to fly a vehicle. The control of modern flight vehicles is supplemented to various degrees by flight control computers. The insights gained from the trim solution can be applied to the development of control laws for automatic flight control systems and in some cases may drive a control solution. In the compound gyroplane example, not only is the optimal lift share between the rotor and wing determined, but the best method by which it may be achieved is discovered, i.e. through the use of tilting the shaft rather than through cyclic flapping. The resulting flight control

architecture for most efficient flight would then break down into a number of control subsystems with sensors and actuators. For the compound gyroplane, the rotor control subsystem would include rotor speed sensors, shaft tilt hinge and actuator as well as hub moment sensors (roll and pitch) and cyclic controls. This method makes the rotor follow along for the ride in cruise and high speed flight, as its effect on steady flight controls in virtually invisible to the pilot flying the fixed wing control surfaces.

6.3 Chapter Summary

The aeroelastic trim performance of an advanced example compound gyroplane is analyzed using the GRG optimal trim method in the comprehensive rotorcraft code RCAS. Two different configurations of the same aircraft were analyzed, one with and one without a steady hub moment. Each configuration was trimmed to a state of steady autorotation. In addition, structural and aerodynamic constraints were fulfilled in the process of determining the optimal trim. The tilting shaft configuration showed better performance due to lower constrained, optimal rotor speed. The determination of these results would otherwise require a complex parametric mapping of the multivariate, constrained trim space for each gross weight condition. The results obtained for this problem shows the utility of the optimal trim method.

CHAPTER 7
CONCLUSION

The purpose of this thesis is to develop and apply a systematic method to reach the best or optimal trim solution for rotorcraft configurations that possess constrained, non-unique trim solution spaces. Specific research questions are formulated regarding the application of trim optimization with respect to the following areas: 1) application of NLP methods to the problem of trim optimization in rotorcraft aeroelastic frameworks, 2) the control of rotor speed as a trim variable for variable rotor speed in steady autorotation, and 3) the rapid approximation of rotor blade stress and strain in the aeroelastic analysis for structural constraints in the optimal trim solution. A final purpose of this work is to apply developments in the stated areas to an example advanced rotorcraft problem, one with non-unique trim solutions, to show the utility of the methods. This concluding chapter summarizes the results outlined in this thesis as they relate to the research questions and hypotheses of Chapter 1.

7.1 Summary and Conclusions

An optimal trim algorithm is developed based on the nonlinear programming technique of the Generalized Reduced Gradient (GRG) and is encoded into the comprehensive rotorcraft analysis code RCAS. The conjugate gradient based search direction is modified to accommodate the radii of convergence of the various independent variables in a novel manner. The optimal trim algorithm is then applied to a series of increasing complexity optimal trim helicopter problems. Inequality constraints are fulfilled by a slack variable method which treats rotor speed as a dependent variable, and a penalty function method which treats rotor speed as an independent variable. The optimal trim algorithm as implemented converges on the independent variable values that produce the minimum power solution, as determined from a parametric mapping of the solution space. Results from Chapter 3 affirm the hypothesis to the primary research question in that *an*

optimal trim solution can be systematically found through the use of the Generalized Reduced Gradient (GRG) NLP method.

The phenomenon of autorotation is discussed with specific reference to the fact that rotor speed varies as steady flight conditions change and its value is not known a priori. A method is developed which captures the rotor speed variation by controlling rotor speed as a trim control parameter in a Newton-Raphson iterative method. The method is validated against isolated wind tunnel rotor data and steady level flight data of a small gyroplane. Application of the optimal trim method allows rotor speed to vary as an independent variable, rather than a dependent variable, and still satisfy the requirement of zero average torque in conditions where multiple zero torque solutions exist. These results affirm the hypothesis to supporting research question 1 in that *rotor speed treated as a trim control parameter allows the rotor speed to be known at a fixed value during each trim iteration, yet vary between iterations until autorotative equilibrium is reached.*

A novel method to rapidly approximate elastic rotor blade stresses and strains in aeroelastic analyses is developed. The method approximates the maximum cross-sectional stress/strain response with an artificial neural network (ANN) surrogate trained by stress/strain values from VAM analysis. The surrogate is a function of 1-D beam forces and moments for the cross-section. The method is validated by comparison of the surrogate predicted loads against the VABS recovered loads for a complex, anisotropic beam cross-section loaded in time. A comparison of the individual strain component values from the surrogate and VABS shows good correlation. Results from Chapter 5 confirm the first hypothesis to supporting research question 2 in that *blade stress and strain can be captured by a surrogate model as a function of the 1-D beam forces and moments.*

The aeroelastic trim performance of an advanced example compound gyroplane is analyzed using the GRG optimal trim method in the comprehensive rotorcraft code RCAS. The optimal lift share between the wing and rotor is determined while keeping the rotor in steady autorotation by driving the average shaft torque to zero. Maximum

rotor blade von Mises strain at the critical spanwise location is computed via a surrogate model and used to constrain the optimal solution to one that ensures blade strain is below endurance limits. Results from Chapter 6 confirm the second hypothesis to supporting research question 2 in that s*urrogate stress/strains can be computed with significantly less time and in a convenient form to be used during the trim optimization.*

7.2 Future Work

In the development of trim in this thesis, the configuration design parameters have been fixed. The development of trim optimization presents an opportunity in certain design applications (which are configuration dependent) where the trim solution and some design element can be optimized simultaneously, with the possibility of finding a better solution than trim and design optimized in isolation. Aside from the possibilities of simultaneous trim/design optimization, three additional areas present an opportunity for further development with potential for advancing optimal trim and surrogate loads utility. The first area is in regard to the step-size and search direction in each optimal trim line search. In the rotorcraft trim class of problems, the radii of convergence of the independent variables vary significantly in magnitude, specifically when rotor speed becomes an independent variable. This condition causes inefficiency as a large number of function calls are required each time the line search step-size must be reduced. This issue was dealt with by developing a somewhat ad hoc method of modifying components of the step size along the search direction. The application of a hybrid search direction and step-size method based on quadratic programming is briefly discussed in 2.2.2.3 as developed by Parkinson and Wilson [37]. This approach simultaneously optimizes both the search direction and step-size based on a number of linearized constraints in a quadratic programming sub-problem. Additional constraints could be added which include independent variable, radii of convergence. The QP sub-problem method would offer a more theoretically sound, and robust method potentially increasing the trim optimization problem efficiency.

A second area for further development is the extension of optimal trim from performance applications to flight stability and control applications. For configurations with multiple trim solutions, certain trim schemes and trim solution sets may have better stability and handling quality characteristics. For example, one trim solution set may show to have less sensitivity to pilot control input perturbations than another. The goal would be to find a trim solution that optimizes some handling quality metric based on the trim control parameters values. This application could draw from the discipline of robust design methods where control parameters are adjusted to minimize variability. In the handling qualities application, a variable set could be chosen such that changes in the vehicle rigid body states are minimized.

A third area for further development is in regards to a tool for the surrogate loads method. The example problem in this thesis captured a single response for one cross-section, the maximum von Mises strain. For some applications, more than a single stress or strain parameter for an entire cross section is required. This is particularly the case for the application of cumulative damage assessment in the situation where the maximum stress/strain jumps to different locations in the cross-section. Tracking the strains from multiple responses in different cross-sectional locations would provide a better estimation of actual fatigue damage accumulated throughout a given time loading sequence. This approach may be particularly useful for the determination of stress/strain in multiple layers or in the inter-laminar matrix for composite beam cross-sections. The main requirement would be the development of a capability that intelligently and easily identifies gauss points of interest in the cross-section and relates them to a particular response to be captured. An interface that graphically allows a user to specify cross-sectional locations of interest and relate them to a response is desirable. The accurate tracking and accumulation of stress/strain damage in specific geometric locations in a computationally fast manner has the potential to improve the quantification of composite beam fatigue and cumulative damage.

REFERENCES

1 Peters, D.A., and Barwey, D., "A General Theory of Rotorcraft Trim," Proceedings of the 36th AIAA/ASME/ASCE/AHS/ASC Structures, Structural Dynamics and Materials Conference, New Orleans, LA, April 1995, Paper No. 95-1451, pp. 2558-2595.

2 Karem, A., Optimum Speed Rotor, U.S. Patent Number 6,007,298, December 1999.

3 Warwick, G. "Gyro Revival," *Flight International*, February 21, 2006.

4 Carter, Jay Jr., "CarterCopter – A High Technology Gyroplane," Proceedings of the American Helicopter Society Vertical Lift Aircraft Design Conference, San Francisco, CA, January 2000.

5 Ashby, Dale, and Eadie, William, and Montoro, Guy. J., "An Investigation of the Reverse Velocity Rotor Concept and its Application to High Speed Rotorcraft," Presented at 2002 Biennial International Powered Lift Conference, November 2002.

6 Ganguli, Ranjan, "Survey of Recent Developments in Rotorcraft Design Optimization," *Journal of Aircraft*, Vol. 41, No. 3, May-June 2004.

7 Celi, R., "Recent Applications of Design Optimization to Rotorcraft – A survey," *Journal of Aircraft*, Vol. 36, No. 1, Jan-Feb 1999.

8 Hohenemser, K.H., "Hingeless Rotorcraft Flight Dynamics," AGARDograph No. 197.

9 Saberi, H., Khoshlahjeh, M. Ormiston, R.A., and Rutkowski, M.J., "Overview of RCAS and Application to Advanced Rotorcraft Problems," AHS 4th Decennial Specialist's Conference on Aeromechanics, San Francisco, CA, January 21-23, 2004.

10 Peters, D.A., Bayly, P., and Li, S., "A Hybrid Periodic-Shooting, Auto-Pilot Method for Rotorcraft Trim Analysis," Proceedings of the 37th Annual AHS Forum, Washinton D.C., June 4-6, 1996.

11 Yen, J.G., Corrigan, J.J., Schillings, J.J., and Hseieh, P.Y., Comprehensive Analysis Methodology at Bell Helicopter: Conference," Proceeding of the Aeromechanics Specialists Conference, San Francisco, January 19-21, 1994, Paper PS. 2.

12 Anon. RCAS Theory Manual, Version 2.0, Technical Report USAAMCOM/AFDD TR 02-A-005, US Army Aviation and Missile Command, Moffett Field, CA, June 2003.

13 Johnson, W., *Helicopter Theory*, Dover Publications, New York, 1994, pp 154.

14 Gessow, A., and Myers, G.C., *Aerodynamics of the Helicopter*, Fredrick Ungar Publishing, 1952.

15 Peters, D.A., and Ormiston, R.A., "Flapping Response Characteristics of Hingeless Rotor Blades by a Generalized Harmonic Balance Method," NASA TN D-7856, February 1975.

16 Eipe, Abraham, *Effect of Some Structural Parameters on Elastic Rotor Loads by an Iterative Harmonic Balance*, Doctor of Science Thesis, Washington University in St. Louis, December 1979.

17 Peters, D. A, and Izadpanah, A. P., "Helicopter Trim by Periodic Shooting with Newton-Raphson Iteration," Proceedings of the 37th Annual AHS Forum, New Orleans, May 1981.

18 Achar, N.S., and Gaonkar, G.H., "Helicopter Trim Analysis by Shooting and Finite Element Methods with Optimally Damped Newton Iterations," *AIAA Journal*, Vol. 31, No. 2, February 1993.

19 Peters, M.H., and Peters, D.A., "Discrete Control Theory and Dynamic Observers Applied to Rotorcraft Stability and Trim," Presented at the 54th AHS Forum, Washington, D.C., May 20-22, 1998.

20 Peters, D.A., Kim, B.S., and Chen, H., "Calculation of Trim Settings for a Helicopter Rotor by an Optimized Automatic Controller," *Journal of Guidance, Control, and Dynamics*, Vol. 7, No. 1, 1984.

21 Peters, D.A., Bayly, P., and Li, S., "A Hybrid Periodic-Shooting, Autopilot Method for Rotorcraft Trim Analysis," Proceedings of the 52nd AHS Forum, Washington D.C., June 4-6, 1996.

22 Enns, Russell, and Si, Jennie, "Helicopter Trimming and Tracking Control Using Direct Neural Dynamic Programming," *IEEE Transactions on Neural Networks*, Vol. 14, No. 4, July 2003.

23 Riviello, Luca, *Rotorcraft Trim by a Neural Model-Predictive Auto-Pilot*, Masters Thesis, Georgia Institute of Technology, April 2005.

24 Jacob, H.G., and Lehmann,.G., "Optimization of Blade Pitch Angle for Higher Harmonic Rotor Control," *Vertica*, Vol. 7, No. 3,. 1983.

25 Chopra, I., and McCloud, J.L., "A numerical Simulation Study of Open-Loop and Closed-Loop and Adaptive Multicyclic Control Systems," *Journal of the American Helicopter Society*, Vol. 28, No. 1, January 1983.

26 Taylor, R.B., Farrar, F.A., and Miao, W., "An Active Control System for Helicopter Vibration Reduction by Higher Harmonic Pitch, " AIAA Paper 80-0672, 36th AHS Forum, Washington, C.C., May 1980.

27 Friedmall, P.P., and Millot, T.A., "Vibration Reduction in Rotorcraft Using Active Control: A Comparison of Various Approaches," *Journal of Guidance, Control and Dynamics*, Vol. 18, No. 4, 1995.

28 Ormiston, R.A., "Further Investigations of Helicopter Rotor Induced Power," Presented at the 61st AHS Forum, Grapevine, Texas, June 1-3, 2005.

29 Cheng, R.P., Celi, R., "Optimum Two-Per-Revolution Inputs for Improved Rotor Performance," *Journal of Aircraft*, Vol. 42, No. 6, November-December 2005.

30 Vanderplaats, Garret N., *Numerical Optimization Techniques for Engineering Design*, Vanderplaats Research and Development Inc., 2001.

31 Sandgren, E., and Ragsdell, K.M., "The Utility of Nonlinear Programming Algorithms: A Comparative Study – Parts 1 and 2," *ASME Journal of Mechanical Design*, July 1980, Vol. 102, pp. 540-551.

32 Schittkowski, K., "Nonlinear Programming Codes: Information, Tests, Performance," Lecture Notes in Economics and Mathematical Systems, Vol. 183, Springer-Verlag, New York, 1980.

33 Wolfe, P. "Methods for Linear Constraints," *Nonlinear Programming*, J. Abadie (ed), North Holland, Amsterdam, 1967.

34 Wolfe, P., "Methods of Nonlinear Programming," *Recent Advances in Mathematical Programming*, R.L. Graves and P. Wolfe (eds), McGraw-Hill, New York, 1963.

35 Abadie, J., and Carpentier, J., "Generalization of the Wolfe Reduced Gradient Method to the Case of Nonlinear Constraints," *Optimization*, R. Fletcher (ed), Academic Press, 1969.

36 Gabriele, G.A., "Large Scale Nonlinear Programming Using the Generalized Reduced Gradient Method," Ph.D. Thesis, Purdue University 1980.

37 Parkinson, A., and Wilson, M., "Development of a Hybrid SQP-GRG Algorithm for Constrained Nonlinear Programming," *ASME Journal of Mechanisms, Transmissions, and Automation in Design*, January 1988.

38 Leishmn, G.J., "Development of the Autogiro: A Technical Perspective," *Journal of Aircraft* Vol. 41, No. 4, July–August 2004 pp. 765-781.

39 De la Cierva, J., "The development of the Autogiro," *Journal of the Royal Aeronautical Society*, Vol. 30, No. 181, 1926, pp. 8-29 (including discussion).

40 Schad, J.L., "Readers Forum - Small Autogiro Performance," *Journal of the American Helicopter Society*, July 10, 1965, pp. 39-43.

41 De La Cierva, J., *Engineering Theory of the Autogiro*, Unpublished.

42 Wheatley, J. B. "The Influence of Wing Setting on the Wing Load and Rotor Speed of a PCA-2 Autogiro as Determined in Flight" NACA Technical Note Number 523, December 1934.

43 McCormick, B. W., "Numerical Analysis of Autogyro Performance," AIAA 2002-5950, Presented at the AIAA Biennial International Powered Lift Conference, Williamsburg, Virginia, November 5-7, 2002.

44 Ward, J.F., "Exploratory Flight Investigation and Analysis of Structural Loads Encountered by a Helicopter Hingeless Rotor System," NASA TN D-3676, 1966.

45 Houston, S.S., "Analysis of Rotorcraft Flight Dynamics in Autorotation," *Journal of Guidance, Control and Dynamics*, Vol. 25, No. 1, 2002.

46 Houston, S.S., "Modeling and Analysis of Helicopter Flight Mechanics in Autorotation," *Journal of Aircraft*, Vol. 40, No. 4, July-August 2003.

47 Wheatley, J.B., "An Aerodynamic Analysis of the Autogiro Rotor with a Comparison Between Calculated and Experimental Results," NACA Report No. 487, January 1934.

48 Wheatley, J.B., "Lift and Drag Characteristics and Gliding Performance of an Autogiro as Determined in Flight," NACA Report No. 434, May 1932.

49 Wheatley, J.B., and Manley, J. H., "Full-Scale Wind-Tunnel Tests of a PCA-2 Autogiro Rotor," NACA Report No. 515, December 1934.

50 Gessow, A. and Myers, G.C., "Flight Tests of a Helicopter in Autorotation Including a Comparison with Theory," NACA Technical Note No. 1267, April 1947.

51 Jhemi, A.A., Carlson, E.B., Zhau, Y.J., Chen, R.T.N., "Optimization of Rotorcraft Flight Following Engine Failure," *Journal of the American Helicopter Society*, April 2004, Volume 49, No. 2.

52 Houston, S. S., "Validation of a Rotorcraft Mathematical Model for Autogyro Simulation," *Journal of Aircraft*, Vol. 37, No. 3, May-June 2000.

53 Rutherford, J. W., and Wells, V. L., "An Air-Launched Self-Recovering Autonomous Vehicle Concept," *Aircraft Design Journal*, Vol. 2, No. 2, 1999,pp. 81–94.

54 Groen, J., "GBA Gyros in the 21st Century," AIAA 2003-2519, AIAA/ICAS International Air and Space Symposium and Exposition, 14-17 July 2003, Dayton, Ohio.

55 McCormick, B. W., "Numerical Analysis of Autogyro Performance," AIAA 2002-5950, Presented at the AIAA Biennial International Powered Lift Conference, Williamsburg, Virginia, November 5-7, 2002.

56 Morillo, J. A., *A New Harmonic Balance Approach for Rotor Systems with Engine Dynamics*, Master of Science Thesis, Washington University, Saint Louis, Missouri, 1996.

57 Hodges, D.H., "A Review of Composite Rotor Blade Modeling," *AIAA Journal*, Vol. 28, No. 3, March 1990, pp. 561-565.

58 Jung, S.N., Nagarag, V.T., and Chopra, I., "Assessment of Composite Rotor Blade Modeling Techniques," *Journal of the American Helicopter Society*, Vol 44, No. 3, July 1999, pp. 188-205.

59 Cesnik, C.E.S., and Hodges, D.H., "VABS: A new Concept for Composite Rotor Blade Cross-Sectional Modeling," *Journal of the American Helicopter Society*, Vol. 42, No. 1, January 1997, pp 27-38.

60 Yu, W., Volovoi, V., Hodges, D.H., and Hong, X., "Validation of the Variational Asymptotic Beam Sectional Analysis," *AIAA Journal*, Vol 40, No. 10, October 2002, pp. 2105-2112.

61 Yu, W., and Hodges, D.H., "The Timoshenko-like Theory of the Variational Asymptotic Beam Sectional Analysis," presented at the 44th AIAA/AS<E/ASCE/AHS Structures, Structural Dynamic and Materials Conference, 7-10 April 2003, Norfolk,Virginia.

62 Yu, W., Hodges, D.H., Volovoi, V., and Fuchs, E.D., "The Vlasov Theory of the Variational Asymptotic Beam Sectional Analysis," 45th AIAA/ASME/ASCE/AHS Structures, Structural Dynamics and Materials Conference, 19-22 April 2004, Palm Springs, CA.

63 Fletcher, R. and C.M. Reeves, "Function Minimization by Conjugate Gradients," *Computer Journal*, Vol. 7, No. 2, 1964.

64 Sun, W., Yuan, Y., *Optimization Theory and Methods*, Springer Science 2006.

65 Gabriele, G.A., and Ragsdell, K.M., "The Generalized Reduced Gradient Method: A Reliable Tool for Optimal Design," *Journal of Engineering for Industry*, ASME, Series B, Vol. 99, No. 2, May 1997, pp. 394-400.

66 Kelley, T.C., *Iterative Methods for Linear and Nonlinear Equations*, Society of Industrial and Applied Mathematics, 1995.

67 Prouty, R., *Helicopter Performance, Stability, and Control*, Krieger Publishing, Malabar, Florida, 2002.

68 Wimperis, H.E., "The Rotating Wing in Aircraft," Aeronautical Research Council, ARC R&M 1108, London, 1926.

69 Nikolsky, A.A., Seckel, E., "An Analytical Study of the Steady Vertical Descent in Autorotation of Single-Rotor Helicopters," NACA TN 1906, 1949.

70 Nikolsky, A.A., Seckel, E., "An Analytical Study of the Steady Vertical Descent in Autorotation of Single-Rotor Helicopters," NACA TN 1906, 1949.

71 Bailey, F.J. Jr., "A Study of the Torque Equilibrium of an Autogiro Rotor," NACA Report 623, 1938.

72 Wheatley, J.B., and Bioletti, C., "Wind-Tunnel Tests of a 10-Foot-Diameter Gyroplane Rotor," NACA Report No. 536, April 11, 1935.

73 Dadone, L.U., *U.S. Army Helicopter Design Datcom Volume I – Airfoils*, May 31, 1976.

74 He, Chengjian, *Development and Application of a Generalized Dynamic Wake Theory for Lifting Rotors*, Doctor of Science Thesis, Georgia Institute of Technology, Atlanta, Georgia, July 1989.

75 Houston, S.S., and Brown, R.E., "Rotor-Wake Modeling for Simulation of Helicopter Flight Mechanics in Autorotation," *Journal of Aircraft* Vol. 40, No. 5, September-October 2003.

76 Houston, S.S., "Longitudinal Stability of Gyroplanes," *AIAA Journal*, January 1996.

77 Houston, S.S., "Identification of Autogyro Lognitudinal Stabilty and Control Characteristics," *Journal of Guidance, Control and Dynamics*, Vol. 21, No. 3, May-June 1998.

78 Houston, S.S., "Validation of a Rotorcraft Mathematical Model for Autogyro Simulation," *Journal of Aircraft*, Vol. 37, No. 3, May-June 2000.

79 Schaefer, R.F., and Smith, H.A., "Aerodynamic Characteristics of the NACA 8-H-12 Airfoil Section at Six Reynolds Numbers From 1.8E06 to 11.0E06," NACA Technical Note, 1998, December 1949.

80 Coton, F., Smrecek, L., and Patek, Z., "Aerodynamic Characteristics of a Gyroplane Configuration," *Journal of Aircraft*, Vol. 35, No. 2, 1998.

81 Bisagni, Chiara, Lanzi, Luca, and Ricci, Sergio, "Optimization of Helicopter Subfloor Components Under Chrashworthiness Requirements Using Neural Networks," *Journal of Aircraft*, Vol. 39, No. 2, March-April 2002.

82 Baker, C.A., Grossman, B., Haftka, R. T., Mason, W.H. and Watson, L.T., "High Speed Civil Transport Design Space Exploration Using Aerodynamic Response Surface Approximation," *Journal of Aircraft*, Vol 39, No. 2, 2002, pp 215-220.

83 Sevant, N.E., Bloor, M.I.G., and Wilson, M.J., "Aerodynamic Design of a Flying Wing Using Response Surface Methodology," *Journal of Aircraft*, Vol. 37, No. 4, 2000, pp. 562-569.

84 Henderson, J.L., Walsh, J.H., and Yound, K.C., "Application of Response Surface Techniques to Helicopter Rotor Blade Optimization Procedure," Proceedings of the AHS National Technical Specialist Meeting on Rotorcraft Structures: Design Challenges and Innovative Solutions, 1995.

85 Ganguli, R., "Optimal Design of a Low Vibration Helicopter Rotor Using Response Surface Approximation," *Journal of Sound and Vibration*, Vol. 258, No. 2, 2002, pp. 327-344.

86 Abdi, Herve, "A Neural Network Primer," *Journal of Biological Systems*, Vol. 2(03) 1994, pp. 247-283.

87 McCulloch, W.S., and Pitts, W.H., "A Logical Calculus of Ideas Immanent in Nervous Activity," Bulletin of Mathematical Biophysics, Selected Papers on Optical Neural Networks, Vol, 96, No. 5 1943, pp. 115-133.

88 Myers, R.H., Montgomery, D.C., *Response Surface Methodology – Process and Product Optimization Using Designed Experiments*, Wiley, New York, 1995.

89 Gosse, Jon H., "Strain Invariant Failure Criteria for Polymers in Composite Materials," AIAA-2001-1184.

90 Tay, T.E., Tan, S.H.N., Tan, V.B.C., and Gosse, J.H., "Damage Progression by the Element-Failure Method (DFM) and Strain Invariant Failure Theory (SIFT)," Elsevier 2005.

91 Hodges, D. H., *Nonlinear Composite Beam Theory*, AIAA, Virginia, 2006.

92 Rustenburg, J.W., Skinn, D., and Tipps, D.O., "An Evaluation of Methods to Separate Maneuver and Gust Load Factors from Measured Acceleration Time Histories," DOT/FAA/AR-99/14.

93 Floros, M. W., Johnson, W., "Performance Analysis of the Slowed-Rotor Compound Helicopter Configuration," Presented at the AHS 4th Decennial Specialists' Conference on Aeromechanics, San Francisco, California, January 21-23, 2004.

94 Wilde, E., Bramwell, A., and Summerscales, R., "The Flapping Behavior of a Helicopter Rotor at High Tip Speed Ratios," British Aeronautical Research Council, Report CP 877, 1966.

95 Hohenemser, K., "Remarks on the Unloaded Rotor Type of Convertiplane," Proceedings of the 11th Annual AHS Forum, Washington D.C. 1955.

96 Peters, David A., Hohenemser, K.H., "Application of the Floquet Transition Matrix to Problems of Lifting Rotor Stability," *Journal of the American Helicopter Society*, Vol 16, (2), April 1971.

97 Floros, Matthew W., Johnson, Wayne, "Stability Analysis of the Slowed-Rotor Compound Helicopter Configuration," Presented at the American Helicopter Society 60th Annual Forum, Baltimore, MD, June 7-10, 2004.

98 Sissingh, G.J., "Dynamics of Rotors Operating at High Advance Ratios," *Journal of the American Helicopter Society*, 13, (3) July 1968.